THE UNIVERSITY OF HULL

DEVELOPMENT OF A MICROFLUIDIC DEVICE FOR THE *IN SITU* PRODUCTION OF SINGLET OXYGEN FOR CHEMICAL AND BIOLOGICAL APPLICATIONS

being a Thesis submitted for the Degree of Doctor of Philosophy

in the University of Hull

by

Emily K. Lumley MChem (Hons) BA

August 2012

Acknowledgements

I would like to thank my supervisors Prof. Ross W. Boyle, Dr. Nicole Pamme and Dr. Charlotte Dyer for their support and guidance throughout my studies over the last four years. Also thanks to the Clinical Biosciences Institute for financing this project. Special thanks to Dr. Charlotte Wiles, Dr. Francesca Giuntini and Dr. Cristina Alonso for their help and guidance in the lab with practical work. I would also like to thank Huguette Savoie for all her help and guidance with the cell work and for putting up with me in her lab using her equipment and making a mess. Also my thanks to Steve Clarke for chip fabrications and Nigel Parkin for making the syringe pump holder, chip holders and the black box set-up.

To all those that I have shared labs with and that have helped me when things weren't working; Mike Benstead, Aaron Bullous, Chris Welch, Mark Tarn, Sal Peyman, Kirsty Shaw, Jane Woods, Sam Hattersley, and Leanne Josefson. Especially I would like to thank those special friends who helped so much over the last two years and who shared lunch and a number of very special dinner parties; Mark Ward, Emma Hope, Louis Allott and Kati Nicholson, Francesca Bryden and Rachel Smith.

My family have been wonderful also, supporting me with love and prayers over the good times and the bad; I love you all and appreciate everything you have done for me. Last, but by no means least to my husband, Jason; he made me a better person by loving me and encouraged me to be the best I could be, I couldn't have done it without you.

Thank you all.

Abstract

Cancer cells are derived from cells that are termed, and recognised as being 'self', meaning that the immune system does not target them. Many treatments target the tumour through its requirement for large quantities of nutrients. However, this causes healthy cells to be destroyed and unpleasant side effects for the patient. Recently research has found that cancer cells treated *ex vivo* with photodynamic therapy will initiate an immune response on re-introduction to the patient. Photodynamic therapy is the use of a photosensitiser drug, in the presence of oxygen, being irradiated with light and thus producing singlet oxygen which is toxic to cells in the region.

The purpose of this work was to immobilise a photosensitiser to the glass channel walls of a microfluidic device which could be used to produce singlet oxygen *in situ*. This device could then be used for chemical applications, in photo-oxidation reactions, and for a specific biological application, the efficient production of a PDT-generated cancer vaccine.

A method was developed to immobilise a porphyrin, bearing an isothiocyanate group on the inner glass channels of the fluidic device, pre-silanised to present amino groups. This method was optimised using rhodamine B isothiocyanate on glass beads and within the microfluidic device before the porphyrin was used in its place. To determine the success of this reaction the porphyrin-immobilised chips were used to oxidise cholesterol and compared to the same reaction with the porphyrin in solution, both on chip, and in batch conditions. Further photo-oxidation reactions were conducted with α-terpinene and citronellol and compared to the equivalent reaction in batch conditions. It was found that the on-chip reaction gave a lower yield, but was more efficient, at producing oxidation products.

Finally the porphyrin-immobilised chip was used to determine the effect on cultured cancer cells pumped through in the presence of light. The cationic porphyrin used for the chemical

applications was found to cause dark toxicity, and therefore a neutral hydrophilic porphyrin was used. This was found to give a difference between the cell death in the dark and in the light that was statistically significant. However, the expression of heat shock protein 70, a key marker for immunogenicity of cells, was not found.

The microfluidic chip was successfully functionalised with porphyrin molecules, and was found to efficiently produce singlet oxygen for the purposes of chemical oxidation reactions. The chip was capable of causing cell death to cancer cells and proven to be due to the irradiation of the porphyrin, however, it was not discerned whether they would be capable of initiating an immune response.

Abbreviations

$^1O_2$	Singlet oxygen
$^1\Delta$	Lowest energy state of singlet oxygen
$^1\Sigma$	Highest energy state of singlet oxygen
$^3\Sigma$	Ground state triplet oxygen
AFM	Atomic force microscope
APC	Antigen presenting cell
APTES	(3-Aminopropyl)triethoxysilane
AuNP	Gold nanoparticle
BPD	Benzoporphyrin derivative
CI	Chemical ionisation
CPTMS	3-Chloropropyl trimethoxysilane
CRT	Calreticulin
DAMP	Damage associated molecular patterns
DC	Dendritic cell
DCA	9,10-Dicyanoanthracene
DMF	Dimethylformamide
DMSO	Dimethyl sulfoxide
DNA	Deoxyribonucleic acid
DPBF	1,3-Diphenylisobenzofuran
ESI	Electrospray ionisation
FTIR	Fourier transform infrared
GC-MS	Gas chromatography-Mass spectrometry
HMGB	High mobility group box

Hp	Hematoporphyrin
HpD	Hematoporphyrin derivative
HPV	Human papilloma virus
HSP	Heat shock protein
IL	Interleukin
INF	Interferon
IR	Infrared
ITC	Isothiocyanate
ITO	Indium tin oxide
LB	Langmuir Blodgett
LC-MS	Liquid chromatography-Mass spectrometry
LED	Light emitting diode
LSPR	Localised surface plasmon resonance
MB	Methylene blue
MHC	Major histocompatibility complex
NK	Natural killer
OTS	Octadecyltrichlorosilane
PCR	Polymerase chain reaction
PDMS	Polydimethylsiloxane
PDT	Photodynamic therapy
PMMA	Poly(methylmethacrylate)
PPIX	Protoporphyrin IX
PVSZ	Polyvinylsilazane
RB	Rose bengal
RhB	Rhodamine B

ROS	Reactive oxygen species
S/V	Surface to volume
SAM	Self-assembled monolayer
$scCO_2$	Super critical carbon dioxide
T_C	Cytotoxic T cells
TCSPP	Tetrakis(4-chlorosulfonylphenyl) porphyrin
TDCPP	Tetra(2,6-dichlorophenyl) porphyrin
TDP	1,1-Thiocarbonyldi-2(2*H*)pyridine
T_H	Helper T cells
TMPyP	Tetramethylpyridiniumyl porphyrin
TNF	Tumour necrosis factor
TPP	Tetraphenylporphyrin
TSPP	Tetra(4-sulfonatophenyl) porphyrin
TTP	Tetratolylporphyrin

Table of Contents

Figures

Schemes

Tables

Chapter 1. Introduction

This introduction will serve to explain the principles behind the research in this thesis and review the literature relevant to it. Initially the general concepts of the research are outlined which include a definition of cancer and the issues that are involved in treating it (section 1.1). A brief overview of the biological applications will be included (section 1.2) including an explanation of photosensitisers, singlet oxygen and photodynamic therapy (PDT) in order to expand this later to include the development of PDT-generated cancer vaccines. An outline of the chemistry mediated by singlet oxygen and specifically photo-oxidation reactions will be given (section 1.3) which will subsequently be expanded to incorporate the research that is pertinent to this thesis (section 1.6). Finally microfluidic technology will be presented (section 1.4), which will later be dealt with in the context of its utility for specific applications. Following on from this, literature dealing with silanisation and functionalisation of glass and silica substrates will be presented (sections 1.5). A review of photo-oxidation reactions in homogeneous conditions, with solid supported photosensitisers and on-chip will be outlined (section 1.6). Finally a more in depth look at PDT and the immune response to it is provided, leading to an explanation of the recent work on PDT-generated vaccines (section 1.7). It is the aim of this literature review to introduce the gap in the wider research into which this thesis is placed.

1.1. Cancer

The term cancer is used to describe a large number of diseases which are linked by common features. Some of these can now be efficiently treated or managed, especially if they are detected early enough. Others are more likely to be terminal and can cause the patient a great deal of pain and distress, especially throughout the treatment. Cancer can occur in almost any location within the body, possibly affecting any number of different cells, tissues and organs. The most common cell to be affected by cancer is the epithelial cell, which is found in the gastro-intestinal tract, bladder, lungs, vagina, breast and skin, and accounts for around 70% of cancers.[1] There are a series of six "acquired capabilities" that a cell gains that signifies it as cancerous, as defined by Hanahan and Weinburg:[2]

1. **Self-sufficiency in growth signals:** Whereas normal cells require specific growth signals (often originating from other cells in close proximity to them), cancer cells gain the ability to create their own growth signals, allowing them to grow independent of other cells around them.
2. **Insensitivity to antigrowth signals:** Normal cell growth is regulated by antigrowth signals to ensure that a healthy balance is maintained. When a tumour grows, the cancerous cells become insensitive to these signals, allowing them to grow eternally.
3. **Evading apoptosis:** Programmed cell death (apoptosis) ensures that when a cell gets damaged or old they are removed to keep equilibrium in the body. The tumour becomes a greater burden due to the tumour cells ability to evade apoptosis.
4. **Limitless replicative potential:** Whereas most cells have a limited replication potential, cancer cells gain the ability to infinitely replicate.

5. **Sustained angiogenesis:** In order for a cell to gain all the necessary nutrients it is estimated that it needs to reside within 100 μm proximity to a blood vessel. Therefore, tumours are able to create new blood vessels in order for it to grow.
6. **Tissue invasion and metastasis:** Finally, a tumour will spread throughout the body establishing and growing in new sites.

Figure 1 illustrates that it is the combination of all six factors that identify a cell as cancerous.

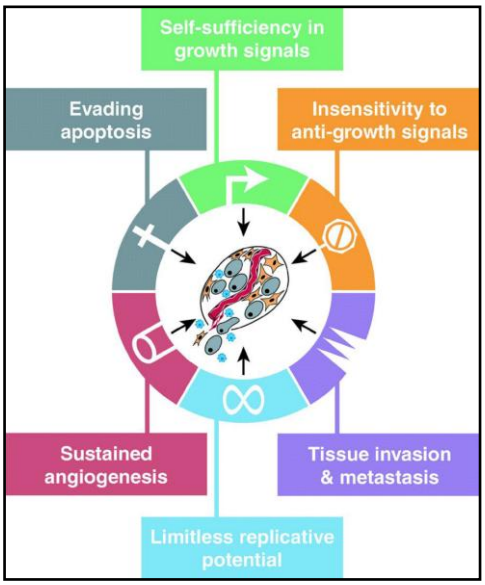

Figure 1: The acquired capabilities of cancers as postulated by Hanahan and Weinburg.[2]

The factors that affect the cells, and are considered to initiate tumorigenesis, are almost as numerous as the types of diseases that are caused by them. These range from lifestyle choices and living environments to a genetic predisposition to developing a specific type of cancer. Lifestyle choices such as smoking and a high calorie diet are now well established as increasing the risk of developing certain cancers.[3] Cancers can also be caused by viruses and bacteria, such as the human papilloma virus (HPV), which is known to contribute to the development of cervical cancer.[4] Carcinogens have been identified which include ionising radiation and chemicals of various types, such as asbestos, arsenic and aniline dyes.[5] Many

of these chemicals have been used in industrial processes, or were workplace hazards of many jobs. Finally, genetics is well established as playing a part in a number of cancers. It is easy to track the inheritance of certain cancers, such as breast and ovarian cancer through a familial line.[6]

Cancer cells are mutations of cells recognised as self and therefore effectively invisible to the immune system. The ability to become self-sustaining within the body has meant that cancer is particularly difficult to treat. Many of the current treatments work on the basis that a drug will be taken up more by the cancer cells than by other cells in the body, and therefore the damage will be extensive to the tumour cells. However, this means that they have many side effects as they accumulate in other healthy cells in the body and cause a reduced quality of life for the patient and their family.[7] In order to provide an effective treatment for cancer it is necessary to find a therapy that will act more specifically on the cancer cells and will be less damaging to other healthy cells in the body. One method being looked at to target the cancer cells specifically is personalised cancer vaccines,[8, 9] based on the killed vaccine theory; by starting with the patient's own cancer cells these could be killed in a fashion that has been shown to initiate an immune response. Reintroduction of the treated cells to the patient should then trigger the adaptive immune response to recognise the cancer cells as non-self. It will enable those antigens expressed by the cancer cells, and not by normal cells, to be targeted specifically to achieve directed recognition and eradication of cancer cells. The intention of this work is to realise the production of a PDT-generated cancer vaccine which could be produced efficiently and in a simple manner. Therefore it is important to understand the principles behind PDT as a treatment for cancer which will be presented in the following section.

1.2. Principles associated with the biological applications

Photodynamic therapy (PDT) involves the drug, known as a photosensitiser, which on irradiation with light of a specific wavelength, will be promoted to an excited singlet state. Due to certain characteristics a percentage of the excited singlet photosensitiser will transfer to the triplet excited state by intersystem crossing, and in the presence of molecular oxygen will undergo energy transfer to the singlet ground state promoting oxygen to the singlet excited state. This singlet oxygen is highly cytotoxic and causes cell death of the cancer cells, which can initiate an immune response to the cancer. The main components of this effect, the photosensitiser and the singlet oxygen will be explained followed by a more in-depth look at PDT as a cancer treatment as it is utilised presently.

1.2.1. Photosensitisers

Photosensitisers are molecules which, in the presence of light and oxygen can produce singlet oxygen and other reactive oxygen species. They are used and investigated in relation to photodynamic therapy (PDT), but can also be used for certain chemical reactions that require the production of singlet oxygen such as ene reactions and [2+2] or [4+2] Diels-Alder like cycloaddition reactions.[10] Photosensitisers can be loosely categorised into porphyrin based and non-porphyrin based.[11] The most common types of photosensitiser for PDT are porphyrin based molecules;[10, 12, 13] however non-porphyrin photosensitisers are also being investigated.[14-17] For chemical applications methylene blue[18, 19] and rose bengal[20-27] are two of the most common photosensitisers, however *meso*-tetraphenylporphyrin[28-30] has also been used. In general they are highly conjugated and/or have heavy atoms present which causes them to efficiently convert molecular oxygen into singlet oxygen *i.e.* the singlet oxygen quantum yield. To look in more detail at porphyrin-based photosensitisers, the basic structure of porphine (**1**) is composed of four pyrrole units attached by methine bridges to

form a macrocycle. This basic structure is known as porphine, however, when further substituted at the *meso* or β positions it becomes known as porphyrin (Figure 2).

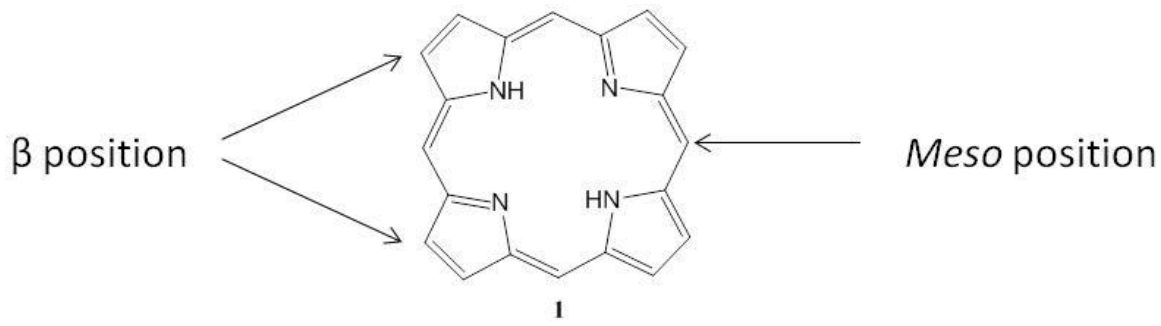

1

Figure 2: Basic porphine structure comprised of four pyrrole units attached by methine bridges and showing possible sites for attachment of further groups to form substituted porphyrin molecules.

To this core aromatic structure it is possible to attach a number of other groups, introducing functionality or altering the ground and excited state photophysical properties, a metal atom can also be chelated by the four nitrogen atoms pointing into the central cavity. Functional groups can be added to either the β position or the *meso* position. This makes porphyrin molecules particularly versatile and gives many avenues for improvement over numerous uses. There are also a number of variations on the basic structure of porphine which can alter aspects of its use. For example chlorins (**2**) and bacteriochlorins (**3**) have one and two of the double bonds in the pyrroles reduced respectively (Figure 3). Phthalocyanines (**4**) have an extra benzene ring fused to the pyrroles along with extra nitrogens to bridge the pyrrolic rings.

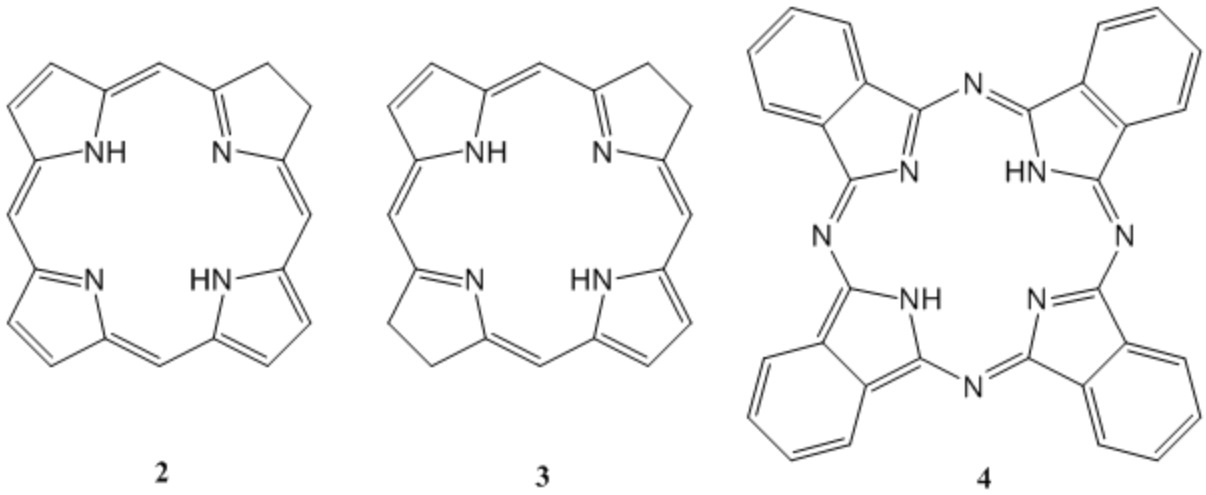

Figure 3: Structure of chlorin (2), bacteriochlorin (3) with one and two double bonds reduced and phthalocyanine (4) with an extra benzene ring and nitrogen bridging the pyrollic rings.

Porphyrins occur naturally in blood as haem, which is iron(II) protoporphyrin IX (PPIX). A dihydrated analogue of PPIX, haemotoporphyrin (Hp) was found to be useful for imaging tumours by fluorescence, however, it was later found that a synthetic polymer formed from Hp, hematoporphyrin derivative (HpD) had increased tumour localising properties. It was this material that was then found to be useful for photodynamic treatment of tumours.[31] HpD itself is a complex mixture of many different monomers and oligomers. A purified form of HpD is now used clinically in PDT and has the trade name Photofrin™. Due to the labour intensive method for synthesising porphyrins, non-porphyrin molecules have also been investigated for use in PDT, as have other porphyrin derivatives.[32] All these photosensitiser molecules have one thing in common, and that is their ability to initiate the production of reactive oxygen species, and more specifically singlet oxygen, which is the cytotoxic aspect in PDT. A comprehensive compilation of the many photosensitisers and their singlet oxygen quantum yields was produced in 1999 by Redmond and Gamlin.[33] A common method of improving the quantum yield of a photosensitiser is to attach heavy halogen atoms, and this method is often utilised for xanthene dyes. These atoms have a two-fold improvement by

increasing the intersystem crossing, which in turn increases the amount of long lived triplet state, but also, for biological applications, it can shift the activation into the red region of the spectrum which improves transition of the light through tissue.[34] The next aspect important to both the biological and chemical applications is how photosensitisers produce singlet oxygen.

1.2.2. Singlet oxygen

When a photodynamic sensitiser is excited by light in the presence of oxygen, it results in the transformation of ground state triplet oxygen to excited state singlet oxygen which is the toxic agent most often implicated in PDT, and also the active reagent in singlet oxygen-mediated oxygenation. A modified Jablonski diagram can help to understand how singlet oxygen ($^1O_2$) is produced through the excitation of a photosensitiser by light (Figure 4).

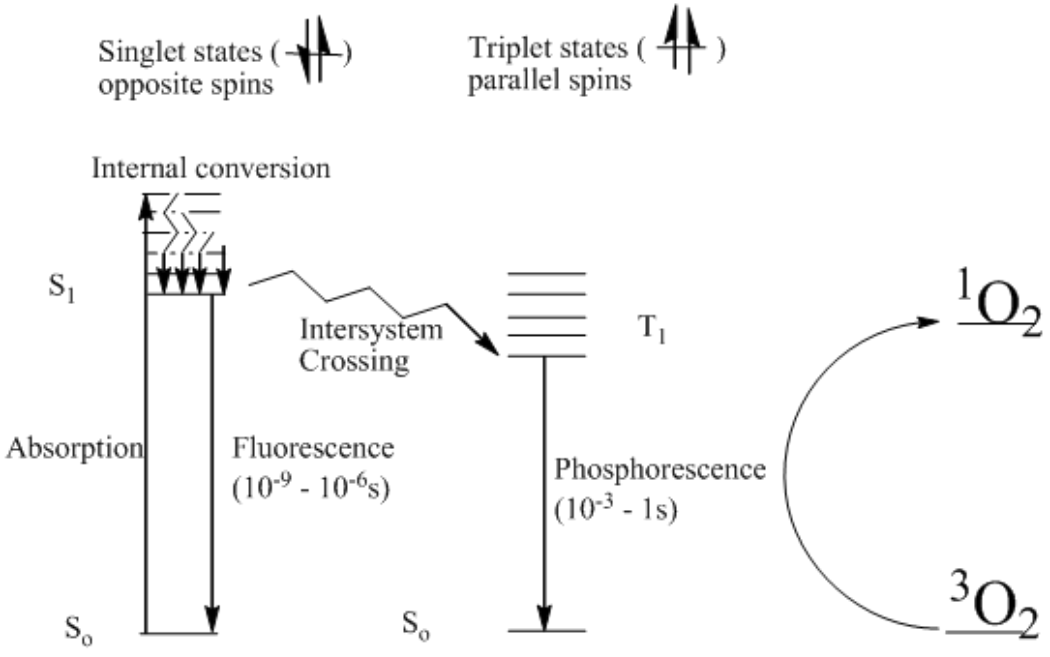

Figure 4: Jablonski diagram to show the production of singlet oxygen. The photosensitiser, in the ground state (S_0) absorbs a photon of light to promote it to the excited singlet state (S_n), and then relaxes to the first excited singlet state (S_1). Through intersystem crossing it gains parallel spins and is in the triplet excited state (T_1). Energy transfer can then occur as the photosensitiser returns to the singlet ground state (S_0) and triplet molecular oxygen is promoted to excited singlet oxygen ($^1O_2$).

When a photosensitiser is illuminated with light of an appropriate wavelength, it is promoted into the excited singlet state. From here there are a number of pathways it can take to relax to the ground state. Internal conversion first relaxes the molecule to the lowest vibrational level of the electronic excited state (S_1), by emission of a photon the molecules can then return to the ground state by fluorescence which is a spin "allowed" transformation resulting in a short fluorescence lifetime of $10^{-9} – 10^{-6}$ s. Certain molecules have a tendency, from the S_1 state, to undergo intersystem crossing to an excited triplet (T_1) state in which two electrons have parallel spins, and then by emission of a photon, can return to the ground state by phosphorescence. Due to the spin forbidden nature of a triplet to singlet state transition, the phosphorescence lifetime of $10^{-3} – 1$ s is significantly longer than that of fluorescence.[10] The quantum yield of total radiative transitions for a compound will always be equal to 1. For an effective photosensitiser a high quantum yield is essential as this indicates how efficiently the molecule can turn light energy into the relevant process (for instance the production of singlet oxygen). For example the singlet oxygen quantum yield of Hp in various solvents ranges from 0.04 (solvent PBS, pH 7.4 irradiated at 630 nm) to 0.75 (CH_3OD).[33]

In the presence of oxygen the transfer of energy that is required for the photosensitiser to return from the triplet state to the ground state can cause a photochemical reaction (Type II) which converts triplet oxygen to the highly reactive singlet oxygen species ($^1O_2$). It is this reactive oxygen species that is believed to be the major cause of the cytotoxic effect in PDT.[31] Type I reactions can also occur from the triplet excited state of the photosensitiser ($^3P^*$). In the absence of oxygen the triplet state photosensitiser can react directly with organic substrates in close proximity to it, producing oxidised substrates (S^+) and reduced photosensitiser (P^-) or reduced substrates (S^-) and oxidised photosensitiser (P^+), depending on the redox potential of both reagents. These are represented in the equations in figure 5.

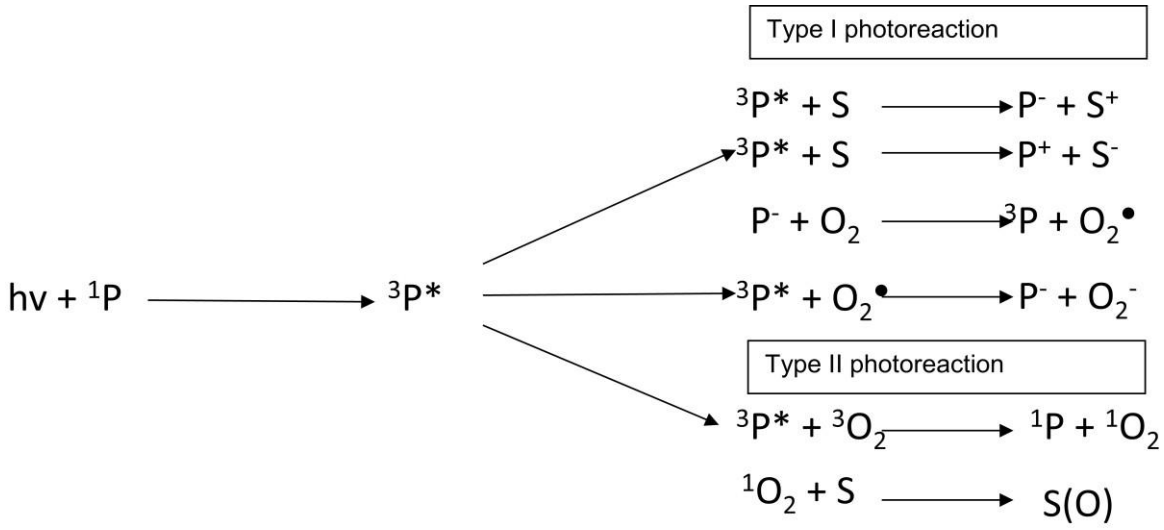

Figure 5: Type I reactions can occur from the triplet excited state ($^3P^*$), in the absence of oxygen it can react directly with organic substrates in close proximity producing oxidised substrates (S^+) or reduced substrates (S^-) depending on the redox potential of the reagents. With low concentrations of oxygen the superoxide anion (O_2^-), this can then react to form highly reactive radicals. Type II reactions involve a direct energy transfer from the excited photosensitiser to ground state triplet oxygen to form highly reactive singlet oxygen.

If there is a small amount of oxygen present the reduced photosensitiser will react with it to produce a superoxide anion (O_2^-). The excited triplet state photosensitiser can also react directly with superoxide radicals to produce the superoxide anion (O_2^-). These superoxide anions can then react further to form the highly reactive hydroxyl radical ($OH^\bullet$).

There are two singlet states for molecular oxygen, and one triplet state. Unlike most molecules, it is the triplet state that is the ground state and the two singlet states that make up the excited states. In the ground state the two electrons of highest energy (π_x^* and π_y^*) each occupy one orbital and are unpaired ($^3\Sigma$), whereas in the excited energy state they are either in the same orbital and paired ($^1\Delta$) or paired in different orbitals ($^1\Sigma$) (Figure 6).[35]

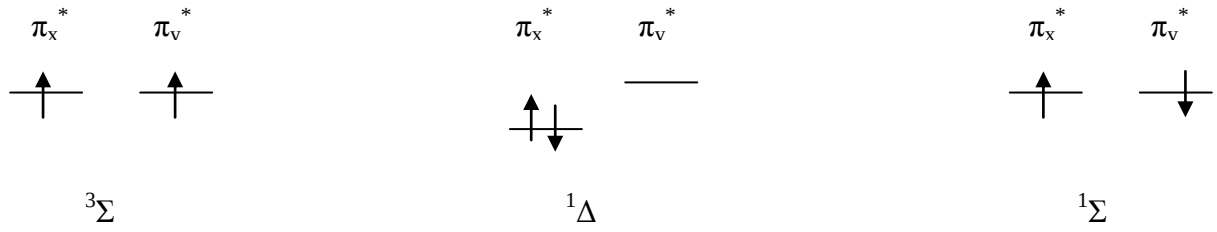

Figure 6: The two electrons of highest energy (π_x* and π_y*) in ground state oxygen occupy one orbital and are unpaired ($^3\Sigma$). In the excited state energy state they are either in the same orbital and paired ($^1\Delta$) or paired and in different orbitals ($^1\Sigma$) and it is the $^1\Delta$ state that is the longest lived, and therefore most commonly referred to as singlet oxygen ($^1O_2$).

The $^1\Sigma$ energy state has a very short lifetime ($<10^{-11}$ s) and when formed is quickly quenched to the $^1\Delta$ state in aqueous solutions.[35] The $^1\Delta$ energy state is thus the predominant species in the photochemical reaction involved in PDT and chemical reactions, and is the state referred to as singlet oxygen ($^1O_2$) in the rest of this report. $^1O_2$ has a very limited lifetime; in organic solvents it is in the range 10-100 μs, however in water it is reduced to just 2 μs, due to the similarity between the energies of the excited state oxygen and the O-H stretching frequency.[36] So, in organic solvents $^1O_2$ can have an effective spherical volume of activity of about 10 nm diameter. For a more in depth review on singlet oxygen and its uses see Schweitzer and Schmidt[37]

1.2.3. Photodynamic therapy

PDT is the use of a photosensitiser, which accumulates in the tumour of the patient, and is then irradiated with light *in situ*, to produce toxic $^1O_2$ killing the tumour cells and initiating tumour regression. A tumour is a solid mass of cells that are no longer under normal physiological controls, and can be cancerous or non-cancerous. Current PDT protocols target only solid tumours, they involve injecting the patient with a formulation of the photosensitiser; the patient is then left for 24-48 hours to enable the photosensitiser to accumulate in the tumour. The tumour is finally irradiated with light to activate the

photosensitiser and create $^1O_2$. Due to endogenous chromophores present in mammalian tissue and light scattering, only light of wavelength 600-800 nm will penetrate effectively through the tissue, thus the photosensitiser needs to have a significant absorption in that region. This is one of a number of properties that make a photosensitiser suitable for use in PDT.[38] Thus molecules should have:

1. Chemical purity,
2. High quantum yield of singlet oxygen production,
3. Absorption in the long wavelength region (600-800 nm),
4. Preferential tumour localisation,
5. Minimal dark toxicity (toxic in the absence of light) and delayed phototoxicity,
6. Stability and be easily dissolved in injectable solvents (formulation).

Photofrin™ is a clinical PDT agent; however, it does not fulfil many of these properties. Aside from the fact that it is a mixture of many different components, Photofrin™ has a low molar extinction coefficient of 1170 M^{-1} cm^{-1} and only absorbs at 630 nm meaning that a high concentration of both photosensitiser and light are required for the treatment. It does have reasonable preference for tumour localisation, although the drug still accumulates in non-cancerous tissues meaning that the patient is required to stay out of sunlight for 4 weeks after the treatment.[11] Despite these disadvantages it is still considered the "gold standard" for new PDT agents, especially for solid cancers and other skin tumours.[11] According to Shuitmaker *et al.* in 1996 Photofrin™ was mainly used in superficial bladder cancer, lung cancer, malignant and non-malignant skin diseases and upper aerodigestive tract.[39] Photofrin™ thus has a wide scope and still remains one of a very small number of PDT agents that are clinically approved.[11]

The Type II photoreaction and production of $^1O_2$ considered to be the dominant cause of cell death in PDT requires a supply of oxygen. In order to maintain enough oxygen within the tumour site for the Type II photoreaction to be effective it is important to manage the light dose carefully. The light dose within PDT is known as the fluence (J cm^{-2}), and when this is considered with the time taken for the dose to be delivered it is referred to as the fluence rate (W cm^{-2}). In order to ensure an effective PDT treatment it is important to have a low fluence rate, this ensures that the oxygen present in the vasculature and the tissues is not exhausted too quickly. Therefore, for *in vivo* PDT it is necessary to control the concentration of the photosensitiser and the fluence rate, in order to ensure the optimal amount of $^1O_2$ is produced and as much of the tumour is treated as possible.[40] Further considerations of PDT are discussed in section 1.7 in relation to its use for the production of personalised vaccines.

1.3. Principles associated with chemical applications

There are a several types of reactions that utilise singlet oxygen. The most common of these is the ene reaction which results in an endoperoxide and a shift of the double bond and, [2+2] and [4+2] reactions which involve the addition of dioxygen to an alkene group. Alkenes are electron rich and attract the electrophilic singlet oxygen in a suprafacial reaction.[41] Heteroatom oxidations are of a similar nature, the heteroatom contains an electron pair attracting singlet oxygen. Nitrogen, phosphorous, sulphur and selenium are all known to react readily with singlet oxygen, also certain transition metal complexes such as iridium or rhodium.[42] Another significant area of singlet oxygen chemistry involves heterocyclic oxidations; furans and benzofurans make up a high percentage of these reactions. Heterocyclic compounds are commonly found in biological substrates, and are often used for detecting the presence of singlet oxygen. The reaction of pyrroles and indoles with singlet oxygen could be used to model the oxidation of molecules such as tryptophan which are biologically significant. Photo-oxidation of oxazoles enables the production of a number of compounds including triamides and spiro-hydroperoxy lactones. Other heterocyclic compounds that are capable of reacting with singlet oxygen are thiophenes, thiazoles and imidazoles, however, they are less useful in synthetic applications.[42] Examples of some of these reactions are shown in Scheme 1.

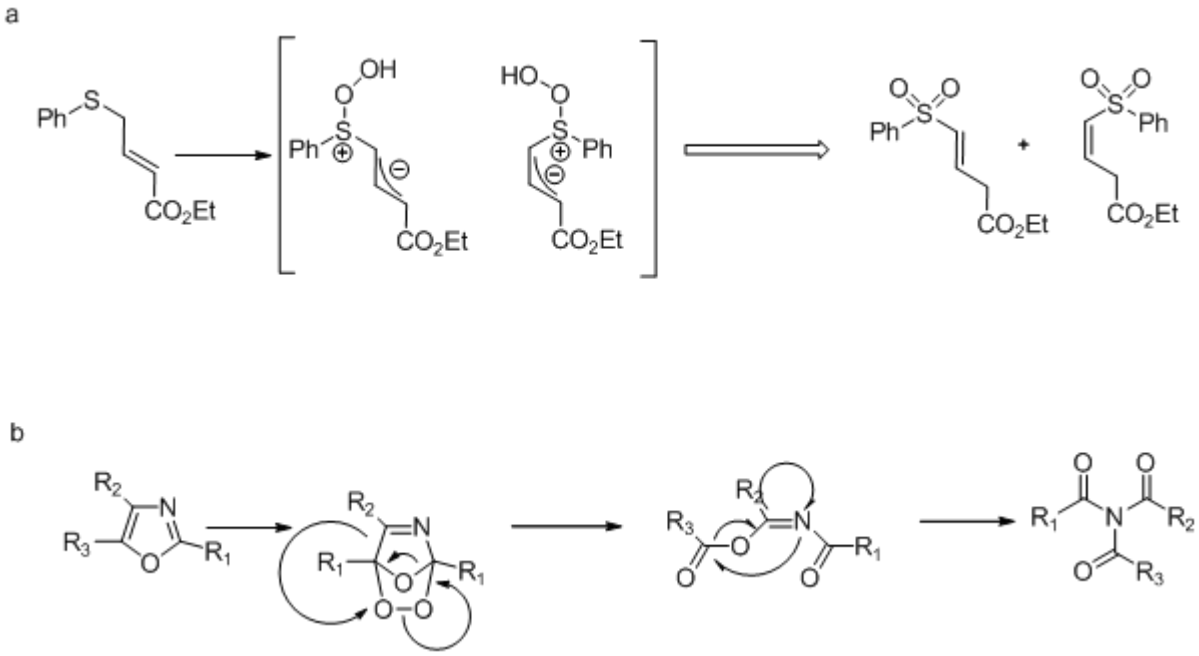

Scheme 1: Example of some oxidation reactions; a) an heteroatom oxidation with sulphur as the heteroatom and b) an oxazole oxidation to yield the triamide[42]

The use of singlet oxygen in chemical synthesis is widespread and of use in the development of many drug compounds.[43, 44] It is also useful in studying the possible effect of singlet oxygen damage to biologically important compounds, which also helps in the development of future phototherapeutic agents.[45, 46] So although the primary interest is in the development of a personalised cancer vaccine, it is possible that further possibilities would be to use the system in drug development, by making photo-oxidation steps easier and more efficiently managed.

1.4. Principles of microfluidic applications

Microfluidics concerns fluid handling in channels in the μm scale and is used to manipulate small volumes (μL, nL, pL or fL), for analysis and reactions. The potential applications of microfluidics ranges from microelectronics through chemical reactions and analysis to biodefence and molecular biology.[47] The areas that are of interest relating to this work are primarily molecular biology involving cell manipulation and chemical reactions, especially those related to singlet oxygen. Therefore, these aspects are reviewed below and are split into the biological and chemical applications.

1.4.1. Biological applications

Molecular biology within microfluidic devices is of particular interest in research covering a wide range of applications such as sequencing, separation and analysis of proteins and DNA, polymerase chain reaction (PCR) techniques, manipulation and culture of cells, on-line diagnostics and immunoassays.[48] A benefit of conducting biological assays and analysis on chip is the possibility to make microfluidic devices mimic the presentation of cues found in the body. Conventional laboratory procedures for investigating cells under culture *in vitro*, take place in 2D environments, usually on plastic surfaces. Therefore the ability to mimic conditions in 3D environments within microchannels enables a more effective method of controlling and monitoring cells *in vitro*. This capacity to control cells has led to a large number of chip-based devices being designed for work from cell culture to cell sorting and biochemical analysis (Figure 7).[49] It is also possible that it will lead to fast and efficient methods for screening new drugs, by mimicking bodily functions and reaction to new drugs by creating and supporting artificial tissue systems.

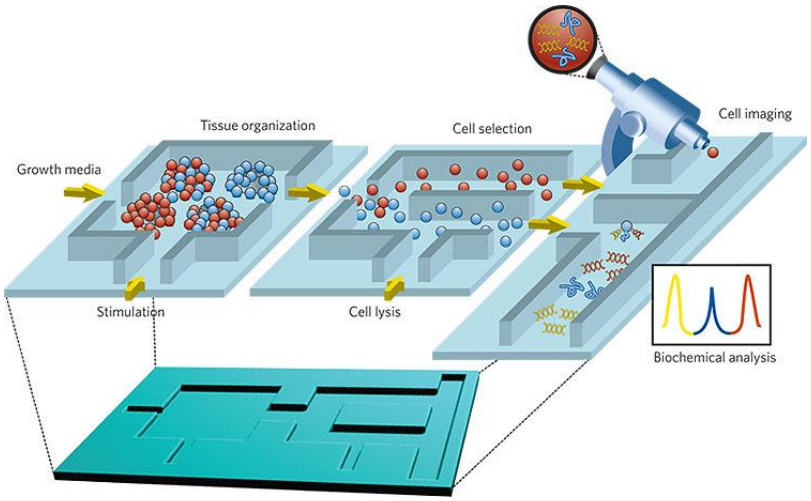

Figure 7: Vision of tissue organisation allowing for growth and stimulation of tissue, culture and enabling selection of lysis and analysis including staining and imaging in microsystems from El-Ali *et al.*[49]

The use of microdevices for medical applications is not without its difficulties; the adherence of certain cell types to surfaces creates a bigger challenge in microfluidics than it does in larger scale laboratory equipment due to a higher ratio per unit volume of surfaces.[49] An example of this effect is PCR, which is conventionally undertaken in a reaction tube in which the surface to volume (S/V) ratio is approximately 1.5 mm^2 μL^{-1}. This ratio will increase ~5 fold for a capillary tube (20-100 µL), and ~13 fold for a typical microchannel of a microfluidic device.[50] Increasing the surface area available for attachment can therefore create unwanted side-effects. However, by coating the microchannel surfaces it is possible to minimise any unwanted reactions. The purpose of surface modification is to change the surface charge of the microchannel wall, making them more or less hydrophilic, as necessary. For the project described herein, surface modification is very important, as it provides a basis for immobilising photosensitiser onto the glass surface in the microchannel.

1.4.2. Chemical applications

Along with the biological applications, there are a large number of chemical reactions that can be conducted in microchips.[51] Small quantities of reagents and waste make the use of

microfluidics more economical for chemical reactions, in addition heating and cooling of liquids within the small channels, through the absorption and dissipation of heat becomes more efficient. For highly exothermic reactions, conducting them within a microfluidic device is much safer as it reduces the total volume reacting at any one time, and allows for the dispersion of heat from the reactor due to large S/V ratio and good heat conduction of chip material.[52]

The use of microreactors in photochemical reactions has been reviewed by Coyle and Oelgemöller,[53] in which they comment on the benefits of microfluidics for photochemistry. Due to the small depth of the microreactor (<1000 μm) it is possible to irradiate the whole sample efficiently. The ability to perform continuous flow photochemistry and instantly change conditions such as irradiation time by adjusting the flow rate enables optimisation of reactions. As mentioned above the ability to transfer heat effectively allows for rapid cooling, which is specifically useful for strong light sources. In order to reduce heat accumulation it is possible to utilise smaller less powerful light sources, such as light-emitting diodes (LEDs) as there are less reactants to irradiate, making it more energy efficient.[54] Finally, by designing the microfluidic device, it is possible to introduce a number of other features such as on-line monitoring of the reaction, or additional flow/waste streams.[55] Also the reduced volume of solvents and oxygenated solvents, which are highly flammable, is an added safety advantage.[26] "Micro-photochemistry" is, therefore, a particularly efficient means of performing photochemistry, and removes many of the inherent dangers and problems associated with macroscale reactions. This will be reviewed in more detail in section 1.6.3.

1.5. Functionalisation of glass surfaces

There are two main purposes for the functionalisation of glass and other glass-like substrates such as silica gel and silica particles. The first is merely to change the inherent charge associated with the bare glass, the second is in order to attach further moieties onto the glass, such as biological entities, molecular catalysts and sensing molecules. Herein a description is given of the various approaches to the silanisation of glass and other glass-like substrates through organic-, aqueous-, or vapour-phase deposition. In order to focus the review only those working with (3-aminopropyl)-triethoxysilane (APTES) and a small number of other amino functionalised agents have been selected as these relate more specifically to the work conducted herein. Other silanising agents are available and there is much literature associated to them, the most common one being octadecyltrichlorosilane (OTS).[56] The general schematic of a silanisation reaction is shown in scheme 2 (section 1.5.1). Also the focus has been on the use of glass, or silica substrates, as again this relates directly to the intention of the work conducted.

Finally, current work in functionalising glass substrates for both chemical and biological applications will be considered. This will be a very general review as there is a large amount of literature available, and it is not all directly relevant to the work conducted. In section 1.6.2 a more specific review into photosensitiser-functionalised substrates for photooxidation reactions will be given which will be more significant to the work conducted in this thesis.

1.5.1. Silanisation

The silanisation of glass surfaces is part of a larger field of research into self-assembled monolayers (SAMs). Although silanisation using APTES does not always results in a monolayer on the surface of the substrate, many of the principles of formation are very similar to those of the SAM. The review by Ulman[56] goes into great detail of the many

varied type of SAMs including fatty acid monolayers, semiconductor surfaces, alkanethiolates of gold in addition to monolayers of organosilicon derivatives which include APTES layers on glass and silica substrates. It is interesting to note from this review that the use of SAMs started as early as 1946 by Zisman[57] adsorbing a surfactant onto a metal surface in what would later be classed as self-assembly. Since then alkanethiolate monolayers on gold substrates are the most commonly studied,[56] however, there is still a large amount of interest in organosilicon monolayers. These usually consist of alkylchloro- or alkylalkoxysilanes with either alkyl chains or ω-functionalised alkyl chains which impart the functionality onto the substrate, and the silane which is used in the production of a covalent bond with the substrate. Due to the strength of the Si-O bond, these monolayers are most stable when utilising hydroxylated or oxidised substrate surfaces.[56] Glass is comprised of silicon oxide bonds, and the glass surface consists of hydroxyl groups, making them ideal for the formation of these Si-O bonds with the silanising agent. Other surfaces are used, such as metal and silicon; however these need to be oxidated prior to the silanising reaction being performed.

Two reviews by Ishida *et al.*[58, 59] in the late 1970s and early 1980s go into detail of the various theories that had been presented in the early years of amino-silanisation. They proposed that when the silanes are in water they form 5- or 6-membered rings with interaction of either the nitrogen directly with the siloxane or a zwitterionic form in which the protonated amine is interacting with an unreacted silanol respectively (Figure 8). They also include in the later review details of the work by Chiang *et al.*[60, 61] in which they agree that the aminopropyl group bends to create a six-membered ring with a hydroxylated ethoxy group.

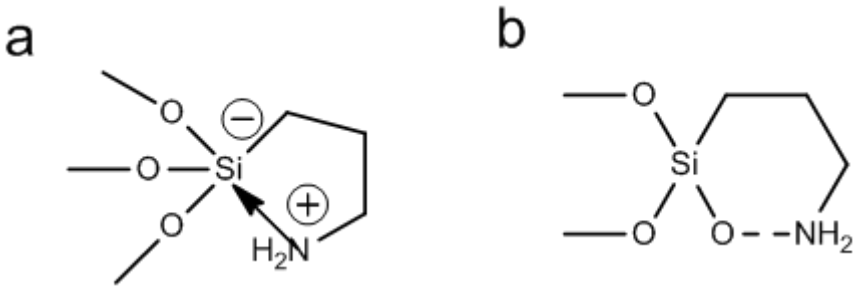

Figure 8: a) the 5-membered ring formation with a co-ordinate bond between the amino group and the silicon and b) the 6-membered ring formation with hydrogen bonding between the amino group and an hydroxyl group on the silicon suggested in the review by Ishida *et al.*[58, 59]

At the point of the final review in 1984 they conclude, in respect to aminosilane interactions, that they are incredibly complex, especially in the uncured form, and this has led to documents of many various hypotheses on the structures. Caravajal *et al.*[62] sum up these various hypotheses shown in Figure 9

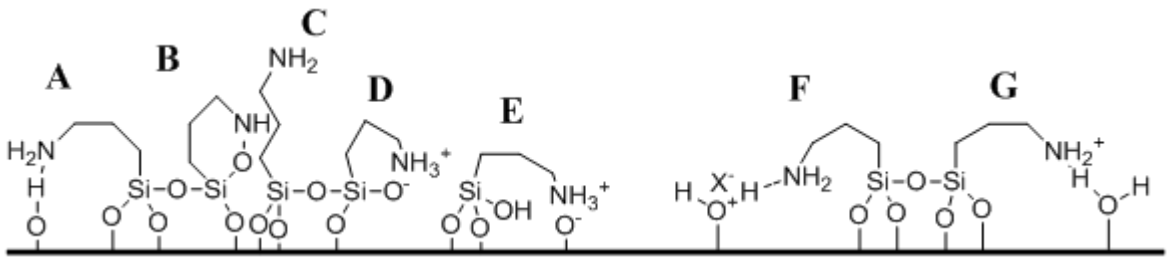

Figure 9: Possible structures anticipated from the reaction of APTES with glass surface, showing various forms of ionic bonding (D-G) and hydrogen bonding (A and B) as well as the straight form (C) from Caravajal *et al.*[62]

Throughout the decades in which SAMs have been investigated there have been a large number of hypotheses regarding these structures and how to control the reactivity of APTES on oxidised silica substrates. In the following review these conditions are investigated in various areas; a) the effect of the reaction solvent and different deposition phases used, b) the effect of curing, c) the remaining reaction conditions (concentration, time and pH) and d) methods for increasing amine reactivity.

Reaction solvent and deposition phase

There are three general procedures used in the literature for silanisation reactions; organic-phase deposition (normally using toluene), aqueous-phase deposition and vapour-phase deposition. In the 1970s a reaction mechanism of silanising agents with silica substrates was suggested by Arkles (Scheme 2).[63]

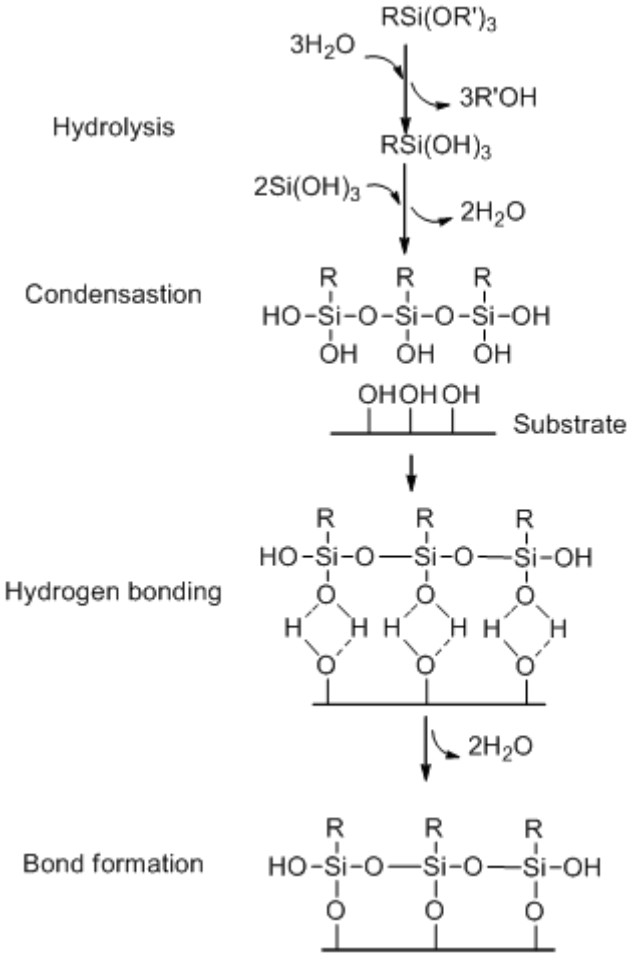

Scheme 2: Theoretical mechanism for the deposition of silanes on to oxygenated silica surfaces proposed by Arkles.[63]

Arkles stated the need for water to be present in order for this process to be possible, either added to the solvent, present on the substrate surface or from the surrounding atmosphere. This suggested that organic-phase deposition was preferred, but with the addition of water to enable the reaction to proceed. It was also made clear that an increase in the water content

would increase the degree of polymerisation of the silane which could potentially decrease the formation of bonds with the substrate.

This is a concept that has been corroborated by other groups through experimental evidence. Caravajal *et al.*[62] in the late 1980s agreed that the presence of water in the reaction would increase the number of siloxane bonds with the surface, however, an aqueous environment would reduce this number significantly. This is explained by Vandenberg *et al.*[64] and Chu *et al.*[65] as being due to organic solvents facilitating the formation of a covalent monolayer or surface anchored groups, whereas, aqueous solvents favour electrostatic interactions of the silanising agent with the substrate. This would suggest that an aqueous solvent stabilises the hydrogen bonding seen in Arkles mechanism (Scheme 2) but is unable to undergo bond formation.

As more advanced techniques of investigating the surface structures of ATPES were used these theories have been proven. Kim *et al.*[66] have shown through Fourier-transform infrared spectroscopy (FTIR) and ellipsometry that APTES layers, formed in the organic phase, initially covalently bound with the surface to form a monolayer, and after further time can form multilayers *via* covalent and electrostatic interactions with the initial layer. However, they show that in aqueous phase deposition, the depth of the layers stays the same over extended periods of reaction. APTES is shown to be adsorbed on to the substrate surface largely through electrostatic interactions of the protonated amine with limited covalent bonding. Simon *et al.*[67] examined the surface through atomic force microscopy (AFM) and found that layers deposited from an anhydrous organic phase were formed homogeneously and were stable in comparison with those formed through aqueous-phase deposition.

Another method which has been used for the deposition of APTES layers is through the vapour-phase. This involves pulling the vapours of the reaction mixture over the substrate surface. As early as 1978 the idea of conducting this reaction with vapours was tried by Haller[68] and was found to remove the haze that can form on substrates with the previously mentioned methods. He also found that this method yielded a monolayer on the substrate surface with the removal of "polymeric globules" which can be formed from aqueous- or organic-phase deposition. Haller also used the layer to perform further reactions at the surface, showing that the amino groups were reactive in a similar manner to free primary amines. Much later, in 1995, Wilson and Schiffrin[69] also used vapour-phase deposition, comparing it to organic-phase deposition by the reactivity of the resultant amines on the surface. The reaction of fluorescamine (**5**) with primary amines yields a fluorescent configuration that could be quantified with a fluorimeter (λ_{ex} = 396 nm) (Scheme 3). They conducted the reaction by introducing the reagents between the silanised slide and a clean slide by capillarity, this would not be possible on-chip, although the reaction may still occur by flowing the reagents through the chip. Fluorimetry would not be possible on-chip, but it may be possible under the fluorescence microscope.

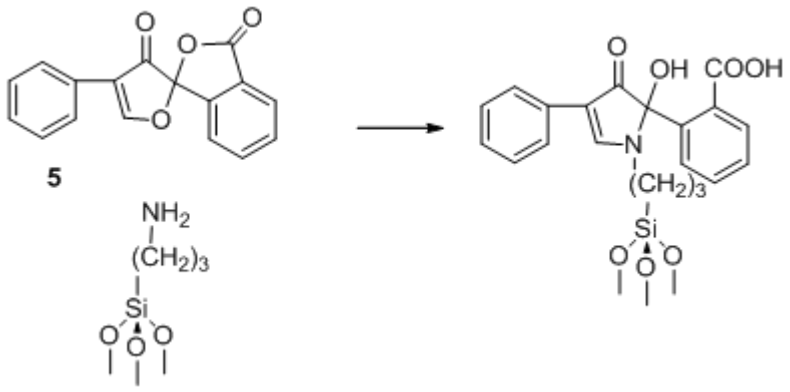

Scheme 3: Reaction of fluorescamine (5) with the primary amine of the substrate-bound APTES by Wilson and Schiffrin.[69]

In this report they found no difference in amine reactivity between organic- and vapour-phase depositions. Wang and Vaughn[70] in 2008, however, found that using vapour-phase deposition gave more available amines for reacting, whereas using toluene resulted in an inert surface. This seems to be in complete disagreement with the majority of the work conducted on silanising substrates using APTES. In most work, the use of toluene for organic-phase deposition has been preferred,[69-79] and results in varying degrees of mono- or multilayers, which are capable of reacting further with amine reactive moieties. Although the use of vapour-phase deposition, overall, could be advantageous, in light of the findings by Wilson and Schiffrin, the improvement may not be as significant as proposed by Wang and Vaughn.

Reaction conditions

There are many other experimental parameters that have been shown to effect the resultant layers, including concentration, reaction time, temperature and pH. In a comprehensive examination of many of these aspects Howarter and Youndblood[72] found that reaction time determined the film thickness and that concentration and temperature influenced the roughness of the film, with reaction time having a limited effect on this aspect. In general they found that the longer the reaction was allowed to proceed; the thicker the resultant layer (Figure 10). This is in agreement with Kim *et al.*[66] who determined that in an organic phase the layers of APTES grew over time due to both covalent and electrostatic interactions.

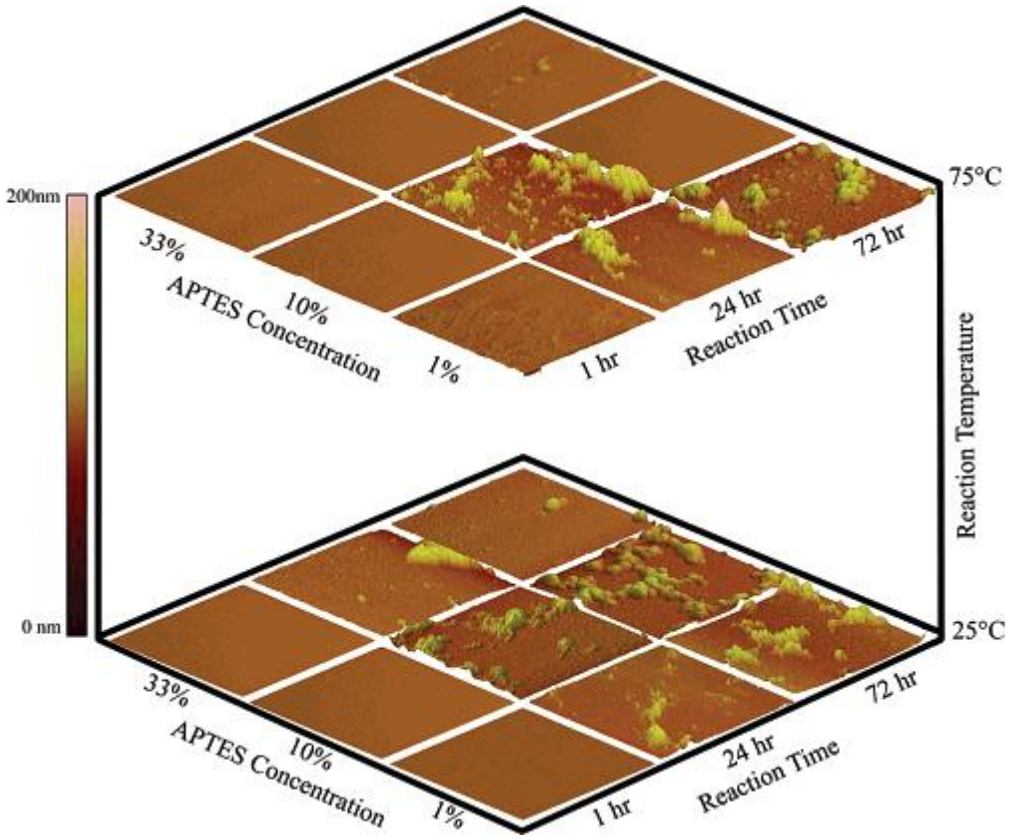

Figure 10: Figure from Howarter and Youngblood showing the effect of reaction time, concentration and temperature on the surface roughness and thickness of APTES layers on silica surfaces.[72]

The concentration of APTES was also suggested to determine film thickness by Arkles.[63] Whereas, two decades later Okabayashi *et al.*[80] were looking more closely at the effect that concentration had on the structure of the film. Using toluene in an organic-phase deposition they determined that low concentrations of APTES (0.08 mol L^{-1} or 1.9 % v/v) yielded cyclic structures involving the protonated amine form (NH_3^+), whereas higher concentrations (0.72 mol L^{-1} or 16.8 % v/v) yielded more accessible amines in the NH_2 form. Most groups seem to favour either low concentrations of approximately 1%[71] or slightly higher concentrations of 5%,[81] however, there are few uses of a concentration as high as 17% as seen here from Okabayashi *et al*.

The last of the reactions conditions is the pH of the reaction mixture, which can relate to both organic and aqueous phase deposition. As early as 1972 Bascom[82] suggested that the reaction was autocatalytic, meaning that the amino group at the end of the propyl chain aids in the reaction of the silane group with the surface hydroxyl groups. This was corroborated by Naviroj *et al.*[83] who determined that this related to a basic solution with a pH of 10.6. They also suggested that making the solution more basic was not advantageous to the reaction. However, Kallury *et al.*[73, 84] determined that the reaction was improved with the addition of base. They suggested that base could increase the amine reactivity by orienting the amine groups away from the substrate surface.

Curing

Another important experimental parameter that can be altered in this reaction is the curing step. This is thought to polymerise the surface silanol groups, making the structure more stable and relates to the bond formation step in scheme 2. However, opinions differ on the extent of curing that is required. Arkles[63] comments on the need for curing in order to form covalent bonds as opposed to adsorption *via* electrostatic interactions, which is also stated by Chiang *et al.*[61] Waddell *et al.*[85] cured their substrate at 80 °C for 3 h and found that the high temperature and time was necessary for stable layers. Caravajal *et al.*[62] concluded that curing at high temperatures was required in order to be effective, however, this was from a comparison of room temperature over 150 °C only. An alternative view by Petri *et al.*[86] was that their method of dip coating in a 1% solution in toluene at 60 °C for 4 min required no curing and so reduced time in the reaction. However, Vandenburg *et al.*[64] and Kim *et al.*[87] also agree that high temperature curing is necessary to produce siloxane bonds at the surface, and to increase the stability of the layer for further amine reactivity. Overall, it seems that the curing step is important for the stability of the covalent bond between the substrate and the

silanising agent, and a curing step was used in this project also. The papers discussed here imply that curing above room temperature from 80-160 °C would be sufficient.

Amino reactivity

This project involves immobilising molecules onto the glass surface through reactions with the amino groups resulting from the silanisation reactions. Therefore, it is of great importance that the amino groups are available for further reactions to take place. Introducing further functionality to silica surfaces will be reviewed later (section 1.5.2), in this section the methods used for determining the availability of those amino groups will be considered. Although APTES is the most widely used silanising agent for imparting amino functionality to a silica substrate, there are also structural variations of APTES that could increase the amine density. The use of fewer alkoxy groups for bonding to the substrate surface is one such alteration. Waddell *et al.*[85] were the first group to look into the use of agents with zero, one or two methyl groups replacing the ethoxy groups in APTES to enhance the stability of the bond. They investigated the amine reactivity through reaction of the surface amines to a Schiffs base with salicylaldehyde and examining the remaining reaction through absorption spectrometry. They discerned that APTES and its analogue with one methyl group ((3-aminopropyl) methyldiethoxysilane) gave similar stabilities; however the effect of two methyl groups ((3-aminopropyl) dimethylethoxysilane) was to reduce the amino-reactivity as it was held at the surface with only one covalent bond which reduced the stability considerably (Figure 11). Moon *et al.*[88] looked at the same aspects and discerned that one methyl group increased stability even over APTES and gave the best stability. They determined the amine reactivity through a reaction with 4-nitrobenzaldehyde to yield an imine on the surface that could be quantified through UV-vis spectrometry. However, the

continued use of APTES over other amino-functionalised silanising agent suggests that the improvement was minimal.

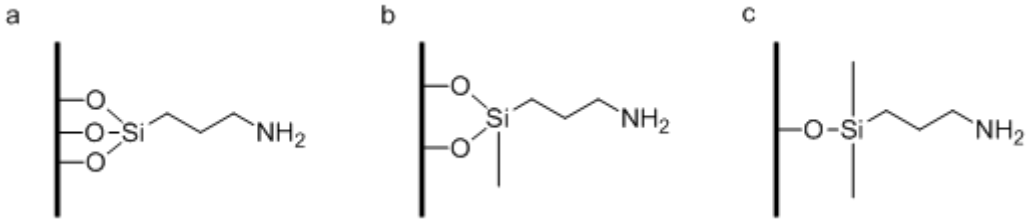

Figure 11: Bonding of silanising agents with one (c), two (b) and three (a) ethoxy groups showing potential stability issues.[85]

Other amino-functionalised silanising agents include those with long alkyl chains, for example those investigated by Bierbaum *et al.*[89] They found, through x-ray photoelectron spectroscopy (XPS) that while short chain films, such as APTES, had little defined organisation, those with longer chains (17 carbons) were completely disordered. This suggests that the use of long chains would not improve the amino reactivity, and short chains are superior. Zhang and Srinivasan[78] investigated the difference between alkyl and aryl linkers between the silane and the amino group through XPS. They found that the amine content of the silica after silanising with aminophenyl triethoxysilane (APhS) was 100% in comparison to 88.6% with (3-aminopropyl) trimethoxysilane (APTMS). They concluded that the phenyl linker group imparts a greater rigidity to the structure preventing the interaction of the amine group with the surface. Metwalli *et al.*[90] used silanising agents with additional amino groups in the chain, such as *N*-(2-aminoethyl)-3-aminopropyl trimethoxysilane (**7**) and (3-triethoxysilylpropyl)-diethylenetriamine (**8**) (Figure 12). They found, again through XPS, that the additional chain length, interspersed with amine groups increased the number of surface groups available for further reactions.

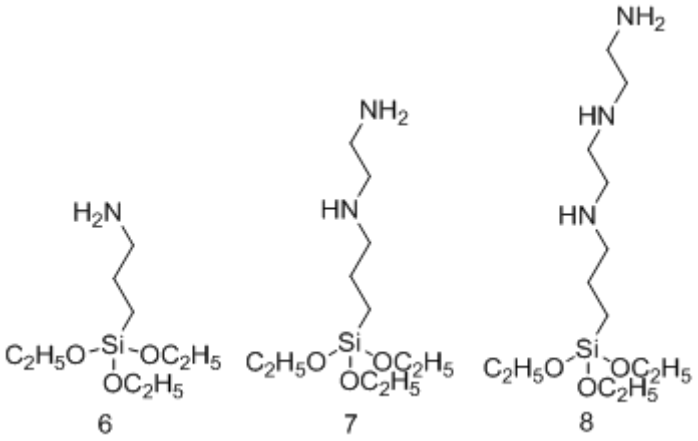

Figure 12: Extended chain lengths with additional amino groups (APTES (6), *N*-(2-aminoethyl)-3-aminopropyltrimethoxysilane (7) and (3-trimethoxysilylpropyl)diethylenetriamine(8)) used by Metwalli *et al.*[90]

Many of these different silanising agents are used in the hope of reducing the interaction of the amino group with the substrate surface. Kamisetty *et al.*[74] attempted to do this in a slightly different way by adding a further silanising agent which consisted of an alkyl chain (butyltrimethoxysilane). The intention was that this silanising agent would react with the remaining hydroxyl groups on the surface of the silica, protecting them from interaction with the amino groups. They claimed that this method also increased the amine reactivity of the silica and quantified it through reaction of the surface amines with the N-hydrosuccinimide ester of Cy3 dye.

On-chip silanisation

The silanisation of glass microfluidic devices is utilised for a variety of reasons and is now common practice. This procedure is often employed for altering the surface characteristics of the glass to avoid undesired effects of the high S/V ratio. It improves handling of biological solutions which often interact unfavourably with the bare glass surface. The use of silanisation for further immobilisation of chemical and biological moieties will be looked at in section 1.5.2. Although silanisation within microfluidic devices is used in many

applications there are not many papers dealing solely with the methodology. Wootton and deMello[91] looked at derivatising glass channels with a copolymer solution that polymerised in a warm environment, whereas Fracassi Da Silva *et al.*[92] used *N*-(2-aminoethyl)-3-aminopropyl triethoxysilane to functionalise glass substrates for the retention of copper (II) ions. In addition to this, there were also two groups that looked at functionalising polydimethylsiloxane (PDMS) microdevices with amino groups. This is more complex than for glass devices as PDMS does not have a natural hydroxyl or oxide layer for a silanisation reaction to occur. Wang *et al.*[93] in 2003 used ozone, produced by a Tesla coil, to oxidise the PDMS surface followed by silanisiation with APTES in toluene before the two plates were bonded. They found that the use of toluene for this reaction had a tendency to make the PDMS swell during the reaction; however, it retained its shape after drying. Sui *et al.*[94] also functionalised PDMS microdevices, however, they performed the reactions *in situ* after the bonding had occurred. To do this, they used H_2O_2 to oxidise the surface followed by a reaction with neat APTES to introduce the amino functionality. This work suggests that the silanisation of microreactors is relatively facile compared to the silanisation of silica gels and glass slides due to the confined environment that it contains. Most of these reactions took place in 30 min and the reactivity of the amino groups was good.

To summarise the findings, organic-phase deposition, with a moderate concentration (1-10 %) and higher temperatures (up to 160 °C) is advantageous for this reaction. Adding a curing step after the reaction can improve the amino reactivity by forming covalent bonds at the surface and reducing the amount of interaction of the amino group with the surface. Finally there are a number of similar silanising agents that have been shown to improve the amine reactivity along with the potential for adding inactive silanising agents to cap the remaining surface hydroxyls.

1.5.2. Immobilisation of further moieties onto amino-functionalised glass

In this section a brief indication of the various uses of amino-functionalised glass will be given. As with the project, this is broken down into biological and chemical applications; the biological applications will be introduced first, followed by a general review of the chemical applications. A more in-depth look at the use of photoactive moieties immobilised on silanised substrates will be presented. Finally there will be a brief review of some of the uses of these immobilised moieties on-chip, showing the progress made thus far.

Biological Applications

There are a large number of biological components that react with amino groups to form a covalent bond. DNA is one of these components, and has been immobilised on amino-functionalised glass by a number of research groups in order to perform *in situ* hybridisation.[95-103] Other groups have immobilised DNA to PDMS substrates through oxidation of the surface with oxygen plasma before the silanisation reaction.[104] Vaidya and Norton[104] also looked at a different attachment mechanism by introducing a maleimide group on the surface and reacting this with a thiol group on DNA to form a thioether bond. Another interest with DNA is the binding force and elasticity; Nguyen *et al.*[105, 106] investigated this by immobilising DNA on to the aminated glass surface, and using atomic force microscopy (AFM) with a biotin-functionalised tip and measuring force versus displacement.

Immunological assays using protein and peptides (made up of chains of amino acids) often require a large amount of washing and reaction steps. Therefore, many groups have immobilised them onto aminated glass surfaces to speed up the analysis, by improving the washing steps.[81, 107-117] Heise *et al.*[118] used this method with silicon wafers and were able to improve the density of surface amines by using a bromo-terminated long chain silanising

agent which was less likely to react with the surface hydroxyls. They then modified the bromo group to an amine (Scheme 4) to which they then bound a polypeptide on the surface in an α-helical comformation.

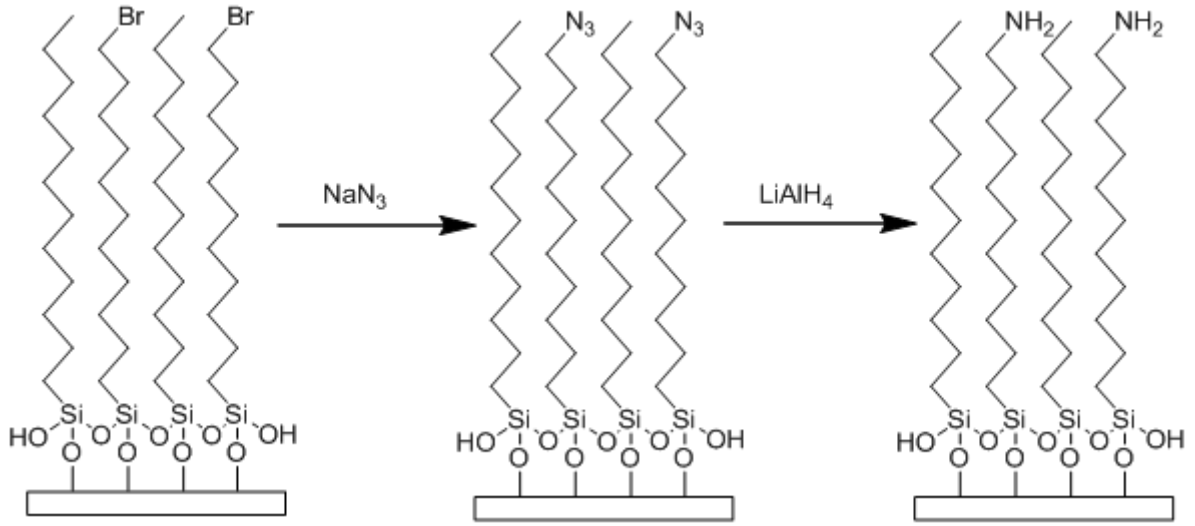

Scheme 4: Synthetic steps used by Heise *et al.* to yield long chain amino-functionalisation from bromo-functionalised silanising agents.[118]

Zhu *et al.*[119] used gold nanoparticles (AuNPs) immobilised on an aminated glass surface to investigate the reaction between them and a protein. Label-free detection of the proteins in bulk suspensions could be achieved by localised surface plasmon resonance (LSPR) of the surface and detection of the difference between AuNPs and those with the protein bound.

The attachment of certain enzymes on the surfaces of amino-functionalised substrates has also been achieved. Arya *et al.*[120] immobilised cholesterol oxidase onto indium-tin oxide (ITO) coated glass slides functionalised with *N*-(2-aminoethyl)-3-aminopropyl triethoxysilane. This could be used to measure cholesterol in solution in the form of a "bioelectrode". Tang *et al.*[121] attached laccase and horseradish peroxidase to an APTES-functionalised ITO electrode with the aim of detecting *Escherichia coli* density in a rapid

method. These examples show the use of biological moieties for detection in a much faster manner than previously realised.

Other biological applications for surface functionalisation are also utilised. For instance Webb *et al.*[122, 123] fabricated a number of functional groups at the glass surface through chemical modification of amine groups to discern the effect on cell attachment, spreading and cytoskeletal organisation. Liu *et al.*[124] investigated glass slides functionalised with a number of different polymer groups as well as APTES to determine the effect of surface roughness on the nucleation of a lysozome on the surface.

Chemical applications

Chemical reactions on solid phases are similar to those in solution, but the kinetics are often different due to fewer collisions. Silanising agents are available with a variety of functional groups, however, especially with long chains, conformational changes can occur. Therefore, it can be advantageous to start with an agent in which the effect of the functional group is known and use chemical reactions to yield the desired functionality. Balachander and Sukenik[125] used hexadecaalkyl chains with bromo-, cyano-, thiocyano- and thioacetate functionality. To the SiO_2 particles with these groups attached, they then conducted chemical modifications to yield an array of different functional groups (Scheme 5).

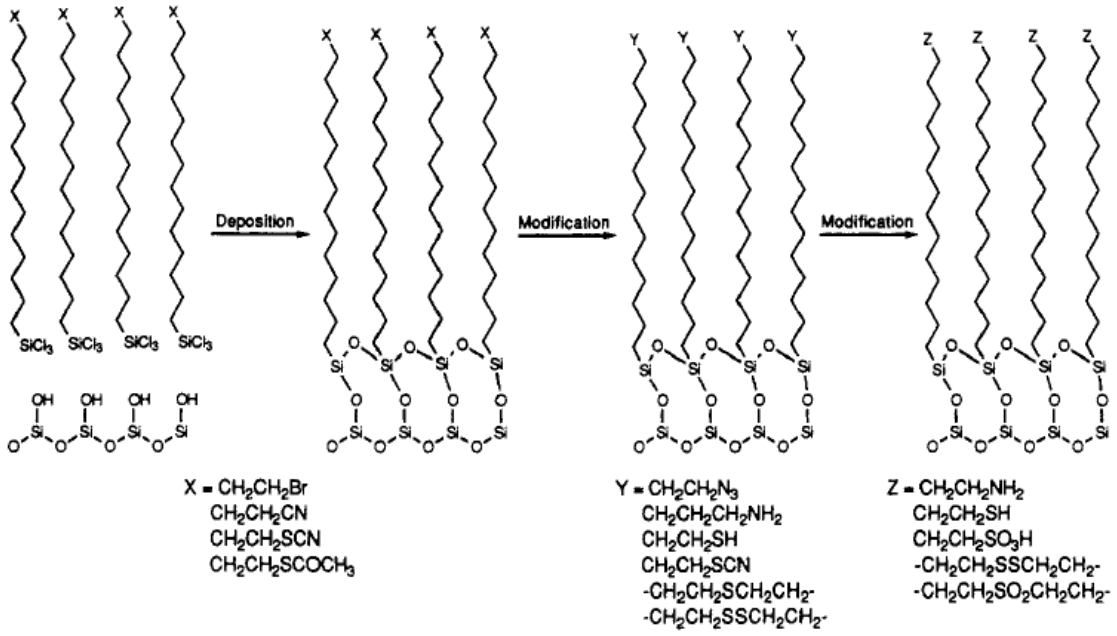

Scheme 5: Deposition (X-functional groups) of silanising agent and subsequent transformations (Y and Z-functional groups) as used by Balachander and Sukenik.[125]

These reactions show that the availability of functional groups on the surface is not limited to silanising agents that can be purchased. Indeed the popular Click reaction has been performed on glass substrates[126] through modification of a bromo-silanising agent to an azide. Click reactions are quick and reliable mechanisms that are designed to mimic nature; the reaction between an azide and an alkyne is known as Huisgen cycloadditions and are catalysed by copper. Also dendrimers have been grown on silica substrates[127] providing an increase in the amine density. Finally a modification of the silanising agent to hydroxyl groups enables the deposition of further layers if this is required.[128]

Manipulation of surface groups enables the introduction of special properties to these silicon substrates for example polymer layers,[129] fluorinated nanodiamonds,[130] and fullerenes.[131] There are also monolayers that impart special applications of the substrate such as ion sensing,[132] reduced wear due to friction,[133] improved conductivity,[134] and molecular probes.[135]

The purpose of this project was to immobilise a photosensitive molecule to the surface in order to produce singlet oxygen for chemical and biological applications. Therefore, the following review will concentrate on the current research into photoactive molecules on solid substrates. There are extensive molecules that are sensitive to light of various wavelengths and for assorted applications; herewith a small number of these are looked at.

Fluorescent molecules are advantageous for binding to substrates, as they allow for quantification or investigation of the silanising step. These molecules include rhodamine B (RhB) thionyl chloride reacting with the amine on APTES-functionalised glass beads,[71] or bacterial light antenna referred to as chlorosomes attached through modification of the APTES-functionalised glass with glutaraldehyde.[136] There are a large number of porphyrin molecules that have been immobilised onto silicon substrates through different attachment methods. Da Cruz *et al.*[137] formed a complex of a metallated (cobalt or zinc) tetraphenylporphyrin (TPP) to the pyridine on 1-((3-triethyoxysilyl)propyl)-3-(pyridine-4-methyl) urea. This was then formed into multilayers of porphyrins with bidentate ligands connecting them (Figure 13).

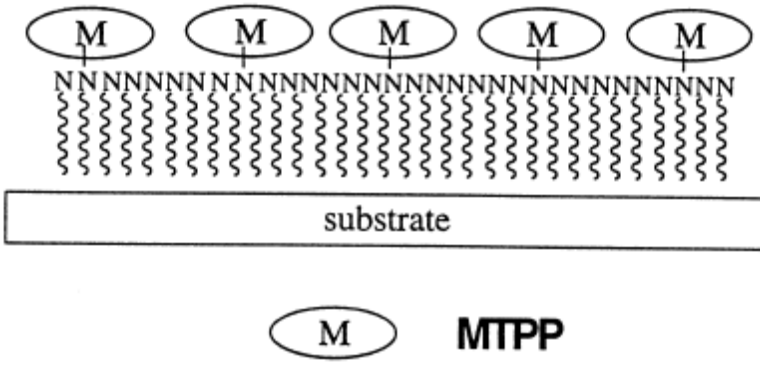

Figure 13: TPP complexed to the substrate surface through the nitrogen of the pyridyl group of the silanising agent.[137]

Zhang *et al.*[138] also formed a porphyrin monolayer through axial ligation of zinc protoporphyrin IX to amino-functionalised glass substrates. Savenije *et al.*[139] looked at the possibility of adsorbing charged porphyrin directly onto glass substrates; they used tetra methylpyridiniumyl porphyrin (TMPyP) either as the free base or metallated with zinc or palladium in a basic solution to achieve a monolayer of porphyrin on the glass. Wienke *et al.*[140] investigated the effect of the number and arrangement of charged side groups on the adsorption of methyl pyridiniumyl porphyrins directly to glass, quartz or silicon substrates.

Although these researchers found that adsorption of these groups on bare glass slides was possible, in the following work, it was shown that this attachment yielded a reduced concentration over covalent bonding of the porphyrin. However, Zhang *et al.*[141] also found that it was possible to adsorb cationic porphyrin and phthalocyanine to anionic pyridine salts on glass and silicon substrates functionalised with APTES, although they did increase the interaction by the introduction of anionic groups. Schick and Sun[142] found that there was little difference between the attachment of tetrakis(4-chlorosulfonylphenyl) porphyrin (TCSPP) to amine-modified and bare silica substrate. They suggested that there was a sulfonamide linkage forming between both the amines when modified and the hydroxyl groups when unmodified. Other research groups using porphyrins include McCallien *et al.*[143] who measured ligand affinity by attaching pentafluorophenyl active ester porphyrin through covalent bonds to the APTES-modified glass and then inserting zinc to the bound porphyrin. The interaction of this bound zinc porphyrin with bidendate ligands was then investigated. Qian *et al*[29] used the Langmuir Blodgett (LB) method to form layers of TPP linked with phenylalanylamino on mica to determine the molecular packing. LB films are another method for producing monolayers. They require the substrate to be accessible for placing the film onto, and therefore, this method is not appropriate for use within microfluidic channels.

Liquid crystals are interesting photoactive molecules, which can change orientation in the presence of light. This is a good example of the ability of molecules to retain photoactive properties on solid substrates. Shashidhar *et al.*[144, 145] and Jain *et al.*[146] looked into the ability of various cinnamoyl derivatives attached to silicon, quartz or ITO to photodimerise for introducing long range order (Scheme 6).

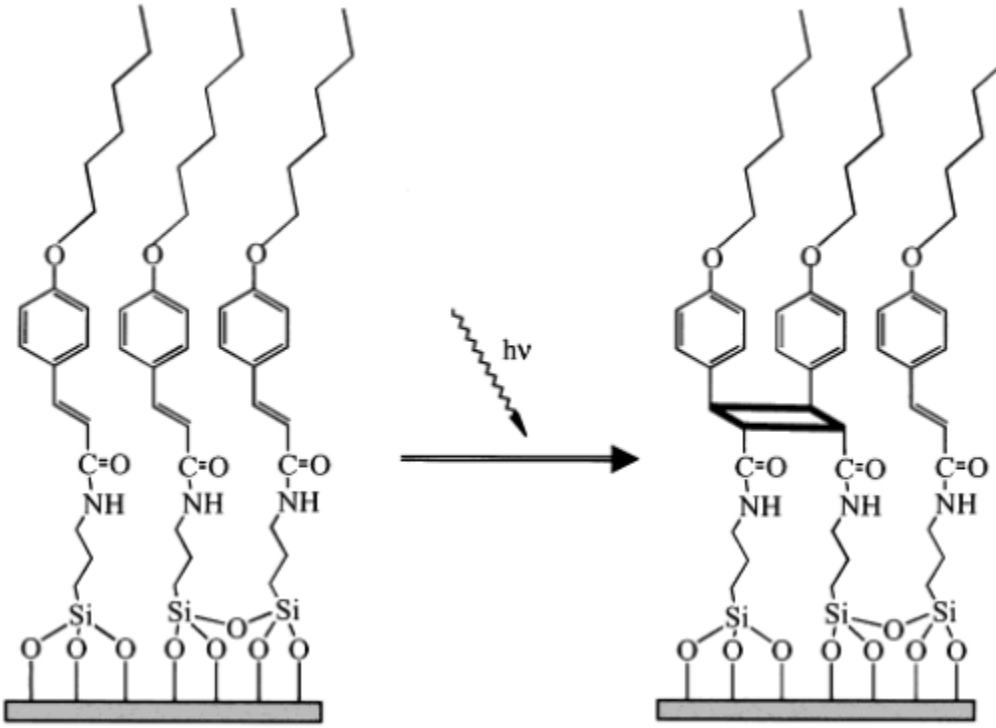

Scheme 6: Photodimerisation of cinnamoyl derivatives from Shashidhar *et al.*[145]

Garcia *et al.*[147, 148] used spiropyran molecules covalently bound to glass surfaces to change the hydrophobic properties of the glass through light. This could enable low volume liquid transport within a microfluidic device or for the attachment and detachment of biological components.

In addition to investigations of monolayers using photoactive molecules as reviewed above, there are other uses for these photoactive molecules. Gas detection, is one of these; as early as 1975 the idea of attaching porphyrin onto surfaces in order to control certain solution

phase characteristics, such as dimerisation, was investigated. Leal *et al.*[28] attached Fe(II) porphyrin to silica gels with a 3-imidizolyl propyl silanising agent, allowing oxygen to be adsorbed by the porphyrin without the hindrance of dimerisation. Then in 1993 Bonnett *et al.*[149] employed the LB method to form multilayers of metallated porphyrin based on *p*-hydroxyphenyl porphyrin on silica gel. They utilised this porphyrin-functionalised silica gel to detect gases such as Cl_2, NO_2, and HCl by comparing absorption maxima before and after exposure. Pilloud *et al.*[150] attached protoporphyrin and hematoporphyrin on to quartz through a thiol-functionalised silanising agent. They used this for measuring interaction between imidazole and carbon monoxide. Most recently Borisov *et al.*[151] covalently attached Pt(II) and Pd(II) tetrakis-(2,3,4,5,6-pentafluorophenyl) porphyrin to silica gel as oxygen sensors.

In a similar manner to the gas sensors, some porphyrin molecules can also be used as ion or pH sensors. Blair *et al.*[152] used an electropolymerisation technique to form a monolayer of the Co(II) complex of *p*-hydroxylphenyl porphyrin on ITO as a pH sensor. Yang and Bachas[153] also used electropolymerisation of Co(II) tetrakis(*o*-aminophenyl)porphyrin onto ITO coated glass slides to provide a nitrile sensor. Liu *et al.*[154] used zinc octakis (β-octyloxyethyl) porphyrin to produce a thin film between layers of ITO or ITO and SiO_2. They found that when the porphyrin was irradiated in the presence of an electric field it was capable of trapping more ions than in the dark. Xiao and Meyerhoff[155] produced amide bonded protoporphyrin on silica gel which they then metallated with zinc, copper, iron, nickel or cadmium for use in ion affinity chromatography. These examples give an idea of the utility of porphyrin films, and show the large number of methods for attaching the porphyrin to silica substrates.

Purposes of immobilisation on-chip

There are many groups investigating immobilisation of chemical or biological moieties on-chip for numerous applications. The majority of these are for biological applications; including immunoassays,[156-161] in which either the antibody or antigen are attached to the microchannel surface in order to make the washing procedures easier to perform and immobilised catalysts[162-164] for investigating the effect on other biological components. Binding of biological entities onto chip surfaces include estrogen receptors,[165] enzymes,[166] cells[167] as well as DNA.[76] In addition Shoffner *et al.*[50] investigated optimum surface modification for performing PCR. Due to the size of the channels with microfluidic devices, they are useful for mimicking *in vivo* channels, and therefore, there is a need to make the microfluidic surfaces as similar to those in the body as possible.[168] For chemical applications Aran *et al.*[169] used surface modification as a type of glue between polymer membranes within glass and PDMS microfluidic devices. As a chemical catalyst Nakamura *et al.*[170] used silica nanoparticles, coating a capillary, functionalised with anatase type TiO_2 for enzyme reactions and photocatalytic reduction of methylene blue. A similar effect was achieved by Lindstrom *et al.*[171] by coating the surface of the channel walls with TiO_2 for the purpose of photocatalytic reduction of methylene blue.

This section of the review has shown some of the many applications for functionalisation of silica surfaces; it has proven the ability of photo-activated molecules to retain their use after immobilisation, it has also provided material for further developing the amine density on the surface. However, the covalent immobilisation of porphyrin directly on the glass channels of a microfluidic chip has not been achieved.

1.6. Photo-oxidation

In this section an outline of the history and the current progress in the field of photo-oxidation is presented. Initially a basic overview of batch reactions in which the photosensitiser dye is in solution with the reagent is given. The use of solid supports for sensitisers gives researchers a more facile method of removing the photosensitiser from the reaction mixture, and the progress made in this area is then presented. Finally an introduction to these reactions on-chip or in microstructured reactions is given to fit the work presented herein into the full context of the previous research and to highlight the omission of any work of the same nature as that in this thesis.

1.6.1. Off-chip batch reactions

The use of light to initiate reactions is not a new concept, and has been used as an energy source for a large number of reactions. In this review the focus is specifically on the use of light to initiate the production of singlet oxygen in the presence of a photosensitiser dye for photo-oxidation reactions. These reactions are generally the ene reaction and Diels Alder type [2+2] and [4+2] reactions. The process is a simple one requiring only molecular oxygen, light and a photosensitiser.[34] Due to this simplicity it is often classed as "green" chemistry as it does not require long heating procedures and is an efficient method of synthesis.[172] "Green" chemistry is essentially a reaction in which the use or production of hazardous substances is limited and energy use is minimised.[173] In the case of large scale photo-oxidation reactions this definition is not strictly true as it involves large volumes of oxygenated solvents, which can easily become heated due to the irradiation of the mixture. However, this definition has the possibility of realisation with the use of less flammable solvents and of miniaturisation of reaction vessels to reduce the total volume of oxygenated solvent and will be discussed in more detail in a later section (1.6.3).

As mentioned, singlet oxygen is largely used in chemistry for reactions involving double bonds which the oxygen can attack. These reactions are the ene reaction to produce allylic hydroperoxides, the [2+2] reaction to produce the dioxane and [4+2] reaction to yield endoperoxides. In addition to these it is also possible to conduct heteroatom and heterocyclic oxidations. Clennan and Pace[42] reviewed a wider range of singlet oxygen reactions, however, in this report the ene, [2+2] and [4+2] reactions only will be looked at. These three reactions have been used as intermediate steps to other functional groups and are easy methods of introducing oxygen to a compound. The mechanism for the ene reaction is still under debate and is often dependent on the reagent being used. Clennan[41] examined three main intermediates that could be formed in the ene reaction; the exciplex intermediate (**9**), the perepoxide intermediate (**11**) and the zwitterionic or diradical intermediate (**10** and **12**) (Figure 14)

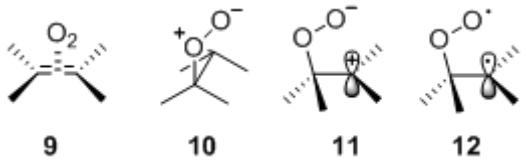

Figure 14: Possible intermediates in the ene reaction to produce an allylic hydroperoxide; the exciplex (9), the zwitterionic (10), the perepoxide (11) and the diradical (12) intermediate.[41]

Clennan also determined that the ene reaction is undertaken in suprafacial manner in which the addition of O_2 and the abstraction of a proton occur from the same face. It was also found that singlet oxygen has a propensity to abstract the proton from the most conjugated side of the double bond.[41] In addition to the mechanistic aspects of the ene reaction, there are also a number of further synthetic steps which can be performed to yield other oxygen-functionalised compounds. Prein and Adam[174] summarised these reactions as shown in Scheme 7:

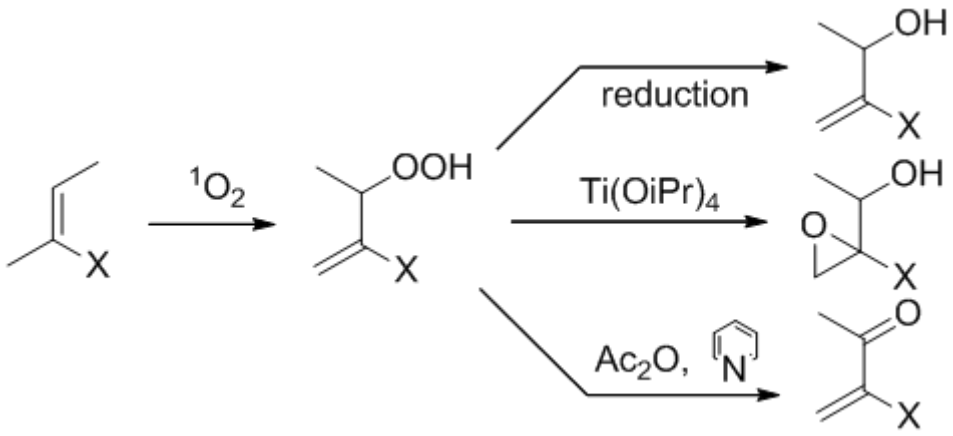

Scheme 7: Synthetic applications of allylic hydroperoxides.[174]

The regioselectivity, solvent effects and synthetic transformations of these reactions is a field of synthetic chemistry in its own right, and is reviewed effectively by Stratakis and Orfanopoulos[175] as well as Clennan *et al.*[41, 42]

There are a large number of synthetically important photo-oxidation experiments that have been conducted. Here is just a brief look at more unusual research or directly relevant to the work that has been conducted in this thesis. In 1975 it was suggested that the only stable product from photo-oxidation was ascaridole (**14**), the product of a [4+2] reaction with α-terpinene (**13)** (Scheme 8).[176]

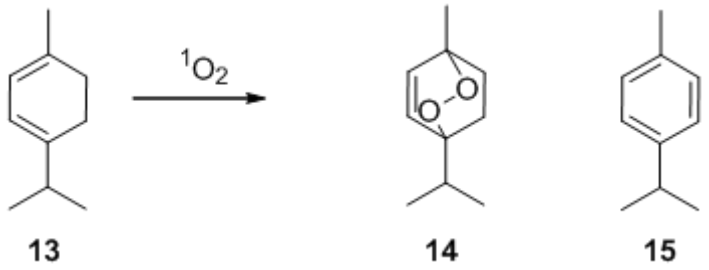

Scheme 8: Oxidation of α-terpinene (13) to yield ascaridole (14) using the [4+2] Diels-Alder type reaction with the production of *p*-cymene (15) as a by-product.

This reaction has subsequently been used as an example reaction for determining the ability of systems to produce singlet oxygen. Many of these reactions take place with immobilised

photosensitisers, and will therefore be looked at in more detail in section 1.6.2. Citronellol is another reagent that is often used for proof of principle reactions.[27, 177-179] It is used in the fragrance industry for producing rose oxide (**19**), which can be produced easily from one of the resultant products of the ene reaction of singlet oxygen with citronellol (**16**), therefore a more efficient manner of producing it would be cost effective (Scheme 9).

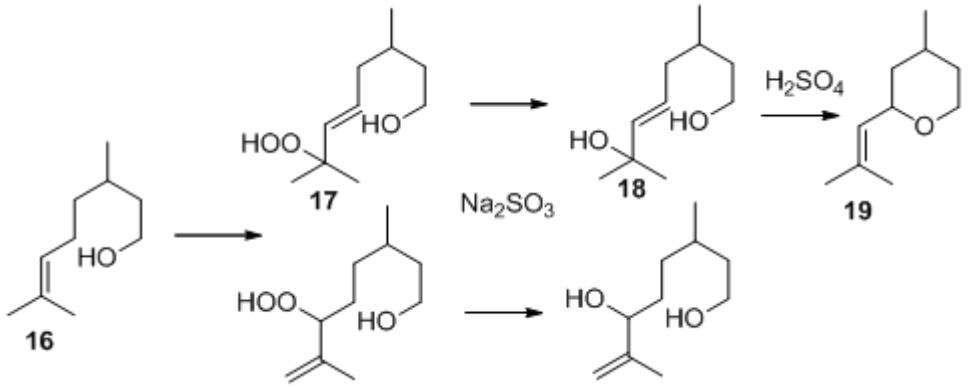

Scheme 9: Oxidation of citronellol (16) using the ene reactions and subsequent synthesis of rose oxide (19).

Photosensitisers that have been used for this reactions include metallated phthalocyanines,[177] where it was found that the zinc phthalocyanine was the most effective. Levesque and Seeberger[178] conducted the photo-oxidation of citronellol in a continuous flow reactor in which the reagents were pumped through a glass channel around a light source, in order to produce high volume throughput of this efficient reaction. Monnerie and Ortner[179] conducted an economic evaluation of this reaction with solar power as opposed to artificial lamp light and found that the cost would be dramatically reduced if this was possible. Oelgemöller *et al.*[27] realised this potential by constructing troughs in which the sunlight would be trapped and the reagents could be placed, and found that the reaction was possible within three hours reaction in strong sunlight. In addition to the reaction of citronellol with singlet oxygen they also investigated the synthesis of juglone (**21**) from 1,5-dihydroxynaphthalene (**20**) in this work and in a further publication (Scheme 10).[180]

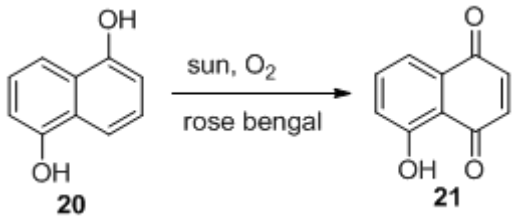

Scheme 10: Oxidation of 1,5-dihydroxynaphthalene (20) to yield Juglone (21).[27]

In this work they used rose bengal, methylene blue and solid supported versions of these two photosensitisers. They found that they could achieve up to 44% yield in non-concentrated sunlight and up to 70% when concentrated, with methylene blue and rose bengal, respectively.

Other methods for producing singlet oxygen have also been investigated such as through the reaction of hypochlorite and hydrogen peroxide by Foote *et al.*[181] and more recently the use of supercritical carbon dioxide by Bourne *et al.*[182] There are also many different uses for singlet oxygen reactions that are more medically centred such as the synthesis of a variety of antimalarial drugs based on artemisinin by peroxide formation.[43] However, these are more unusual, and especially in proof of principle experiments the photo-oxidation of α-terpinene and citronellol are most often seen.

Although these reactions provide proof of singlet oxygen production for new photosensitisers, or photosensitising systems, they do not provide quantitative information on the production of singlet oxygen. There are a number of methods for measuring this in a quantitative way. The only direct measurement of singlet oxygen is the detection of the emission at 1270 nm,[183] however, this can be disrupted by the interference of other emission spectra. Detection of the emission also requires very sensitive equipment. Therefore, the preferred method of quantifying the production of singlet oxygen, and determining the quantum yield is through indirect methods. One of these, which allows for the calculation of

quantum yields is the use of 1,3-diphenylisobenzofuran (DPBF) (**22**); initially a fluorescent molecule, it becomes non-fluorescent on reaction with singlet oxygen (Scheme 11).[36]

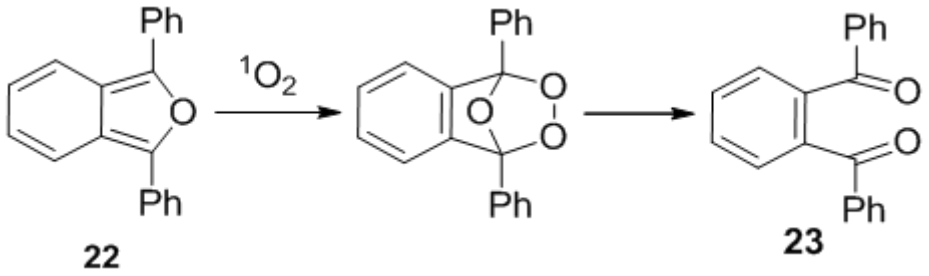

Scheme 11: Reaction of singlet oxygen with 1,3-diphenylisobenzofuran (DPBF) (22) to yield the non-fluorescent product (23) after decomposition through ring opening of the reaction product.[36]

It is possible to determine the singlet oxygen quantum yield of a photosensitiser, or photosensitising system from the extinction coefficient of DPBF. Through use of a number of equations and producing a Stern-Volmer plot of the reciprocal of the quantum yield of loss of fluorescence of DPBF ($1/\Phi_{DPBF}$) versus the reciprocal of the concentration of DPBF (1/[DPBF]) this is achieved.[36, 184, 185] These equations were used by Roitman *et al.*[185] to determine the singlet oxygen quantum yield for the free base and zinc coordinated tetranaphthaloporphyrin. Spiller e*t al.*[184] used them for a series of metallated tetrasulfonated phthalocyanines and determined that the efficiency in singlet oxygen production of them was Zn>Ga>Al>H_2 (free base)>Co. Belfield *et al.*[186] found it particularly useful for two-photon fluorene derivatives as they emitted in the infrared region making the direct method impossible.

Another method which can be used for the comparison of methods in a quantitative manner is the use of cholesterol (**24**) as it photo-oxidises at the double bond. Determination of an absolute singlet oxygen quantum yield from these reactions is not possible because cholesterol reacts through Type I reactions (radical) in addition to Type II reactions (singlet

oxygen). However, it is possible to make a comparison between different systems through the production of oxidation products. Another benefit of using cholesterol is that the products vary between type I and type II photo-oxidation as shown in Scheme 12

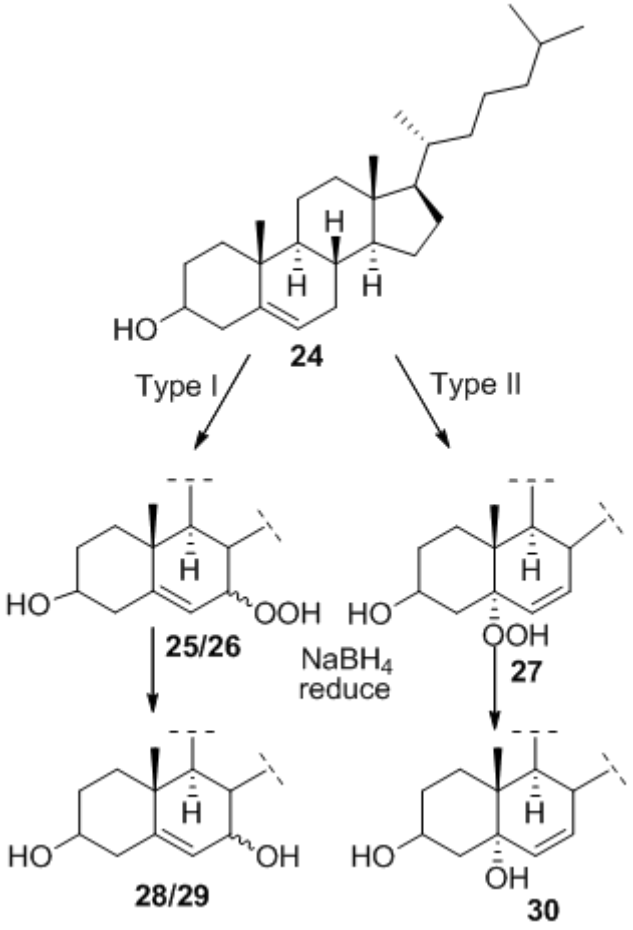

Scheme 12: Photo-oxidation of cholesterol to yield separate products from Type I and Type II oxidation.[35]

Although only the 5α-OOH (**27**) product is shown here from Type II photo-oxidation, it is also possible to get 6α- or 6β-OOH products. However, in general the 5α-OOH product is the most dominant product from this type of reaction.[187-189] Determination of the type of reaction occurring is, in theory possible, however, the 5α-OOH product obtained from singlet oxygen can undergo an allylic rearrangement to 7α-OOH (**25**). In turn this may also epimerise to 7β-OOH (**26**) making it difficult to be completely certain of the reactive mechanism. However, it is more likely that the rearranged 7α- and 7β-products would be in much lower

concentrations in a singlet oxygen-mediated oxidation as these changes happen slowly over time.

In order to quantify results it is necessary to have a method for determining the concentrations of each product. A complex thin layer chromatographic (TLC) method was described by van-Lier[35] for qualitative analysis. This method, in addition to the non-quantitative aspect, is labour intensive and experimental error can occur. However, the ability to separate components on TLC suggests that other forms of chromatography would be possible. The ability to determine the different oxidation products of cholesterol from one another in an easy analysis is a popular area of research especially in respect to food. In 1981 Tsai and Hudson[190] investigated a means to determine a number of oxidation products of cholesterol by high performance liquid chromatography (HPLC). They showed that TLC and gas chromatography (GC) increased the possibility of degradation of the products, whereas HPLC enabled non-destructive analysis. They were able to separate ten different cholesterol oxidation products on a normal-phase column. Maerker *et al.*[191] also used normal phase-HPLC with a flame ionisation detector (FID) detector to separate oxidation products of cholesterol including 7α- and 7β-OH, obtained from the reduction of the hydroperoxy products. Whereas Shen and Sheppard[192] used a reverse-phase (RP) column to separate out products from oxidation including 7α-OH. Both Csallany *et al.*[193] and Caboni *et al.*[194] used UV detectors to determine a large number of oxidation products, however, they included complicated gradients and changes in ultra violet (UV) wavelength or the use of light scattering detectors in conjunction with the UV. HPLC was clearly the preferred method for quantifying oxidation products from cholesterol; however, a robust method was required.[195-197] In 1999 Osada *et al.*[198] determined a method for separating ten different species of cholesterol on an RP-HPLC column. They used an isocratic mixture; however, it was

necessary to couple UV detection (at 210 nm) with evaporative laser light-scattering detector (ELSD). This group required the use of the coupled detectors to separate ten products from the oxidation of cholesterol in foodstuffs.

Other methods have been used to detect these oxidation products such as those by Grandgirard *et al.*[199] They derivatised the cholesterol products with a trimethylsilyl ether which allowed them to be run on GC. However, this requires a longer and more complicated workup of the reaction which may not be necessary in all applications.

1.6.2. Photosensitiser immobilised

The use of photosensitisers immobilised on solid supports began in the 1970s and addresses the issue of removing the photosensitiser from the reaction mixture. By supporting the photosensitisers on resins, gels, or beads they can be easily filtered from the mixture, which can then be purified in a more facile manner. Numerous research groups have worked on this idea resulting in a large array of support structures. Some of these will be reviewed here including polymer and silica supports, dendrimers and polystyrene beads along with molecular sieves and nanoparticles. This review will be broken into general photosensitisers and then look more specifically at porphyrins.

By far the most common photosensitiser supported in this fashion is rose bengal (RB). Blossey *et al.*[200] determined that RB could be immobilised on Merrifield polymers, constituting styrene-divinylbenzene copolymer, and successfully sensitise [4+2], ene and [2+2] oxidation reactions. The group extended this further by looking at more reactions[20] and hydrophilic polymers[21] to show the versatility of this idea. There have also been a number of groups that have taken this polymer supported RB and investigated the effect of different loading concentrations,[23, 24] methods for producing the RB-polymer[201] and compared them to

other solid supported photosensitisers.[202] RB has also been immobilised on silica gel,[22, 203, 204] ion exchange resins,[25, 180] glass plates[19] and porous monoliths.[205]

There are a large number of other photosensitisers that have been immobilised on solid supports. These include methylene blue,[18, 19, 180, 203] C_{60} fullerenes,[206-209] 9,10-dicyano anthracene (DCA),[210-212] ruthenium complexes,[213-215] phthalocyanines[216, 217] along with many others.[54, 218, 219] There are a number of recent reviews that deal with these immobilised photosensitisers in great detail.[220-223] However, porphyrins offer a number of advantages over many of these photosensitisers. They possess many sites in which functionality may be introduced; it is possible to make them cationic, anionic and neutral, as well as the possibility of metallating the centre for improved triplet state yields. This enables great ability to tune them for specific applications, and why they were chosen for this project. Therefore, the rest of this review focuses on porphyrins immobilised on solid support.

Polymer supports offer a range of options in regards to supporting the photosensitiser. Faust *et al.*[224] used poly(methylmethacrylate) (PMMA) to incorporate cationic and anionic porphyrins into the polymer matrix during the synthesis steps. The zinc(II)-5-(4-hydroxyphenyl)-10,15,20-tris-(*N*-methyl-4-pyridiniumyl) porphyrin and zinc(II)-5-(4-hydroxyphenyl)10,15,20-tris(4-sulfonatophenyl) porphyrin were immobilised through the hydroxyl groups to the polymer. It was found that they performed better than polymer supported RB in the photooxidation of imidazole. The resulting transannular peroxide reacts with yellow *N,N*-dimethyl-4-nitrosoaniline to form a colourless product and was used to determine the production of singlet oxygen. Porphyrin was also incorporated with polydimethoxysilane (PDMS) by van Laar *et al.*[225] They investigated the affect of different metal ions in the central cavity such as zinc(II) cobalt (II) and the free base of TPP as well as the free base of 5,15-(2,6-dichlorophenyl)-10,20-(allyloxyl phenyl) porphyrin through the

photo-oxidation of 1-methyl-1-cyclohexene and 2,3-dimethyl-2-butene. They found that the occlusion of these dyes could be advantageous in use with different solvents with the prevention of leaching that may be caused by other methods.

Benaglia *et al.*[226] used a different method, namely attaching PEG polymer to hydroxyl groups on the porphyrin, to form a polymer porphyrin. They used these polymers to successfully conduct photo-oxidation of a number of reactions and found that they were re-useable up to six times (Figure 15).

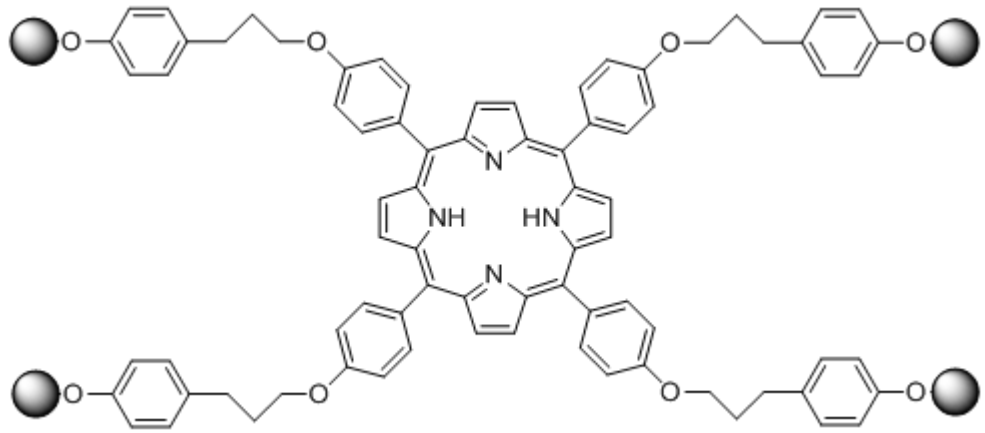

Figure 15: PEG-supported porphyrin synthesised by Benaglia *et al.*[226]

Rogers *et al.*[227] fabricated a polymer monolith with amino-functionality to which they attached hematoporphyrin for oxidation reactions in aqueous and organic solvents. They tested this through the oxidation of anthracene and with a molecular probe called Sensor Green, which reacts specifically with singlet oxygen in type II reactions. They found that these monoliths were successfully producing singlet oxygen for these reactions. Fuchter *et al.*[228] used ring-opening metathesis polymers in a gel and spherical configuration for attaching porphyrinic compounds (zinc-*seco*-porphyrazine). They showed that it was possible to conduct photo-oxidation of [4+2] and ene reactions, and that the spheres were better than the gel. Mosinger *et al.*[229] fabricated polymer nanofibres to which they attached

TPP and measured the singlet oxygen through luminescence at 1270 nm wavelength. They also conducted photo-oxidation reactions including the bleaching of 9,10-anthracenediyl-bis(methylene) dimalonic acid, and suggest that these porphyrin-immobilised nanofibres may have bactericidal properties. Titov *et al.*[230] showed that it was possible to immobilise various metal TPPs (free base, Zn(II) and Mn(II)) to propylene after plasma-chemical treatment and inclusion of acrylamide and 4-vinylpyridine. They analysed the surface, and showed that it was active in generating singlet oxygen through the decomposition of 9,10-diphenylanthracene endoperoxide.

Ribeiro *et al.*[231-233] used Merrifield polymers to immobilise TPP with different halogens attached to the phenyl rings and at least one sulfonated phenyl to attach to the aminated polymer surface (Scheme 13). They used these polymers to conduct a number of photo-oxidation reactions. The purpose of their research was to determine the effect of different halogens, and different spacers between the polymer and the porphyrin, had on the reaction yields. They found that the silanising agent with a C_{12} chain was the most efficient for photosensitised reactions and that the addition of chloro groups on the porphyrin improved the singlet oxygen yield. Finally for polymer supports Han *et al.*[202] compared a large number of porphyrins to RB immobilised on polymer films. They conducted continuous flow reactions using supercritical carbon dioxide ($scCO_2$) and determined that tetra (2,6-dichlorophenyl) porphyrin (TDCPP) with one of the phenyl groups having a carboxylic acid at the 4-position (for covalent binding to the polymer) gave the best space-time yield for the photo-oxidation of α-terpinene and citronellol.

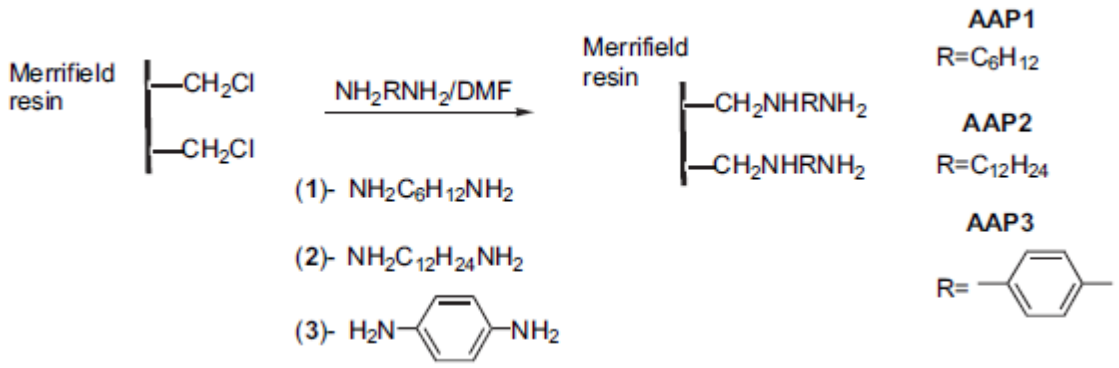

Scheme 13: Reactions conducted on Merrifield resin to yield amino groups with different spacers used by Ribero *et al.*[233]

Polystyrene beads, due to their propensity to swell and shrink in various solvents, allow greater photosensitiser-loading. Various papers by Griesbeck *et al.*[30, 234-236] especially show different methods for immobilising porphyrin on to the polystyrene beads. This includes the adsorption of TPP, tetratolylporphyrin (TTP) and protoporphyrin IX (PPIX)[234-236] using styryl groups on the porphyrin to embed them within the polymeric matrix.[30] They used these porphyrin-immobilised polystyrene beads to conduct solvent free singlet oxygen reactions, by adsorbing the reagents in the beads also, and then extracting the products with small amounts of solvent. This is a good example of the attempt to reduce the quantity of oxygenated solvent needed, and therefore, a potential for "green" chemistry. Inbaraj *et al.*[237] utilised the cationic nature of polystyrene beads with the anionic porphyrin (tetra-(4-sulfonatophenyl) porphyrin (TSPP)) to produce singlet oxygen. They used the bleaching assay with *N,N*-dimethyl-4-nitrosoaniline to determine the relative ability of the free base as opposed to the zinc and cadmium metal porphyrins. It was found that the free base and the zinc complex were almost as efficient as one another but the cadmium complex was not as efficient.

The other main option for immobilising photosensitisers is to use some form of silica substrate, often in the form of a silica gel, or silica particles. Chirvony *et al.*[238] used

nanoporous silica with cationic and anionic porphyrin embedded within it. They found that the silica did not quench the singlet oxygen production of the porphyrin by measuring the luminescence at 1270 nm. It was found that the oxidised silica produced a better result than bare silica. Ribeiro *et al.*[231, 239] compared the porphyrin-immobilised Merrifield polymers, previously discussed, to silica particles in the photo-oxidation of a number of compounds. They found that there was little difference; however, the length of the spacer between the porphyrin and support had a greater influence, with longer spacers giving better singlet oxygen quantum yields.

Shimakoshi *et al.*[240] produced a silica film using the sol-gel method, and immobilised it to a glass plate. A porphyrin-like molecule (porphycene) was attached to the silica gel by synthesising the porphycene with a silane group (Figure 16). They found that this was proficient in the photo-oxidation of 1,5-dihydroxynaphthalene (**20**) to Juglone (**21**) (Scheme 10), and it was reusable over four runs.

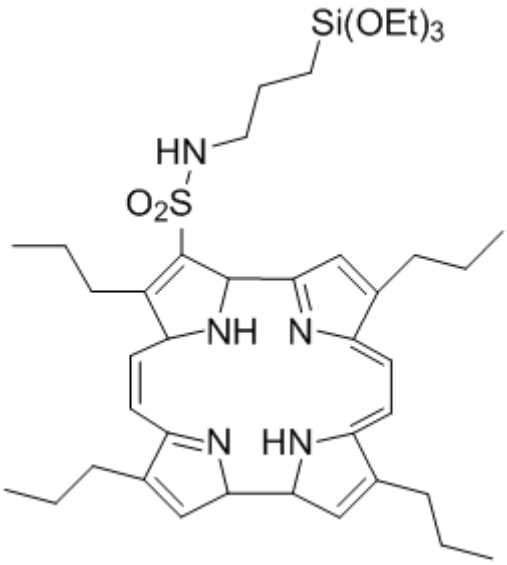

Figure 16: Silane group attached to the porphyrin for immobilising on silica gel.[240]

Aebisher *et al.*[241] used the anionic binding capability of porous vycor glass (PVG) in water to adsorb the cationic porphyrin TMPyP. They detected the luminescence of singlet oxygen and also conducted the photo-oxidation of *trans*-2-methyl-2-pentanoate anions in water and D_2O and found that it was faster in D_2O. This is because the stretching frequency of D_2O is lower than H_2O and therefore does not quench singlet oxygen as quickly. Rossi *et al.*[242] compared the singlet oxygen generation capabilities of free PPIX and the immobilised form on silica nanoparticles. They used the luminescence emission and the loss of fluorescence by DPBF in order to determine the singlet oxygen yield and found that it was higher for the immobilised porphyrin suggesting that this would be a good carrier for PDT. Finally Trytek *et al.*[243] used monolithic silica gels for immobilising a number of porphyrins with water soluble and non-water soluble properties. These included TPP, TMPyP and a tetra-(4-carboxyphenyl) porphyrin. They investigated various solvents to determine the combination that gave the best results and found that chloroform was the best solvent when using the free base of TMPyP for the photo-oxidation of α-pinene. It was found possible to use the system up to thirteen times, but only reproducible up to ten times.

These represent the most common substrates for immobilising photosensitisers, however, there are a number of others that have been used. The use of dendrimers to produce porphyrinic compounds that are of high molecular weight, and are therefore capable of being nano-filtered out of solutions, has been conducted by Chavan *et al.* (Figure 17).[244] The photo-oxidation of 1-methyl-1-cyclohexene and other olefinic compounds were used to test these dendrimers (**31**), and found to be somewhat prone to photodegradation. Other substrates include molecular sieves of various types; the $AlPO_4$-5 type were used with various free base and zinc porphyrins encapsulated into them,[245] and MCM-41 functionalised with APTES with a Ru(II) TDCPP adsorbed *via* a complexation with ruthenium and the

amino group.[246] Whereas the first of these groups did not provide data on the ability to produce singlet oxygen, the latter were able to achieve good yields (61-98%) on photo-oxidation reactions with a number of reagents although taking place over 24 hours. More recently Shi *et al.*[247] have attached TSPP on to CdTe nanoparticles for the photo-oxidation of methionine to the corresponding sulfone, and Lang *et al.*[248] have intercalated TSPP into a Mg-Al layered double hydroxide and measured the lumiscence of singlet oxygen.

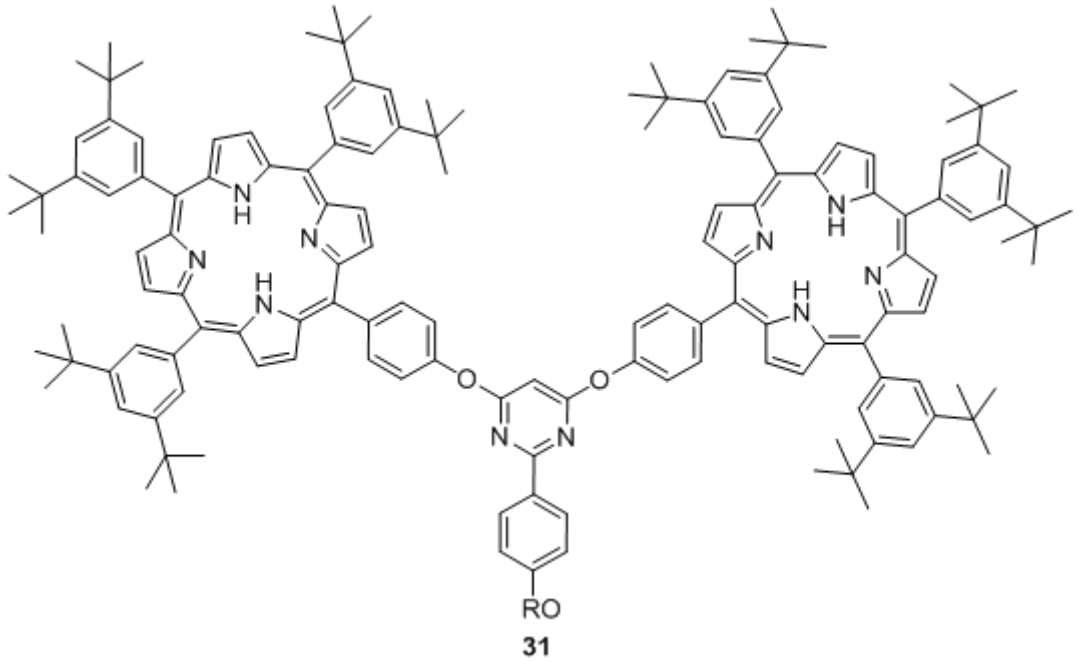

31

Figure 17: Porphyrin dendrimer synthesised by Chavan *et al.*[244]

This review has shown some of the many uses of immobilised photosensitisers within the chemical applications. The immobilisation of porphyrin is extremely varied but has great potential for producing singlet oxygen by altering the porphyrin itself, or the method for immobilising it to the substrate. However, all of these still result in batch-type reactions, in which the photosensitiser needs to be collected after the reaction is complete. The use of microfluidic technology opens up the possibility of continuous flow reactions in which the reaction is quick and efficient.

1.6.3. Photo-oxidation on-chip

The benefits of conducting photo-chemistry on-chip are laid out by Coyle and Oelgemoller:[53]

- Uniform irradiation of the sample through the small microfluidic channels
- Continuous-flow reactions conditions can be easily altered allowing rapid optimisation
- High heat transfer coefficients allowing rapid cooling
- Miniaturised light sources are possible which are more energy efficient
- Microchip design allows integration of reaction monitoring.

Due to these advantages research to improve photo-reactions by conducting them on-chip has increased. Some reactions that have been attempted are cycloaddition [2+2] and [4+2] reactions,[249-253] polymerisations,[254] isomerisations,[255] radical reactions,[55, 256] decarboxylations,[257] and cyanations.[258] There are also a number of microreactor based singlet oxygen reactions that have been successfully conducted. Wootton *et al.*[26] used a solution of rose bengal with oxygen pumped through a serpentine channel chip (Figure 18) to conduct the photooxygenation of α-terpinene (**13**) to ascaridole (**14**) (Scheme 8). Using the set up in figure 19 they found that it was possible to get 85% conversion through the microreactor, as opposed to 67% conversion using batch methods. Another benefit in microfluidic singlet oxygen reactions, is the reduced volume of oxygenated solvents being used making for a safer, less explosive set up. Microreactors have also been used for the Schenck-ene reaction of citronellol (**16**) using a ruthenium polypyridyl complex as the photosensitiser.[259] A serpentine channel was again used and the microreactor was proven to have a better photonic efficiency than a Schenck reactor. The reaction was conducted with an array of forty LEDs proving that this light source was sufficient for the reaction.

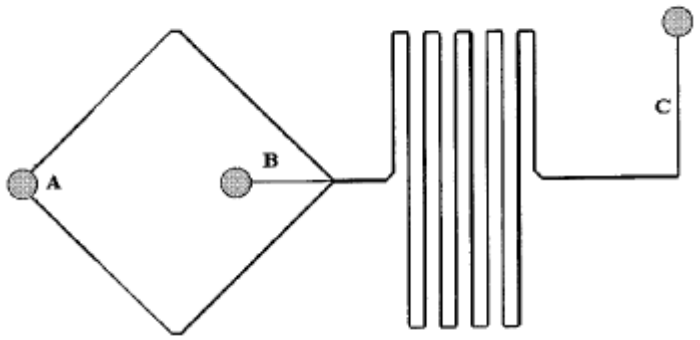

Figure 18: Schematic of glass microreactor for singlet oxygen production in solution, with the divergent channel (A) for the reactants, a secondary inlet (B) for oxygen and the serpentine section for irradiation leading to the outlet channel (C).[26]

Park *et al.*[260] used polyvinylsilazane (PVSZ) to fabricate a dual channel microreactor for separating the reaction mixture and the gas phase, therefore enabling a greater contact between the two. PVSZ was found to be more chemically stable than PDMS enabling a greater array of solvents. They used MB for the oxidation of α-terpinene and citronellol in this device and compared it to batch and plug flow reactors. It was found that the dual channel microfluidic device competed effectively with batch reactions, giving a comparable yield in a much reduced time. The set ups can be seen in Figure 19, showing the increased gas-liquid contact area.

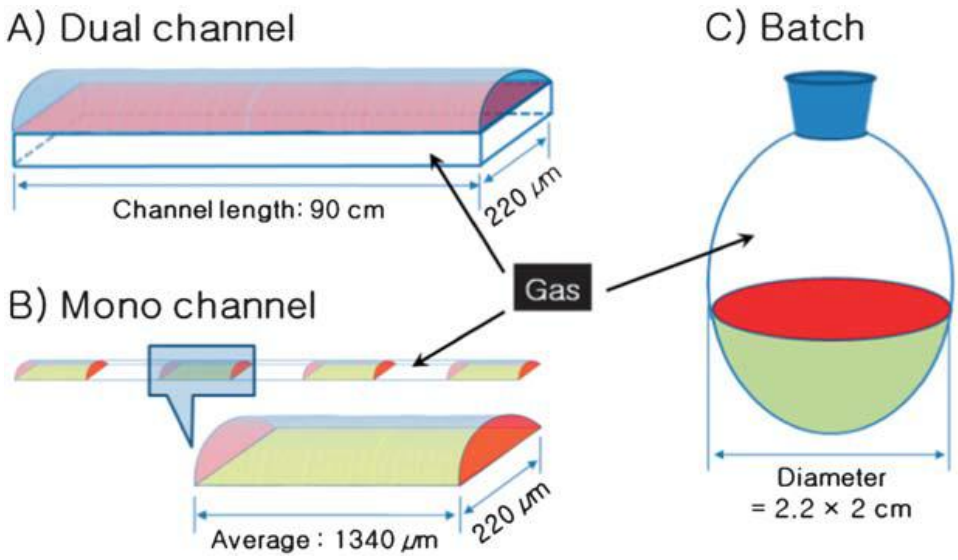

Figure 19: Reaction vessels used and examples of the gas contact areas; A) the dual channel microreactor having a contact area of 1.98 cm^2 and a contact area-to-volume ratio of 50.9 cm^{-1} B) a mono layer channel system with a contact area-to-volume ratio of 14.9 cm^{-1} and C) a batch system using a round bottom flask with a contact area-to-volume ratio of 0.76 cm^{-1}. [260]

Jahnisch and Dingerdissen[261] used a commercially available falling film microreactor for the photooxidation of various olefins. Falling flim microreactors work by the reagents moving through channels of thin films by the force of gravity. These produce residence times from seconds up to one minute. RB in solution was pumped through 32 parallel channels, producing singlet oxygen products to a sufficient quantity for industrial uses. Along with fabricated microreactors, as described above, there is also research into using natural microenvironments for conducting photo-oxidation reactions. These are mostly zeolites[262-265] or Nafion membranes[263, 266] but can also include biological components such as vesicles[263] or liposomes.[267] Tung *et al.*[268, 269] have compiled a review on this type of photo-oxidation, but it will not be looked at further here, as it is not directly relevant to the project.

Immobilisation of substances within microfluidic devices is conducted for a variety of purposes. As has been discussed previously (section 1.5.2), biological assays and cell work is increasingly being conducted on-chip as it can be made to resemble *in-vivo* environments.

Immobilisation of enzymes[270] and immunological receptors[271, 272] along with other biological components[94] on-chip is already used for determining interactions. There are also some chemical reactions which are using immobilised catalysts in order to increase the efficiency of some chemical reactions. These include immobilised Pd for hydrogenation reactions,[273] and immobilised fumarase for the conversion of fumaric acid.[274] However, photo-oxidation reactions within microfluidic devices are limited mostly to coating the channel walls with titanium dioxide to be used as the catalyst for the reaction.[275-281] There is one example of immobilised porphyrin[282] however, the silica support was in the form of silica particles which were incorporated into the device, rather than onto the channel walls. Similarly Carofiglio *et al.*[283] immobilised C_{60} fullerene on to Tentagel® resin beads and silica and incorporated them into a microfluidic chip. These examples show that it is possible to conduct singlet oxygen reactions and immobilise photosensitisers onto the walls of a microreactor, however, they also highlight the absence of photosensitisers directly immobilised on channel walls for singlet oxygen-mediated oxidation.

1.7. Photodynamic therapy-generated vaccines

As described in section 1.2, PDT is the use of photosensitisers, localised in tumours, irradiated with light to catalyse the production of singlet oxygen which is toxic to cells and causes the cancer cells to die. There has been a lot of research conducted into different photosensitisers which could be used in this manner and are effective *in vivo* for causing a reduction in tumour size and viability. Although this area of PDT has directed the information regarding immune responses and ultimately the development of PDT-generated vaccines, there is too much information to go into detail here. There have been a large number of reviews on general photosensitisers,[10, 32] and more specifically porphyrin[12, 38, 284, 285] and non-porphyrin[15, 286] with the most recent commenting on the progress for clinical applications.[11] However, it is the intention here to focus more specifically on information regarding the immune-response that PDT initiates, and how this immune-response has led to certain groups examining the use of PDT-treated cancer cells *ex-vivo* for use in initiating an immune response to the tumour.

1.7.1. Immune response to PDT

The immune response of the body to a tumour is unlike the response to other diseases and pathogens in the body. This is due to the overwhelming odds against the immune system. The amount of antigen recognisable by the T cells on a tumour is low (≤ 100 molecules), it can only be recognised by a small number of T cells (1 in 100,000 or less), and the T cell receptor has a low affinity for it (≤1 μM).[287] It is normally dendritic cells (DCs) which present the T cells with antigens necessary for them to mature. However, it appears that this does not take place in the case of cancer, which could be due to a number of different factors; there may be a lack of functional DCs within the tumour, those DCs that can invade the tumour may lack the necessary components to stimulate T cells, or the tumours may secrete

factors that reduce the development of DCs.[287] It is likely that a combination of these factors is responsible for the low immune response to tumours. However, it has been found that in addition to direct cell death and destruction of vasculature, the photo-oxidation process in PDT activates immune responses against the tumour.[288]

The basic series of events seems to be that the initial PDT treatment cause inflammation within the tumour site, which activates a number of signals through the innate immune response. The result of this is that dendritic cells become activated and move to the lymph nodes where they mature and interact with T cells which form a part of the adaptive immune response. The three main aspects that link PDT treatment and anti-tumour immunity are 1) a specific acute phase response from the innate immune system, 2) the expression of damage associated molecular patterns (DAMPs) and 3) activation and maturation of DCs in the lymph nodes to activate T cell and the adaptive immune system.

An acute phase response occurs during tissue damage to enable a protective atmosphere.[289] It is directly related to the innate immune system and works to remove and "clean up" the site of injury. After PDT treatment, which is designed to kill the cancer cells, this acute phase response is initiated. Phagocytotic cells are amongst the first to arrive at the tumour after PDT as a result of the inflammatory response. However, it has also been noted that neutrophils can act to destroy some tumour cells by damaging the stroma between cells, which can act to expose the tumour cells to cytotoxic effects. Various cell surface proteins are expressed on the cell surface including interleukin (IL) proteins. Gollnick *et al.* have shown that the expression of IL-6 and the resultant down-regulation of IL-10 could be part of the mechanism for increased anti-tumour immunity.[290] They also found that PDT increased the expression of IL-12 in antigen presenting cells (APC), stimulating T-cell proliferation which secreted interferon-γ (INF-γ) increasing APC activity.[291] Korbelik *et al.*[289, 292]

determined that neutrophilia is directly related to the acute phase response, and that this reaction is markedly reduced in adrenolectomised mice. The adrenal-pituitary axis is part of the acute phase response by releasing hormones which activate neutrophilia. They also determined that glucocorticoid hormones are released after PDT which increase a specific protein expression in mice which is part of the acute phase response.[293] Finally Kushibiki *et al.*[294] determined that PDT can induce the expression of IL-1 and IL-6 and reduce the expression of tumour necrosis factor-α (TNF-α) from DCs. These all show that for these specific treatments the acute phase response has been initiated by the PDT treatment.

PDT has also been shown to cause both apoptotic and necrotic cell death to the cells in which it is in contact. These forms of cell death regulate normal cell growth and development; therefore, it would seem inappropriate if these cell death pathways were capable of eliciting an immune response. However, it has been found that the manner of initiating, especially apoptotic cell death, from PDT could contribute to the adaptive immune response.[295] It is the expression of damage activated molecular patterns (DAMPs) on the surface of these apoptotic cells that is thought to be the main reason for them becoming immunogenic.[296] The most characteristic of them is the heat shock protein, HSP-70 which, in addition to calreticulin (CRT) and high mobility group-box-1 (HMGB-1) have been implicated in immune response initiation. When HSP-70 remains outside the cell it can form complexes with tumour antigens, which can then interact with APCs, and in particular cause the activation and maturation of DCs. Gomer *et al.*[297] showed that singlet oxygen could induce the expression of HSP-70 *in vitro* and *in vivo* and that dependent on the photosensitisers these originate from different cellular targets. Korbelik *et al.*[298] demonstrated that as early as 1 hour after PDT treatment HSP-70 is expressed on the cell surface and that this is an important event in the activation of the immune system. This is corroborated by Gollnick *et al.*[295]

finding that the ability of PDT to induce the expression of HSP-70 leads to increased immunogenicity.

Zhou *et al.*[299, 300] also found that HSP-70 was expressed at the cell surface and that this increased the secretion of TNF-α which indicated an important step in the immune response. They also discerned that when PDT was administered at a non-lethal dose HSP-70 took longer to become expressed and that it did not lead to cell death. This suggests that by itself the expression of HSP-70 is not solely representative of the ability to initiate an immune response. However Etminan *et al.*[301] considered the induction of HSP-70 expression to be a key mediator in anti-tumour immunity. More recently other DAMPs have been found to be expressed which are also related to the anti-tumour immunity. Korbelik *et al.*[302] proved that CRT and HMGB-1 were also expressed which they consider to give a further indication of the host response to PDT. This was also determined by Garg *et al.*[303] who found that with hypericin as the photosensitiser expression of CRT was seen in addition to HSP-70. So these DAMPs are, in part, suggestive of an immunological ability of PDT treatment *in vivo* and *in vitro*, however, they cannot be taken on their own as a definitive marker.

Finally, as mentioned HSP-70 can interact with APCs and activate DCs. DCs also digest some of the apoptotic cells, fragments of the necrotic cells and soluble tumour antigens. This causes them to be initiated to migrate to the lymphoid tissues, where they present the appropriate receptors on the surface and hence activate T cells. The T_H cells (helper T cells) and T_C cells (cytotoxic T cells) can aid the innate immune system and directly kill the tumour cells respectively. The first group to discover that the immune system could continue to fight the tumour after PDT was Canti *et al.*[304] They found that after HpD treatment of a tumour in a mouse model, they were able to resist a rechallenge of the tumour. Korbelik *et al.*[305-307] found the importance of a functioning immune system to the success of PDT

treatment. They found that lymphoid populations are essential for an immune response and that the inactivation of various components of the immune system was capable of severely inhibiting the immune response. These were netrophils, macrophages and helper/cytotoxic T cells, and showed a key role in establishing anti-tumour immunity. Finally, it was possible to effect an immune response by recovering immune cells from BALB/c mice and transplanting them into immunodefficient mice. Hendrzak-Henlan *et al.*[308] determined that $CD8^+$ T cells and natural killer (NK) cells were essential for initiating an immune response.

It has been established that DCs activated *ex vivo* can be reintroduced into the body and elicit a specific immune response against the tumour.[287] To be effective it would be necessary to ensure that the DCs were loaded with tumour antigen in order to present these antigens to T cells in the lymphoid organs. DCs, in their immature state reside in most tissues in the body. When they are activated, by coming into contact with an antigen, they will present major histocompatiblity complex (MHC) on the surface and will migrate to the lymphoid tissues. Once they are in the lymphoid tissue, they come into contact with T cells and activate them against the antigen. Therefore, it is important that the DCs, when activated *ex vivo* are replaced in the body at the stage in which they are programmed to migrate to the lymphoid tissues. Once the DCs are fully mature they lose their migratory signals, and would no longer be able to activate the T cells as they would not move to the lymphoid tissues.[309] However, if introduced at the correct time, they could help to initiate a stronger immune response to the tumour. This immune response contrasts sharply with the immunosuppressant effects of other cancer treatements.

1.7.2. Current research into PDT-generated vaccines

The immune responses described above have been instrumental in the theory of PDT-generated vaccines which can be developed *ex vivo* and avoid the possibility of affecting

healthy tissue, whilst still initiating an immune response that will act aggressively toward the tumour. Since initial reports by Gollnick[9] and Korbelik[8], that PDT-generated cancer vaccines had the ability to reduce and/or remove a tumour of the same lineage as that used to raise the vaccine, there have been a small number of other examples of this work. Gollnick *et. al.*, in 2002 were the first to attempt the use of PDT to produce a vaccine.[9] They used cell lysates generated through PDT, which were then mixed with DCs *in vitro* from the host and found that they secreted IL12 which is known to be involved in activating T cells. Although UV treated lysates created as many mature DCs as PDT treated lysates, the IL12 was only found in high numbers in the PDT treated lysates. It was theorised that the PDT-generated cell lysates would have a similar effect in the body, stimulating DCs to initiate an immune response to the tumour. In order to prove this theory they tested the PDT-generated tumour cell lysates in mice and compared them to lysates generated by UV and infrared (IR). The lysates generated using PDT were more effective at initiating an immune response than either the UV or IR-generated lysates.[9]

Korbelik and Sun used whole tumour cells and the photosensitiser benzoporphyrin derivative monoacid ring A (BPD) to reduce incubation time in comparison with Photofrin™.[8] They found that a change in the concentration of photosensitser was not as important in the efficacy of the vaccine as the number of cells used. It was determined that $2x10^7$ cells/vaccination produced the maximum benefit, but any further increase had little obvious advantage. It was also found that other methods of generating the vaccine (in this case X-rays) were not as effective as the PDT-generated vaccine, which confirmed Gollnick's work with cell lysates. This vaccine again showed the increase in immune system response and they were able to show that there was an increase in T and B cells. They postulated that it was heat-shock proteins in combination with the part of the immune system known as

complement that was responsible for the superiority of the PDT-generated vaccine.[8] Complement encompasses a number of serum and cell surface proteins that act in cell lysis, improving phagocytosis and regulating inflammation and immune responses.

Korbelik *et. al.* also found that it was not only the primary tumour that the vaccine affected, but that in mice studies they gained resistance to a re-challenge with the same tumour.[310] This suggests that the use of PDT-generated vaccines could help to combat secondary tumours and tumour metastasis. They also found that the vaccine could be successfully produced using surgically removed tumour cells and PDT treatment *ex vivo*. This is significant because it allows the vaccine to be directly tailored to the patient and the tumour, and avoids the delay in establishing cancer cell culture, making a much more efficient vaccine.[310]

From these initial indications of the ability of PDT-treated cells to initiate an immune response, other groups have also been successful in producing PDT-generated vaccines. Jalili *et al.*[311] have treated murine colon cells (C-26) with Photofrin and found that they showed many of the signs previously discussed regarding PDT-related immune response including HSP-70 and IL-12. When incubated with immature DCs and reinjected into mice they found that they were capable of initiating anti-tumour immunity. Bae *et al.*[312] took HPV tumour cells (TC-1) and treated them with radachlorin photosensitiser to produce immunogenic lysates. They found that when co-injected with another vaccine adjuvant (CpG-oligodeoxynucleotide) the combination was better at activating certain immune responses suggesting good potential for anti-tumour vaccination. Friedberg *et al.*[313] used a murine mesothelioma cell line (AB-1) treated with Photofrin to initiate an immune response in mice. They found that those injected with these cells were more able to resist the tumour growth

than those without the injection. Zhang *et al.*[314] used H22 liver cancer cell lysates treated with hematoporphyrin to again initiate an immune response in mice.

The use of PDT-generated cancer vaccines in personalised medicine is an emerging field. The work conducted to date has proven that the principle works on the mouse model, and with tissue samples as well as cell lysates. However, the preparation of these vaccines was labour intensive and required expert intervention. Producing a microfluidic device that could produce these vaccines in an efficient manner, with little expert intervention would be of great advantage. In addition, by keeping the photosensitiser immobilised to the glass channel walls, it avoids the chance of contamination of the sample with photosensitiser which could cause side-effects *in vivo*.

1.7.3. Immobilised photosensitisers for PDT

The first generation of PDT photosensitisers were based on natural products that were altered to give the optimum conditions for tumour attack. Second generation photosensitisers were specifically synthesised to fulfil the criteria for successful agents in regards to their light activation and toxicity. However, third generation photosensitisers are now being investigated that will enhance the ability to accumulate into the tumour. In order to do this, many groups are looking into immobilising the photosensitiser on to various moieties. These largely constitute nanoparticle supports of polymer,[14, 151, 205, 215, 315] silica,[16, 151, 238, 242, 316-318] or gold.[319, 320] However, there are also those looking at quantum dots,[247, 321] and more biologically significant antibodies.[13, 322] These are, in the majority, designed for *in vivo* applications and are therefore of limited importance in this project, however, they do suggest that immobilising the photosensitiser on to a solid support does not interfere with the ability to produce singlet oxygen and kill cancer cells.

1.8. Conclusion

It has been shown that while the immobilisation of photosensitisers is an established procedure and micro-photochemistry is an emerging field, the combination of the two is limited to a small amount of research. It was the purpose of this thesis to amend this, by immobilising photosensitisers onto the glass channel walls of the microfluidic device, it was hypothesised that photo-chemistry could be conducted in a continuous flow manner to simplify and improve the efficiency of these reactions.

In addition the current research has proven that PDT-generated cancer vaccines are capable of generating an immune response from the patient. The purpose of this thesis was to determine the possibility of using the photosensitiser immobilised chip to produce a similar vaccine. By using the photosensitiser to produce singlet oxygen in the presence of the cells flowing through the chip, it was hypothesised that the device could provide an efficient and simple means of producing a PDT-generated vaccine.

Chapter 2. Immobilisation techniques on glass

In this chapter the methods used to immobilise photosensitisers onto various glass substrates are introduced in conjunction with an outline of the procedure used to synthesise the porphyrins required. In general the photosensitisers investigated were porphyrins, however, rose bengal was also briefly considered. Rhodamine B was utilised in order to determine experimental parameters.

The microfluidic device was fabricated in glass; therefore, various glass surfaces were investigated for immobilising photosensitisers. Glass microscope slides were used to initially test the silanising methods and to determine whether a cationic isothiocyanate substituted porphyrin would immobilise covalently to the functionalised surface through a thiourea bond,[322] or electrostatically between the positive charges on the porphyrin and the negative charges on the glass[247] (section 2.3). Glass beads were investigated, enabling a visual determination of molecules on the glass through a colour change and fluorescence. The colour change and fluorescence was found to be easier to visualise on the beads than on the glass slides due to the cumulative effect of many beads. The procedure for the immobilisation of rose bengal onto controlled pore glass was based on the original solid supported photosensitiser[20, 21, 200] and is briefly discussed in section 2.4.3. The method for photosensitiser immobilisation on the channels of the microfluidic device was optimised in order to reliably bond molecules in an even manner throughout all channels in the chip and is examined here also in section 2.5.

2.1. Aims

The aims for this chapter were to develop an optimised method by which the photosensitisers used in this project could be immobilised on to glass surfaces. The purpose of immobilising photosensitisers on to the glass channels of the microfluidic device was to prevent contamination of either the chemical or biological components[30, 207, 210, 219, 239, 240] with the photosensitising agent while allowing the desired reactive oxygen species to be generated *in situ*. To achieve this, various silanising agents were attached to glass surfaces, bearing functional groups to which photosensitiser molecules could be covalently immobilised. It was hypothesised that porphyrin could be immobilised by reaction of an isothiocyanate group to amino groups on silanised glass using (3-aminopropyl)triethoxysilane (APTES) or (3-aminopropyl) trimethoxysilane (APTMS), while rose bengal could be immobilised by nucleophilic attack of a carboxylate anion on a chloropropyl on silanised glass using (3-chloropropyl) trimethoxysilane (CPTMS).

2.2. Porphyrin synthesis

The synthesis of the cationic porphyrin was conducted as stated in section 5.4 and adapted from the work of Sutton *et al.*[323] Cationic isothiocyanato porphyrins (**35** and **37**) were obtained from 5-(4-acetamidophenyl)-10.15.20-tri(4-pyridyl) porphyrin (**32**), initially by acidic hydrolysis of the acetamido group and treatment of the resulting amino group with 1,1-thiocarbonyldi-2(*2H*)pyridine (TDP). Cationic character was introduced by quaternisation of the three pyridyl groups using methyl iodide in a large excess. This was precipitated from diethyl ether to obtain the cationic porphyrin with iodide counter ions. Alternatively, the crude *N*-methylated product was treated with ammonium hexafluorophosphate followed by tetrabutyl ammonium chloride to yield the cationic porphyrin with chloride counter ions. The hydroxylated porphyrin was derived from the 5-(4-acetamidophenyl)-10,15,20-tri(3,5-dimethoxyphenyl) porphyrin (**38**), which was deprotected using boron tribromide. The isothiocyanato group was also obtained by hydrolysis of the acetamido group and conversion to the isothiocyanate using TDP as described above.

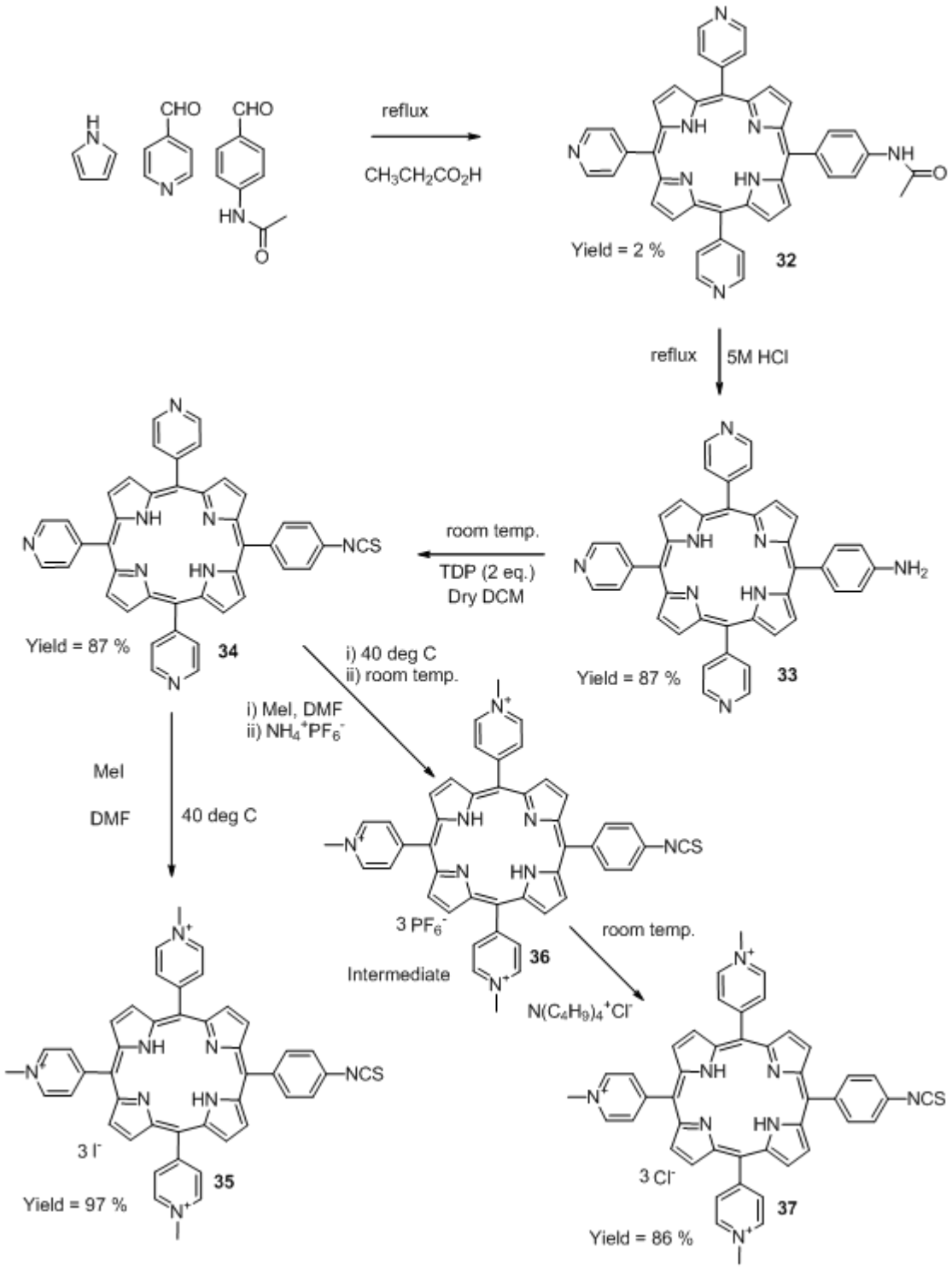

Scheme 14: Cationic isothiocyanato porphyrins obtained from 41, initially by acidic hydrolysis of the acetamido group (33) and treatment of the resulting amino group with 1,1-thiocarbonyldi-2(2H)pyridine (TDP) (34). Cationic character introduced by quaternisation of the three pyridyl groups using methyl iodide to obtain the cationic porphyrin with iodide counter ions (35). Alternatively, crude N-methylated product treated with ammonium hexafluorophosphate (36) followed by tetrabutyl ammonium chloride to yield the cationic porphyrin with chloride counter ions (37).

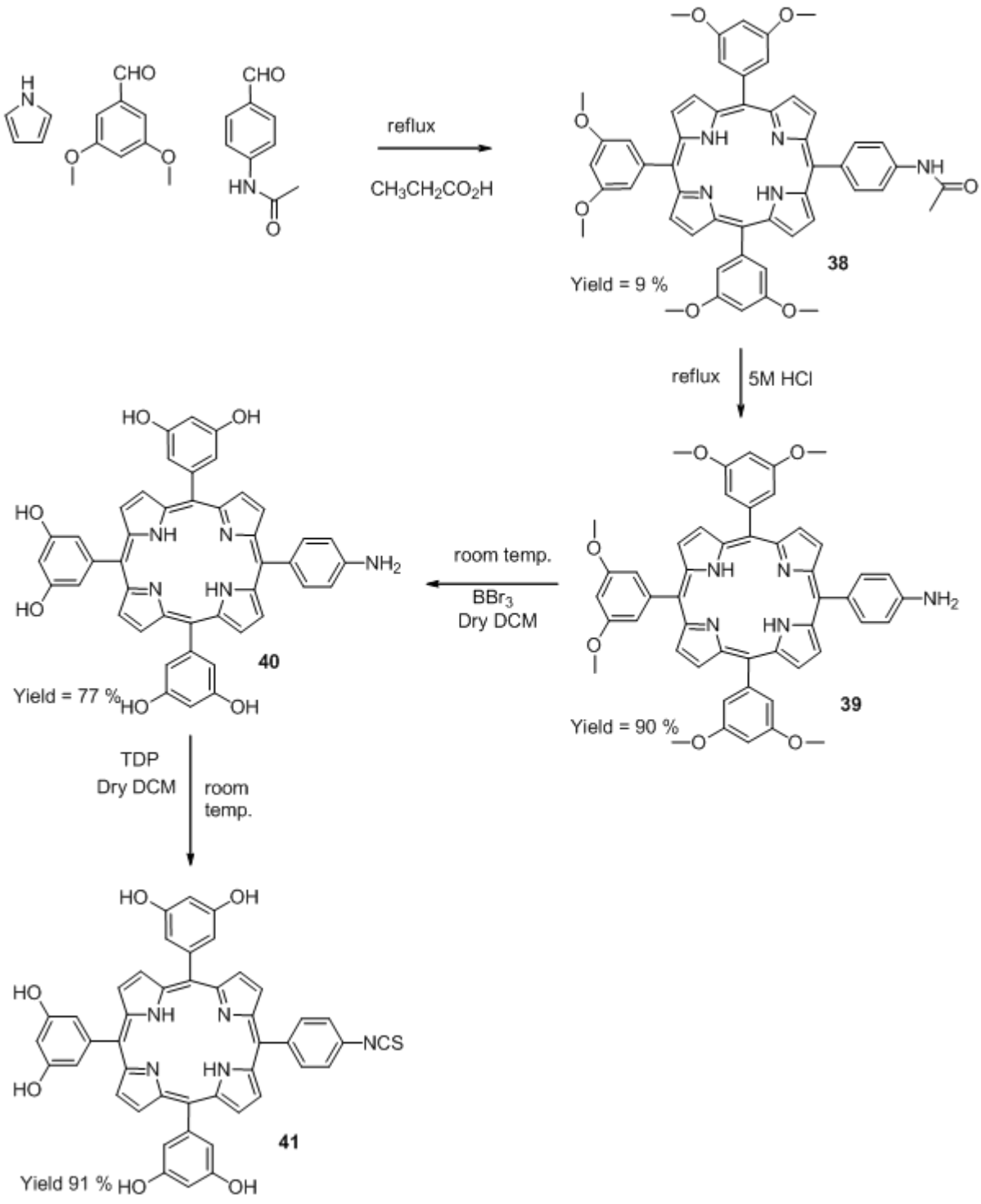

Scheme 15: The hydroxylated porphyrin derived from porphyrin 38, by acid hydrolysis of the acetamido group (39) followed by deprotection of the hydroxyl groups using boron tribromide (40). The isothiocyanato group was also obtained by conversion to the isothiocyanate using TDP (41).

2.3. Glass slides

Glass microscope slides were used to set up a method for silanising glass and to test the effect of different porphyrin molecules on the glass surface. Two different silanising methods were chosen from those in the literature (section 1.5);

- 17.5% silanising agent for 24 h at 65°C [80, 129]
- 0.1% silanising agent for 5 h at room temperature.[64, 324]

These methods the two extremes for the silanising reaction, with high concentrations, heat and a long reaction time compared to low concentrations at room temperature for a shorter reaction time. The first set of experiments used (3-aminopropyl)trimethoxysilane (APTMS)[89, 103, 138] as the silanising agent, however, as the majority of the literature deals with (3-aminopropyl)triethoxysilane (APTES)[70, 111, 134-136, 161, 272, 325-329], as reviewed in section 1.5 this was also used to determine any difference between the two as described in section 5.6. It was recognised that positive charges on the cationic porphyrin could react electrostatically with the negative charges present on the glass,[330] offering a competing reaction to formation of the desired thiourea bond between the glass immobilised amine and the isothiocyanate group on the porphyrin. This could have presented a significant problem, as electrostatic attractions, being much weaker than covalent bonds, could be disturbed during flow experiments, and the porphyrin could potentially contaminate the reaction mixture, or cell suspension. In order to determine whether this reaction would occur preferentially, two porphyrins were examined in relation to their interaction with exposed and silanised glass slides: (5,10,15,20-tetrakis(4-*N*-methylpyridiniumyl) porphyrin tetratosylate (**42**) acted as a control, as it had no reactive functional group for interaction with the amino group, but did present four positively charged quaternary amino groups that could interact with the glass

surface; 5-(4-isothiocyanatophenyl)-10,15,20-tris(4-*N*-methylpyridiniumyl) porphyrin tri idodide (**35**) was used to determine the extent of the reaction of the isothiocyanate group with the amino groups on the glass surface after silanisation (Figure 20) .

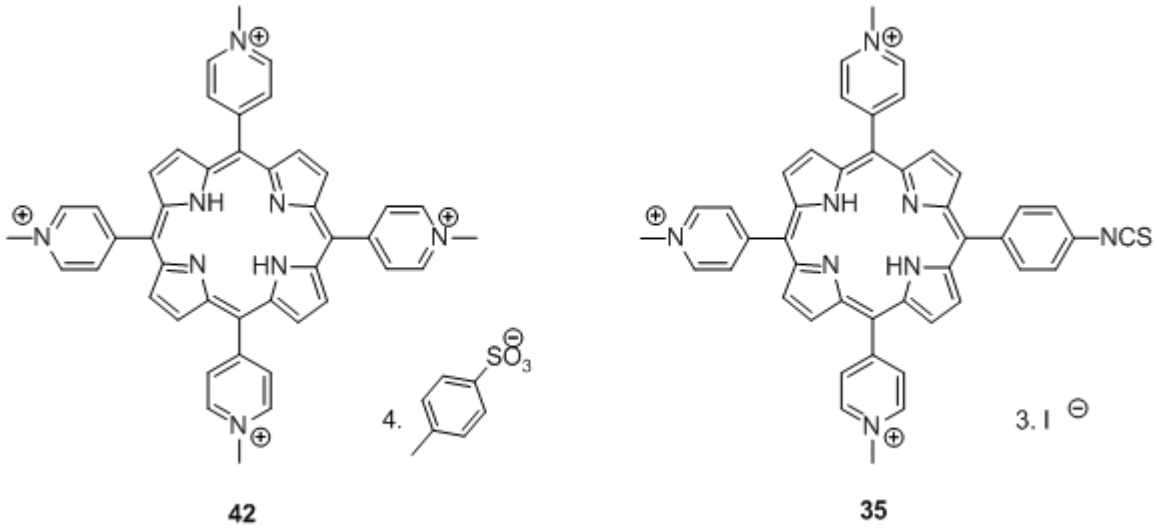

Figure 20: 5,10,15,20-Tetrakis(4-*N*-methylpyridiniumyl)porphyrin tetratosylate (42) and 5-(4-isothiocyanatophenyl)-10,15,20-tris(4-*N*-methylpyridiniumyl)porphyrin triiodide (35) used to investigate their interaction with exposed and silanised glass slides.

The first observation with these experiments was the very low concentration of porphyrin on the glass slides. The surface area of the glass slide was very low (234 mm^2). According to the literature[79], it is usual to achieve a coverage of ~2 amines/nm^2, thus the slide was likely to have less than 1 nmol of porphyrin attached to it, even if it reacted with every amine (surface area of glass slide = 234 mm^2 = $2.34x10^{14}$ nm^2; number of amino groups on glass surface = $2.34x10^{14}$ x 2 = $4.68x10^{14}$; moles of amino groups = $4.68x10^{14}$ / $6.022x10^{23}$ = $7.77x10^{-10}$ mol = 0.776 nmol). In solution, μmolar concentrations are possible to detect with the human eye, when determining the extinction coefficient a concentrations of 0.5 μmol was used, giving an absorbance of 0.135 for the Soret band at 420 nm (Figure 21). With the use of a blank the graph can be extrapolated to zero, however, taking readings at lower concentrations requires

further dilution, and leads to greater errors, therefore, accuracy can be lost at low concentrations.

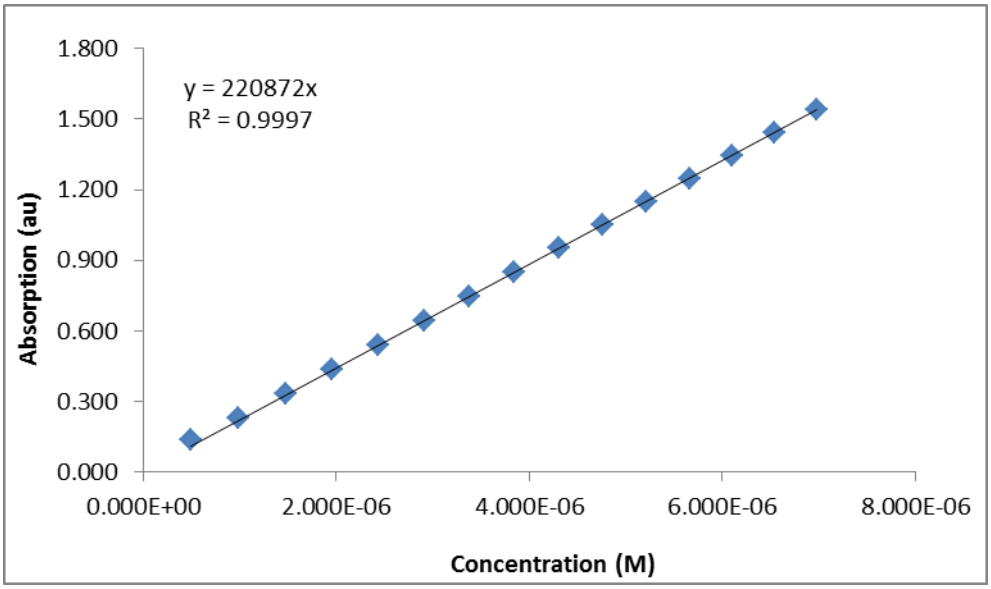

Figure 21: Calibration graph for the absorbance of tetra-cationic porphyrin.

With the high extinction coefficient of porphyrin (ε=253937 $M^{-1}cm^{-1}$ for NCS porphyrin and ε=220872 $M^{-1}cm^{-1}$ for TPyP) nmolar concentrations of porphyrin are detectable using UV/Vis spectrophotometry; however, the determination of exact concentrations are much harder due to possible dilution errors. This technique was used to compare the loading of porphyrin on the glass slide samples as described in section 6.6.2.

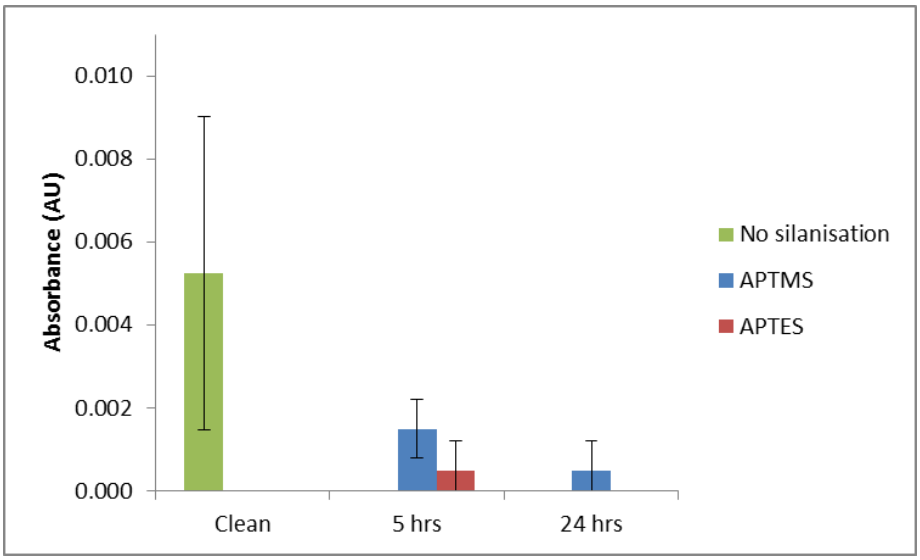

Figure 22: Graph showing the tetra-cationic porphyrin interaction with the glass slide before (clean) and after different silanisation treatments with two different amino-functionalised silanising agents.

When the tetra-cationic porphyrin (**42**) was used, longer silanisation treatments resulted in lower porphyrin concentrations on the glass surface. When there was no silanisation treatment, on exposed glass treated with piranha solution (H_2SO_4:H_2O_2 3:1), the porphyrin concentration was higher relative to those after the silanisation process. This suggests that the cationic porphyrin reacted with the negative charges on the glass surface, however, the high standard deviation shows that the reaction is very variable. The interaction could be dependent on the quality of the cleaning process or the abundance of protonated hydroxyl groups on the surface. The absorbance for the glass slide after the silanisation treatment was reduced. This implies that after the glass surface is aminated the porphyrin no longer reacts significantly with the negative glass surface, indicating that the silanisation treatment blocks the ionisable hydroxyl groups. On average, the APTES silanising agent reduces this interaction more effectively than the APTMS at shorter reaction times (Figure 22).

The tetra-cationic porphyrin was shown to react with the exposed glass surface, therefore it was surmised that the amino reactive porphyrin (**35**), with only three positive charges, would

be less reactive towards the clean glass surface. After a successful silanisation treatment a greater interaction would be expected, as the reactive isothiocyanato group interacts with the amino groups on the surface.

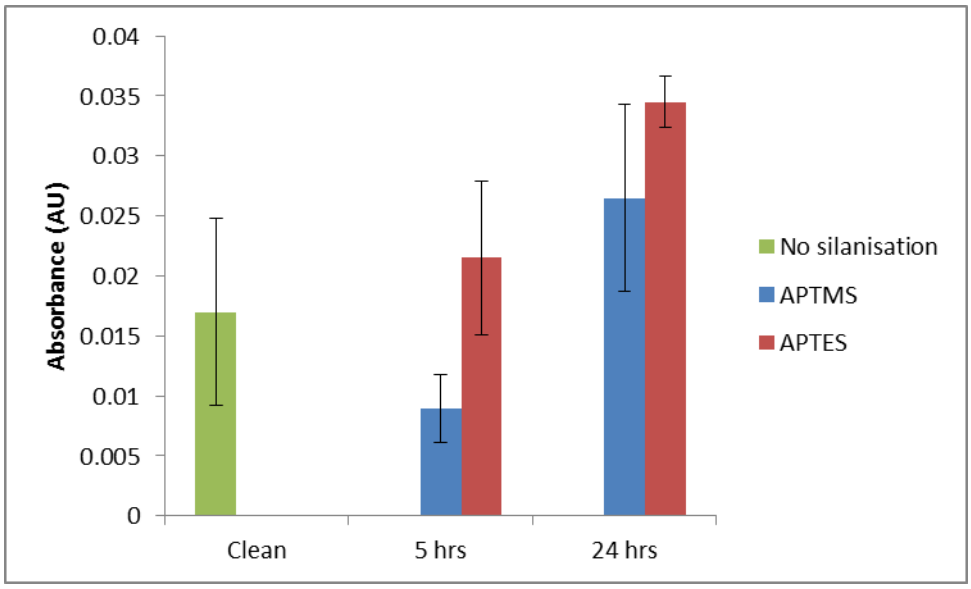

Figure 23: Graph showing the interaction of the amine-reactive porphyrin with the glass slide before (clean) and after different silanisation treatments with two different amino-functional silanising agents.

The absorbance for the amino reactive porphyrin on the exposed glass slide was higher than that of the tetra-cationic porphyrin. This unexpected result could be due to a reaction between the hydroxyl groups and the isothiocyanato groups similar to that between the amino and isothiocyanato groups. After a short silanisation period the amine reactive porphyrin was found to be in a lower (with APTMS), or similar (with APTES), concentration relative to the slide which was not silanated. However, after the longer silanisation reaction the concentration of the porphyrin on the glass slide using APTES was significantly higher than for the clean slide and the slide after 5 h silanisation (Figure 23). Wang *et al.* suggested that organic phase deposition of APTES resulted in thick layers that are rough and relatively inert.[70] Their method which gave this result relates most directly with the shorter silanisation

reaction conducted here (2% APTES solution in toluene stirred for 2 h at room temperature). This may suggest that over time at room temperature, the silanising agent produced a multilayer that rendered the amines unreactive, as they were bonding with one another. The longer silanisation reaction at reflux may enable the amines to be accessible, even if the resulting layer is a multilayer rather than a monolayer.[66, 84]

Whichever way the layers were forming, the porphyrin was reacting with the amines on the glass surface as there was only a minimal reaction between the tetra-cationic porphyrin after silanisation and an increased concentration of porphyrin when the isothiocyanate group was present. However, it also showed that the observable concentration of the porphyrin was very low and it was difficult to determine a significant difference between the concentration on the glass slide. Therefore, it was decided to try a different glass substrate in an attempt to achieve a more definite result.

2.4. Glass beads

Glass beads offer benefits over the glass microscope slides, as it is possible to work with a larger number of them simultaneously and therefore could give the opportunity of visual verification of the functionalisation. The beads used were 2 mm in size, giving them a surface area of 12.56 mm^2 per bead, and the potential of ~0.04 nmol of porphyrin per bead based on a coverage of 2 amines/nm^2 (12.56 mm^2 = $1.26x10^{13}$ $nm^2/6.022x10^{23}$ = $2.09x10^{-11}$ mol x 2 = 0.042 nmol). In large quantities (100 beads) 4.2 nmol of porphyrin could be achieved in one reaction vessel. This would be around 6 times greater than that realised with the glass slides. Further investigation into silanisation treatments suggested that a combination of the previous conditions could prove beneficial to the results. Therefore, the glass beads were refluxed with 5 % APTES in dry toluene for 5 h (as outlined in section 6.6.1).[62, 117, 129] Glass round-bottomed flasks were used for this reaction; reaction vessels of other materials (*e.g.* plastic or metal) were considered, however, plastic would degrade with the use of toluene as a solvent and it is unclear how the silanising agent would react with metal. In order to ensure the silanisation of the round-bottomed flask was not occuring preferentially to the glass beads, the first silanisation reaction was disregarded and the following reactions were conducted in the same glassware for every reaction.

Porphyrin-type molecules are often used as singlet oxygen generating catalysts[34, 176] due to a high triplet quantum yield,[33] which also results in a high singlet oxygen quantum yield. They should also have the ability to phosphoresce, however, this was found to be difficult to image and quantify. Another molecule with a high extinction coefficient and good fluorescence is rhodamine B which is available with the isothiocyante (ITC) group and is often used for imaging species by conjugation with amino groups on the molecules to be labelled.[70, 71]

2.4.1. Rhodamine B isothiocyanate

In order to test the reaction of the silanised glass beads with an isothiocyanate group and determine the sucess of the reaction, rhodamine B ITC (RhBITC) was used as outlined in section 6.6.2.[71, 331] The RhBITC was dissolved in methanol with triethylamine and the silanised beads were stirred in the solution for 24 h. The beads were thoroughly washed and sonicated, yielding glass beads that had a pink hue to them. In order to verify the attachment, the beads were visualised under a fluorescence microsocpe using the green light (λ_{ex} = 550 nm) (Figure 24).

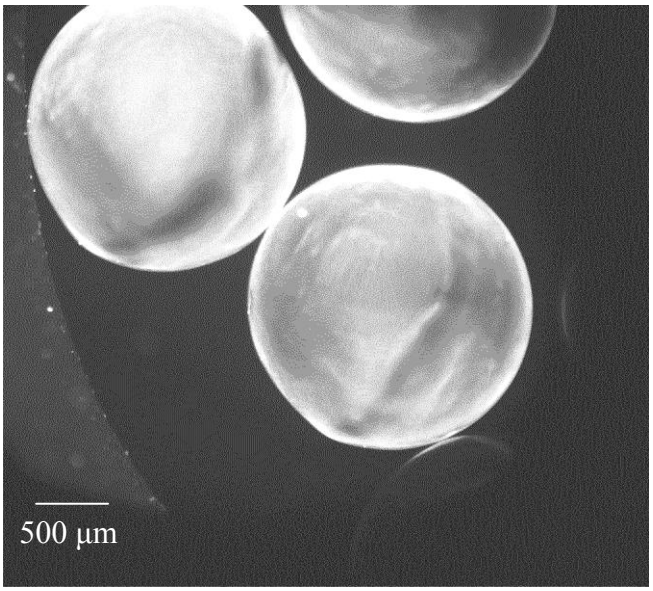

Figure 24: Fluorescent image of rhodamine B isothiocyanate immobilised on 2mm glass beads. The fluorescence can be seen reflecting off non-immobilised beads in the bottom right hand corner.

The glass beads that had not been treated with the RhBITC were also imaged under the microscope to ensure that they did not have an inherent fluorescent property. The edges of these beads can be observed in Figure 24 in the bottom right-hand corner, and are not exhibiting any fluorescence. This showed that the RhBITC was immobilised on the glass beads, and was still capable of fluorescing. This suggested that the glass substrate did not interfere with the absorption of light or the ability of the molecule to fluoresce.

2.4.2. Porphyrin

For immobilising the porphyrin dimethyl sulfoxide (DMSO) was used as the solvent and K_2CO_3 as the base as described in section 6.6.1. Due to the low fluorescence of porphyrin, in comparison to RhBITC, it was not possible to visualise them under the fluorescent microscope. This was due to the microscope used for RhBITC not having the correct filter for the excitation wavelength (λ_{ex} = 420 nm) and the microscope with the appropriate wavelength not having sufficient magnification. The only method used to determine the presence of the porphyrin on the beads was by observing the colour change, before and after the immobilisation procedure.

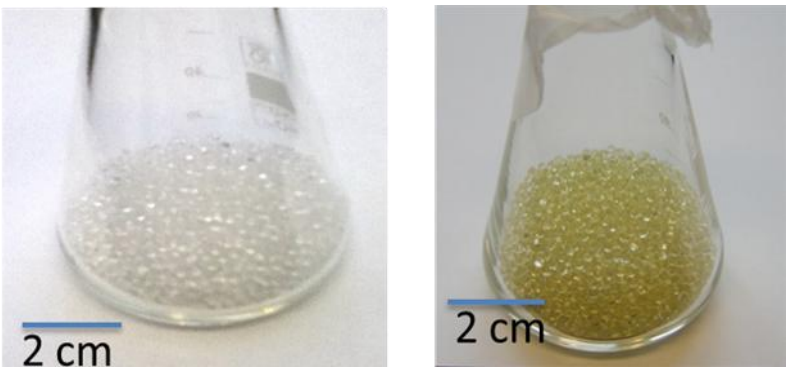

Figure 25: Comparison of the bare glass beads, on the left, to the porphyrin-immobilised glass beads, on the right. A visual identification of the success of the immobilisation was used to confirm.

These pictures show that the porphyrin-immobilised beads had a very clear yellow colour (Figure 25). The cholesterol assay used in section 3.3 for the porphyrin-immobilised chip was used to determine the presence of the porphyrin on the glass beads. It was found that the oxidation of cholesterol was realised using them, proving that the porphyrin was immobilised and that it was capable of producing reactive oxygen species.

The reactions of the RhBITC and the porphyrin with the glass beads were thus used as an alternative to the glass slide and a precursor to the glass channels within the microfluidic device.

2.4.3. Rose bengal

The immobilisation of rose bengal (RB) onto polymers and control pore glass is an established method.[20, 21, 200] The reaction between a chloroalkyl group and the carboxylate anion on RB produces a covalent bond. Using controlled pore glass it was possible to immobilise RB, first through functionalising with CPTMS and then by reacting with RB. This was used to investigate synthetic transformations involving singlet oxygen under flow conditions which will be reported in section 3.2.

2.5. Glass microdevice

2.5.1. Rhodamine B isothiocyanate

In accordance with the methods used for the glass slides and beads, RhBITC was used to determine a successful procedure for immobilisation on the glass channels within the microfluidic device. A number of methods were attempted in order to achieve a consistent coverage of photosensitiser on the glass channels, the final method is outlined in section 5.6. It was found that after cleaning the chip with piranha solution (H_2SO_4:H_2O_2 3:1) it was necessary to neutralise the glass surface by treating it with a basic solution. The piranha solution consists of a strong acid and hydrogen peroxide which strips the surface of any residual organic matter; it was therefore hypothesised that the acid protonated the hydroxyl groups on the surface of the glass. The silanising agent requires the deprotonated form of the hydroxyl groups in order to react efficiently; therefore by passing a basic solution through the chip, deprotonation of the hydroxyl groups should have taken place, leaving them more reactive to the silanising agent. The chips were, therefore filled with an aqueous solution of sodium hydroxide (1 mM) for 1 h prior to silanisation.

It was also found that by backfilling the chip before introduction of the reagent, a more even filling of the channels occurred, giving a complete covering of the silanising agent and the photosensitiser molecule. An optimisation of the method was performed in order to produce a chip, as in Figure 26**,** in which the colour of the immobilised molecule was observable and gave a comprehensive coverage throughout the chip.

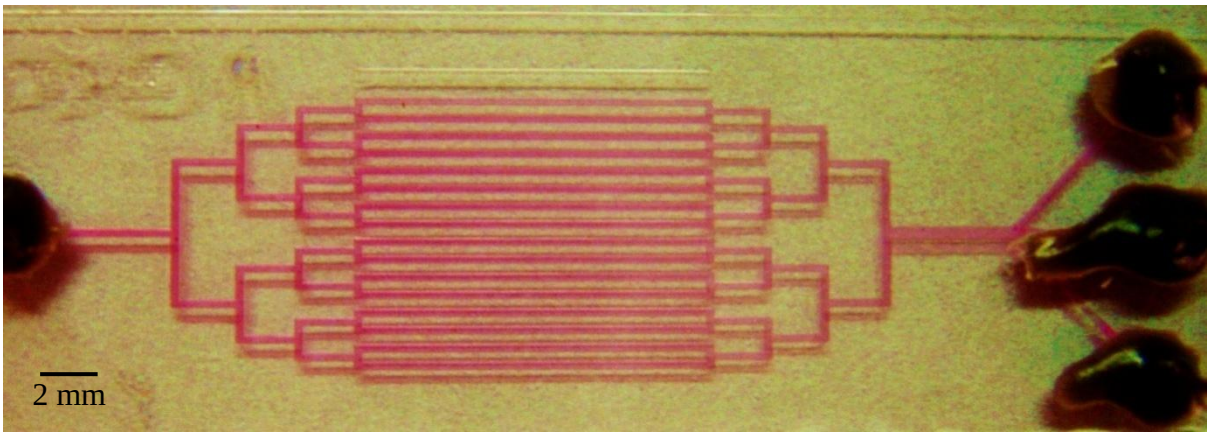

Figure 26: Parallel channel microfluidic chip showing the immobilised RhBITC on the surface of the channels (dry).

As with the glass beads, it was necessary to ensure that the molecule was capable of fluorescing whilst immobilised in the glass channels. Therefore, the chip was imaged under the fluorescence microscope.

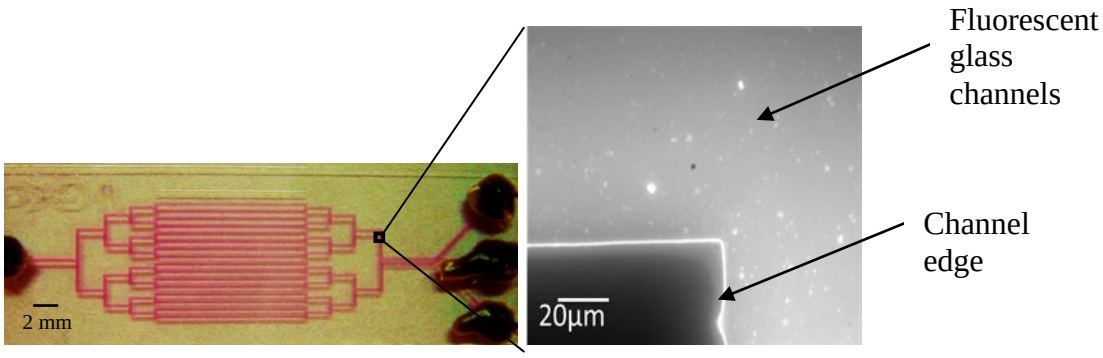

Figure 27: Fluorescent image of RhBITC-immobilsed channel under green light (λ_{ex} = 550 nm).

The image shows that fluorescence was present across the channel. This was a encouraging result for the success of the immobilisation method.

This technique was also attempted for the serpentine chip (design C). The channel width for this design was much smaller than the parallel channel chip (75 µm as opposed to 200 µm), in addition the increase in the length of the channel resulted in an increase in back pressure. This increase in pressure made the process of backfilling the channels, and maintaining a

constant flow of solution through them, much more difficult to accomplish. Therefore, an even coverage of RhBITC on the serpentine channel walls was not possible. A partial immobilisation of RhBITC was observed by eye; however, no fluorescence was observed under the microscope. It may have been possible to optimise this process to make it more successful; however, other factors were considered a higher priority.

2.5.2. Porphyrin

The method that was optimised for RhBITC was then transferred to the amino-reactive porphyrins. It was not possible to visualise the porphyrin in the chip, either by eye or by fluorescence. The only possible way to prove the presence of the porphyrin on-chip was by using it to produce singlet oxygen. These reactions are outlined in the next chapter.

2.5.3. Rose Bengal

The immobilisation of rose bengal onto the surface of the channels inside the parallel channel chip (design B), was attempted. Due to the forcing conditions required for this reaction to take place in solution, it proved difficult to successfully discern the correct conditions for the reactions to take place within the chip. For the silanisation reaction (on controlled pore glass) a much higher concentration of CPTMS is used than for APTES in the previous reactions, both on glass beads and within the chip. This suggests that the reaction is less favourable. This would concur with the information gained from the amination of the glass slides.

The reactions within the chip were conducted with pure silanising agent without diluting it in a solvent. To ensure that it did not cause the chip to block, it was pumped through at a flow rate of 10 μL min^{-1}. Various attempts were made to functionalise the chip with RB after silanisation; a high concentration of RB (4.7 mM) in DMF was pumped through the chip at 5 μL min^{-1} either at room temperature or with mild heating (40 °C). When this was imaged

under the fluorescent microscope it was possible to see RB residue on the channel walls. However, this suggests that it had not coated the channels in the same way as RhBITC. Due to time considerations, the immobilisation of RB onto the glass channels was not continued. In order to further this work it would be useful to have a systematic optimisation of this method. Looking initially at the silanising procedure, with a dilution of CPTMS in toluene, would be a better starting point as it has been shown to work with APTES in this current research.

2.6. Conclusion for immobilisation techniques on glass

This chapter has outlined the methods used to immobilise the porphyrin photosensitiser to the glass channels of a microdevice. By working from the glass slide, to glass beads and then, finally on-chip, it has been shown that it is possible to react the ITC group of fluorescent molecules and porphyrins with the amino groups produced through the silanisation of the glass with APTES.

Although similar experiments were attempted between chloro groups from a silanising agent and the carboxylic acid group of RB, these reactions proved to be more challenging on non-porous glass substrates. Therefore the major focus of the project was directed towards the use of the porphyrin-immobilised microdevice, and the RB-immobilised controlled pore glass for the production of singlet oxygen through chemical transformations.

Chapter 3.

Chemical applications of porphyrin-immobilised chip

In this chapter, chemical applications of the porphyrin-immobilised chip are investigated. The oxidation of cholesterol is used as a model reaction by which to explore the optimal parameters for singlet oxygen production on-chip. Aspects that were looked at are the light source, oxygen concentration, the effect of flow rate, and therefore, residence time, and the impact of repeated exposure on the porphyrin layer. Once the optimum parameters were established, the porphyrin-immobilised chip was used to investigate other singlet oxygen mediated reactions. The [4+2] reaction of α-terpinene, and the ene reaction of citronellol were used, as these are well established procedures in the literature,[26, 27, 34, 172, 176, 178, 179, 182, 206, 216, 228, 231-235, 239, 244, 252, 259, 260, 283, 332, 333] and have been used by other groups to establish the effectiveness of microfluidic devices for reactions involving singlet oxygen along with many other photosensitised reactions.[26, 53, 225, 252-254, 259-263, 268, 269, 275, 280, 332, 334, 335] These are discussed in the introduction, section 1.6, in more detail.

3.1. Aims for chemical applications of the porphyrin-immobilised chip

The aim was to determine how effective the immobilised porphyrin was at producing singlet oxygen. In order to do this, a number of reactions were performed to compare singlet oxygen production in various environments. It has been reported in the literature that rose bengal has been attached to gels and polymers[22, 23, 336] and successfully produced singlet oxygen. The method can easily be used in conjunction with controlled pore glass (CPG). The starting point of these experiments was to use rose bengal immobilised on CPG and packed into a microfluidic chip (design A) for photo-oxidation of cholesterol. This was compared to rose bengal in solution as a batch reaction, and rose bengal in solution through the parallel channel chip (design B), using cholesterol as the singlet oxygen reactant. This showed that singlet oxygen could be produced within microfluidic devices using an immobilised photosensitiser, giving a starting point for examining the porphyrin-immobilised parallel channel chip (design B).

The porphyrin-immobilised chip should be able to produce singlet oxygen in a reproducible fashion, and it was the aim of this section to determine the optimal procedure for this. Therefore, experimental parameters such as the light source, flow rate, and repeated exposure of the immobilised porphyrin were examined to produce the best results. Once these were optimised the aim was to show that the immobilised porphyrin would be effective for a number of different singlet oxygen mediated chemical reactions.

3.2. Photo-oxidation using Rose bengal as sensitiser

Rose bengal (**43**) (Figure 28) is a good photosensitiser with high singlet oxygen quantum yields (0.76 in MeOH and DCM[33]). It is readily available and easy to manipulate, as it dissolves well in a number of different solvents. It also has a sodium salt of a carboxylic acid group which was used to immobilise it on to chloroalkane groups silanised on to the porous glass. In the following, it was used to explore effective methods for determining singlet oxygen production from immobilised photosensitisers. A light source that gave sufficient fluence for singlet oxygen production was investigated, along with a good singlet oxygen acceptor that would prove useful for comparing the various methods.

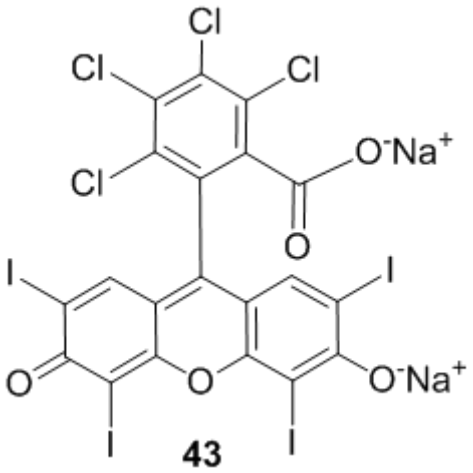

43

Figure 28: Structure of rose bengal showing the salt of the carboxylic acid which is used for attaching to the chloroalkyl- substituted CPG.

3.2.1. Light source

Two light sources were investigated (Section 6.7.2); LEDs emit a cold light, negating the need for any cooling, but their low output (0.27 W) reduces the fluence maximum; the second light source investigated, a Xe arc lamp, produces a lot of heat, due to significant emission in the infrared region, however it also provides a greater power output (3.5 W), resulting in higher fluence maximum. The distance of the light source from the reaction can reduce the power at the working surface, due to diffusion of the beam. In order to determine the power of the effective light on the reaction, it is necessary to measure fluence as near to the point of absorption by the photosensitiser as possible. Fluence is a measure of light intensity over a defined area: W cm^{-2} and can be determined from the output of the light source and the radius of the light beam. The LED had a wide light beam, so even when the light source was at a distance of only 1 cm from the reaction the fluence at the working surface is only 0.11 W cm^{-2}, whereas the Xe arc lamp produces a smaller radius light beam which, coupled with the higher power output, gives a higher fluence of 0.66 W cm^{-2} when the light source is 3 cm from the reaction. In a totally microfluidic regime, an LED is preferred as it is small, and easily incorporated, however, it needs to be as efficient as the bigger, more powerful light source. Experiments comparing the two light sources are discussed in section 3.2.3.

3.2.2. Photo-oxidation of 1,3-diphenylisobenzofuran by rose bengal

1,3-Diphenylisobenzofuran (DPBF) (**22**) can be used as a probe to quantify the production of singlet oxygen in solution,[36] as discussed in section 1.6.1. The starting molecule is fluorescent (λ_{ex} = 415 nm [36]), upon the addition of oxygen the furan ring is cleaved and the resulting molecule is no longer fluorescent (Scheme 11). Further information is given in section 1.6.1. Therefore, fluorescent decay enables determination of singlet oxygen production over time.

The purpose of this work was to determine the extent of singlet oxygen production from RB-CPG (as described in section 6.7.1) within a packed chip in comparison to that of RB in solution. The batch reaction was conducted by mixing a solution of photosensitiser (1, 2 or 3 μM) with a solution of DPBF. It was irradiated with light and the fluorescent decay was analysed on the fluorescence spectrometer following the concentrations in table 3 (section 6.7.1). The production of singlet oxygen by RB-CPG was investigated by packing it into the chip (design A) and pumping a solution of DPBF through the chip. This was irradiated with light, and the solution collected at the outlet. This resulting solution was also measured on the fluorescence spectrometer. The method was first trialled using batch processes; a solution of RB and DPBF in acetonitrile. It was found that the white light from the Xe arc lamp caused some decomposition of DPBF and loss of fluorescence was observed even in the absence of a photosensitiser. Therefore, a solution of DPBF was exposed to the same conditions in the absence of photosensitiser as a control sample. In addition, a bandpass filter was used that allowed transmittance of light between 320-680 nm, exciting RB at 550 nm[26] but reducing the degradation of the DPBF. At 550 nm the transmittance was 62 % which was sufficient to excite the RB. It was found that the DPBF still lost a significant amount of

fluorescence in the absence of RB, but that this was accelerated in the presence of RB (Figure 29).

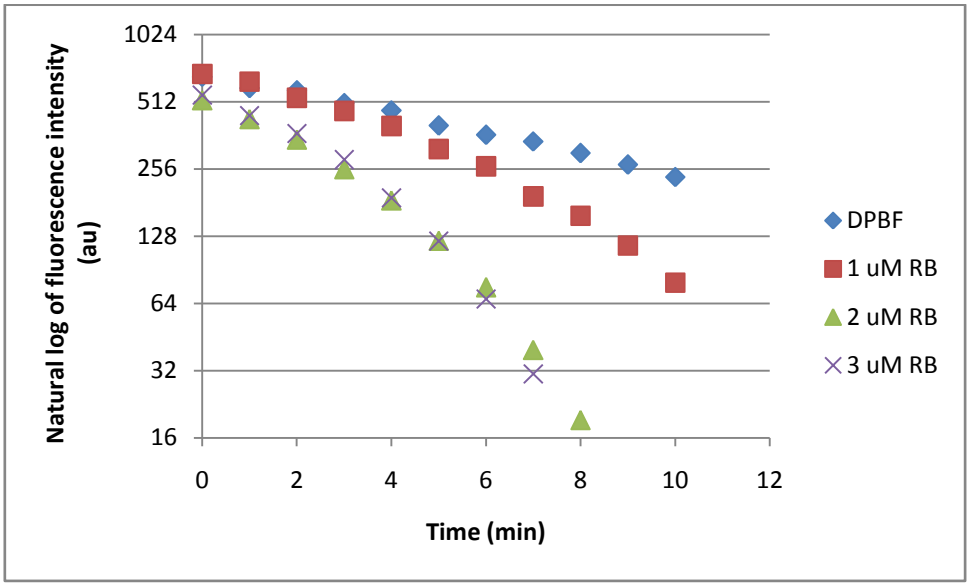

Figure 29: Graph showing the decrease in the natural log of fluorescence intensity of DPBF in the absence of RB and with 1, 2, and 3 µM solutions of RB. It can be seen that the fluorescence decays faster in the presence of rose bengal.

These results were encouraging, showing that RB caused a reduction in fluorescence of the DPBF; however, the fluorescence was also reduced in the absence of RB. This loss of fluorescence without photosensitiser could cause problems in the definite identification of singlet oxygen decay. When this was transferred into the chip packed with CPG-RB the effect was more noticeable (Figure 30). The rapid loss of fluorescence was first attributed to the photosensitiser, but when the experiment was repeated with blank CPG packed in the chip, a very similar loss of fluorescence was observed

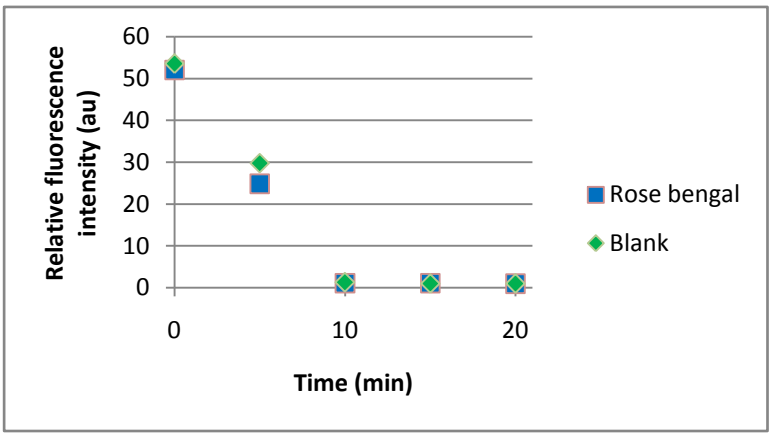

Figure 30: Graph showing the decrease in fluorescence intensity of DPBF through the packed chip when packed with RB-CPG and blank CPG.

The similarity in the plots for the blank experiment and that with RB shows that DPBF in this case was not useful in determining singlet oxygen quantum yields. A different filter may have improved the direct photo-degradation of DPBF by the light, however, it was decided that using a reagent that was less sensitive to light alone would give a better result. Therefore further experiments were conducted with cholesterol as the singlet oxygen probe.

3.2.3. Photo-oxidation of cholesterol by rose bengal

The reaction of cholesterol is a useful marker of the type of photooxidation taking place, as explained in 1.6.1.[35] Here it was used to monitor the production of reactive oxygen species (ROS) by photosensitisers in batch reactions, in solution through the chip and whilst immobilised to the microfluidic channels. The quantitative analysis was achieved using HPLC by comparing the concentration of starting material with the concentration of oxygenated species.

The experiments with RB as a photosensitiser were conducted with the Xe short arc lamp and the LED light to determine the effect that these light sources had on the singlet oxygen production. This is described in section 6.7.2 and the flow rates and fluence rates are

outlined in table 4 of the same section. A solution of rose bengal (20 μM) was made in MeOH:DCM (1:9) and mixed 1:1 with a solution of cholesterol (10 mM) in the same solvent mix. Experiments were conducted with three different reaction vessels. Batch experiments were conducted with 10 mL of the reaction mixture in a conical flask; the packed chip was used with RB-CPG and a 5 mM solution of cholesterol in the same solvent mix and finally the parallel channel chip with 1 mL of the reaction mixture pumped through the chip at various flow rates. Each of these was attempted with the LED and the Xe arc lamp in order to compare their suitability to initiate production of singlet oxygen from the photosensitiser (Figure 31).

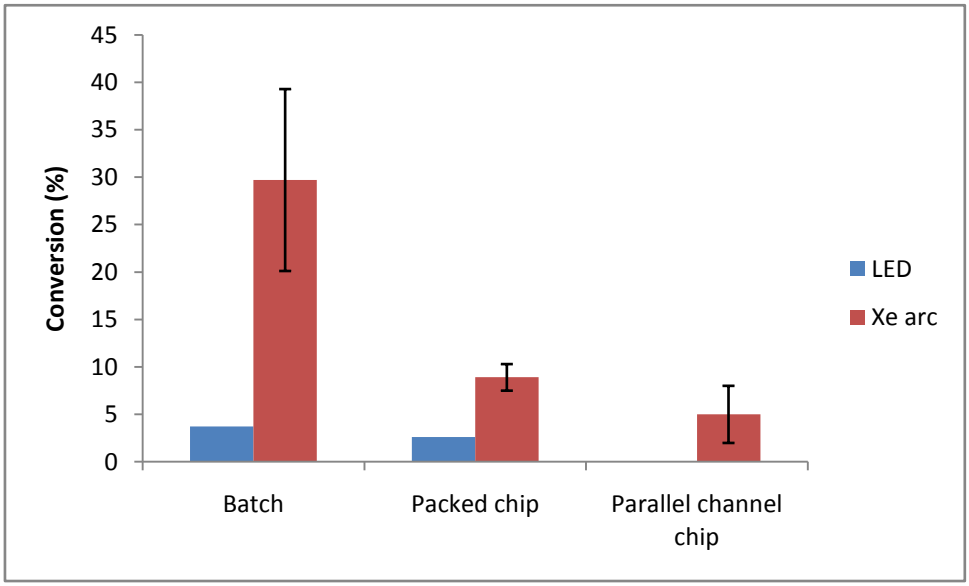

Figure 31: Graph to show the extent of oxygenated cholesterol produced from different light sources. This is calculated as the amount of all oxygenated cholesterol products as a % of all cholesterol species. The superiority of the Xe arc lamp (3.5 W) over the LED (0.27 W) is evident, especially for the parallel channel chip in which no conversion was observed using the LED.

The batch reactions were conducted with the addition of oxygen, and produced a high conversion to the oxidised cholesterol products. The microfluidic experiments were conducted without the addition of oxygen as the packed chip was not designed for oxygen.

These experiments were designed to determine the effectiveness of the light sources which consistently proved that the Xe arc lamp was more effective than the LED (Figure 31). Therefore, the Xe arc lamp was used exclusively for all other experiments.

By changing the flow rate for the microfluidic devices the residence time of the solution in the chip and therefore the fluence rate of this light was also altered. A set of experiments was conducted to determine the effect changing flow rate would have upon the oxidation of cholesterol (Figure 32). The experiments were conducted as stated above for the effect of the light source but concentrating purely on the microfluidic regime to determine the effect of flow rate. The reaction conditions are outline in table 5 (section 6.7.2)

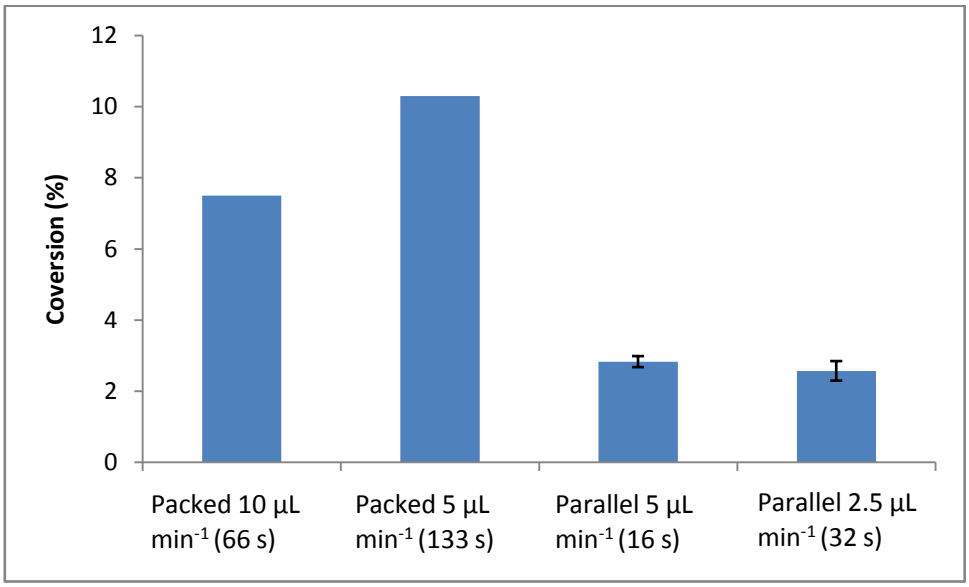

Figure 32: Graph showing the effect flow rate had on the photo-oxidation of cholesterol within the microfluidic devices. Packed (design A) at 10 and 5 µLmin^{-1} (giving a residence time of 66 and 133 seconds respectively) and Parallel (design B) at 5 and 2.5 µLmin^{-1} (giving a residence time of 16 and 32 seconds respectively). Conversion was calculated by taking all the oxidised cholesterol products as a % of the total cholesterol species.

This showed that for the packed chip, although only one experiment was conducted for each flow rate, reducing the flow rate to 5 µL min^{-1} (residence time of 133 seconds) resulted in an increase in the production of singlet oxygen. For the parallel channel chip, in which the

photosensitiser was in solution with the cholesterol, there was no significant difference in the production of singlet oxygen. The packed chip at 5 μL min^{-1} gave the best microfluidic production of singlet oxygen. This was because the residence time for this reaction was much longer than for the other reaction conditions. Also the constant irradiation of the immobilised photosensitiser would lead to more ROS, and the increase in residence time resulting from the slower flow rate would enable a more efficient oxygenation process for the cholesterol solution. Also, with an increase in total volume in the packed chip compared to the parallel channel chip, the total residence time, and therefore, irradiation time is increased. At the slowest flow rates, the maximum residence time of 133 s for the packed chip is much higher than for the parallel channel chip (32 s). Therefore, there would be more time for the reaction to take place in the packed chip than the parallel channel chip. The fastest flow rates were chosen to ensure that there was a measurable quantity of oxidised products to analyse. It was found that by reducing the flow rate below 2.5 μL min^{-1} an increase in temperature (>35°C) caused the small volumes of solvent to evaporate and caused problems in analysis. Therefore, these flow rates were used throughout the project.

In order to produce singlet oxygen for the oxidation of cholesterol, molecular oxygen is needed. As the reaction occurred without the addition of oxygen to the system, there must be some present in the system, however, it is possible that it was used up quickly, as is known to happen with *in vivo* PDT[40]. Therefore, the addition of oxygen to the system should increase the oxidation of cholesterol. To test this hypothesis, various experiments were repeated with oxygen introduced to the system. Due to the design of the packed chip (with only one inlet) there was no way of introducing oxygen to the packed chip; hence this investigation was conducted as a batch reaction and through the parallel channel chip only, but at different flow rates for the chip reaction (Figure 33).

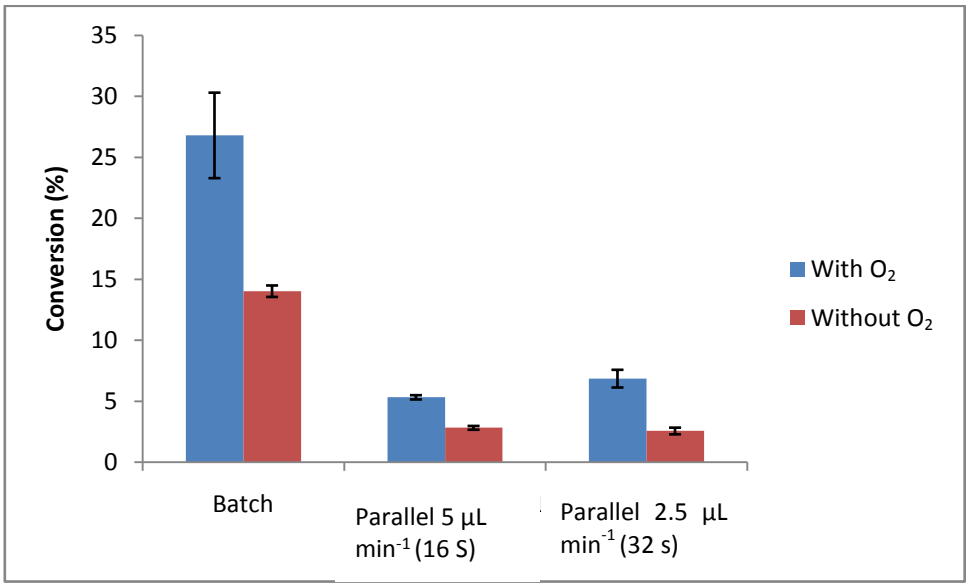

Figure 33: Graph to show the effect of additional oxygen to the system for the oxygenation of cholesterol in a batch and parallel channel chip configuration. Conversion is calculated by taking the oxidised cholesterol products as a % of total cholesterol species

The addition of oxygen to the system increased the oxidation of cholesterol in all three experiments. This is to be expected as it would produce a greater supply of oxygen to be transformed into singlet oxygen for the reactions. The addition of oxygen to the parallel channel chip experiment also caused a greater difference between the two flow rates. The increase between the two flow rates is still minimal, but shows that the reaction produces more singlet oxygen at the slower flow rates and with additional oxygen. By halving the flow rate, the residence time doubles from 16 s to 32 s. The batch reaction took place over 60 min (3600 s) and was therefore, much less efficient. Further examination into the efficiency of these reaction vessels will be given in section 3.3.4.

3.3. Photo-oxidation using porphyrin as sensitiser

As described in chapter 2, the immobilisation of porphyrin was conducted within the glass channels of the parallel channel chip. To determine the effectiveness of this immobilisation and whether it is capable of producing ROS, various chemical reactions were conducted on-chip. Initially the ene reaction of singlet oxygen with the double bond in cholesterol was used to determine if the porphyrin was present. Once this was verified, other industrially useful reactions were attempted within the chip to compare with the same reaction in batch mode. First the [4+2] reaction of α-terpinene with singlet oxygen was conducted, then another ene reaction with citronellol.

3.3.1. Photo-oxidation of cholesterol by porphyrin-immobilised chip

Cholesterol is a useful reagent for determining the production of singlet oxygen, as used in the previous section. The effectiveness of the immobilised porphyrin in producing singlet oxygen was determined through comparison of the batch reaction and the porphyrin in solution through the same chip. To ensure comparable results, the same porphyrin that was immobilised to the glass was capped at the isothiocyanato group with propylamine when used for the batch and solution experiments. This resulted in the same thiourea bond used to covalently link the porphyrin to the glass surface, but with a short alkyl chain in place of the glass (Figure 34).

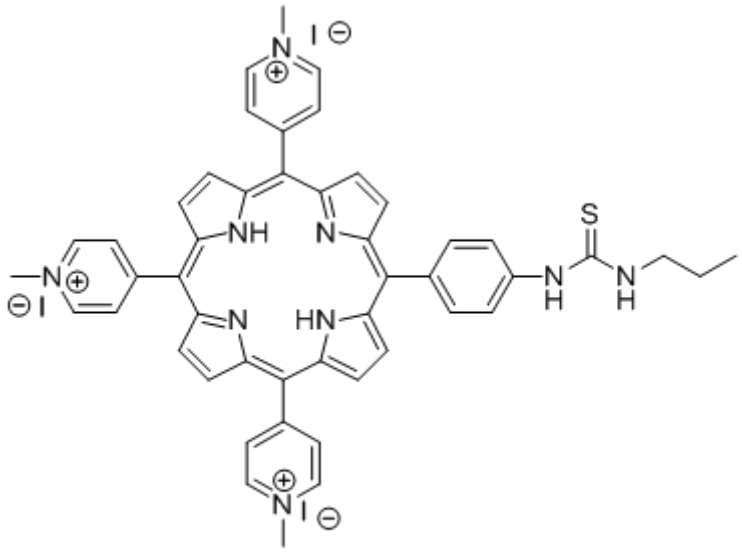

44

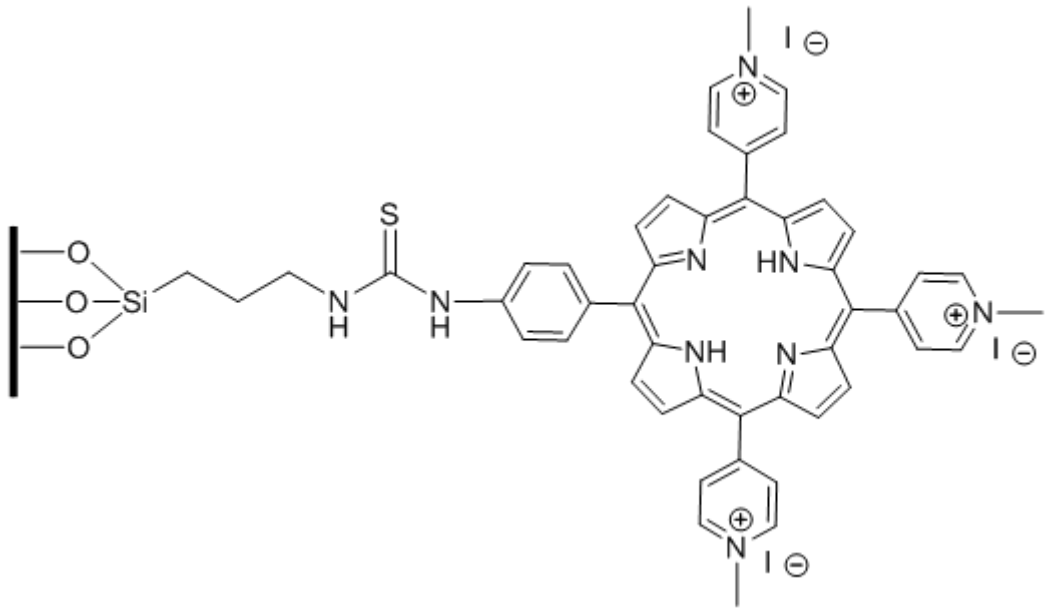

Figure 34: Capped porphyrin (44) used for the experiments with the photosensitiser in solution with the cholesterol and the porphyrin immobilised onto the glass surface of the microfluidic channels.

The capped porphyrin was then made into a 20 μM solution in MeOH:DCM (1:9) to be mixed 1:1 with a 10 mM solution of cholesterol in the same solvent mix. As the 10mM solution of cholesterol was subsequently mixed with the porphyrin solution the resulting cholesterol concentration in the reaction mixture was 5 mM. Therefore, the experiments with

the porphyrin-immobilised chip were conducted with a 5 mM solution of cholesterol in the same solvent (Figure 35). These conditions are summarised in table 6 (section 6.7.2).

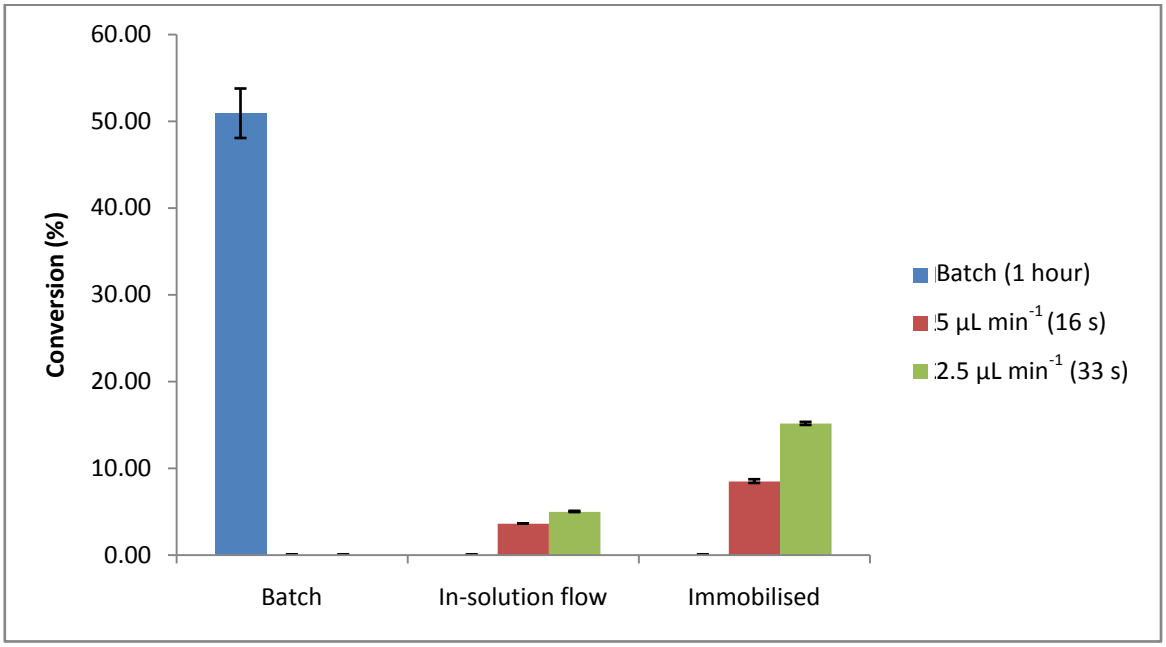

Figure 35: Graph to show the effectiveness of the immobilised porphyrin to cause the oxidation of cholesterol in comparison to the porphyrin in solution in batch and through the chip. Conversion is calculated by taking the oxidised cholesterol products as a % of total cholesterol species.

This proved that porphyrin was immobilised onto the glass surface of the chip, and that it was capable of producing ROS. This was an encouraging result, showing that the immobilisation procedure was effective. In addition to this, it also appeared that the immobilised photosensitiser was more effective at oxidation of the cholesterol than when it was in solution. This is a similar result as seen for the CPG-RB packed chip in comparison to RB in solution through the parallel-channel chip. This was a positive result as it proved that the glass was not effecting the photosensitiser and it was still capable of producing singlet oxygen.

With the ability of the immobilised porphyrin to produce singlet oxygen proven, the next aspect was to determine the stability of the porphyrin over time, as photobleaching is a well-

known phenomenon for photosensitisers generally. For these experiments, 100 μL fractions were collected sequentially from the chip whilst constantly irradiating and the resulting oxidation of cholesterol was determined as previously (Figure 36). The irradiation times equate to 20 and 40 min per 100 μL for a flow rate of 5 and 2.5 μL min^{-1} respectively.

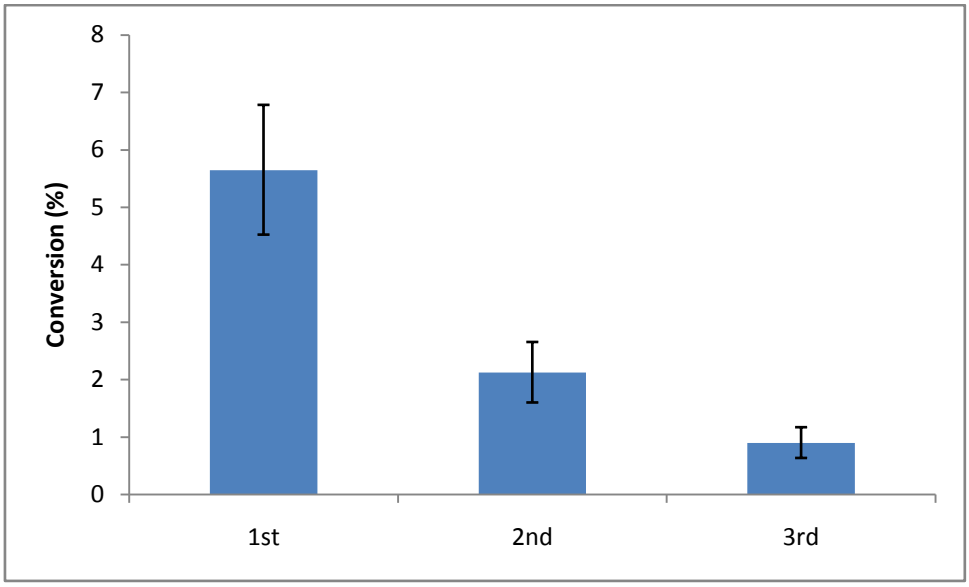

Figure 36: Graph to show the effect of repeated exposure of the immobilised porphyrin to light. Conversion is calculated by taking oxidised cholesterol products as a % of total cholesterol species.

The data shown in Figure 36, which relates to a flow rate of 2.5 μL min^{-1}, clearly shows a decrease in effectiveness of the porphyrin. This could be a problem for the applications of the porphyrin-immobilised chip, either for chemical or biological applications. It may be possible to investigate other porphyrins, or alternatively to utilise a metal complex of the porphyrin. Some metals are known to increase the photostability of the porphyrin and would be a good starting place for further investigation.[184] However, cleaning and coating of the chips is a relatively routine process, so if necessary multiple chips could be rotated in a use – clean – coat cycle, to ensure maximum efficiency of the photosensitiser.

3.3.2. Photo-oxidation of α-terpinene using porphyrin-immobilised chip

A well-known synthetic transformation involving singlet oxygen is the conversion of α-terpinene (**18**) to ascaridole (**19**), which proceeds in high yield when performed in batch (Scheme 8, section 1.6.1). In order to analyse the results from these experiments it was necessary to be able to determine the starting material from the more polar product or other by-products. GC was used initially as this gave a good separation between the starting material and the product. However, problems occurred with the batch reactions in which the porphyrin, which was in solution with the reagents, would block the GC column, as it has low volatility, and hence did not evaporate, but combusted at higher temperatures. RP-HPLC was then investigated, which appeared to give good results and a good separation between α-terpinene and ascaridole. After a number of experiments were conducted, it appeared that the starting material was oxidising over time, and the starting material had a high percentage of ascaridole present. This was based on observing an increase in signal at 11.5 min during the batch reaction; however, this was based on the assumption that this was ascaridole. To determine the validity of this assumption the starting material was analysed by LC-MS. However, it did not prove possible to obtain an MS on this product in the electrospray ionisation mode (ESI). It was tested again on the GC-MS and a good separation was obtained, in addition to determination of the constituents. With careful workup of the mixture after the batch reaction, it was possible to dissolve the products in hexane, in which the porphyrin is not soluble, and thereby analyse all experiments solely using GC-MS as described in section 6.7.3. It was found that α-terpinene produced some oxygenated products such as eucalyptol and other oxabicyclo structures in the early stages of the photo-oxidation. These have similar structures to ascaridole and could have been seen on the HPLC-UV with

the same retention time. However, after further irradiation, the ascaridole was formed in high yields, in the batch experiments (Figure 37).

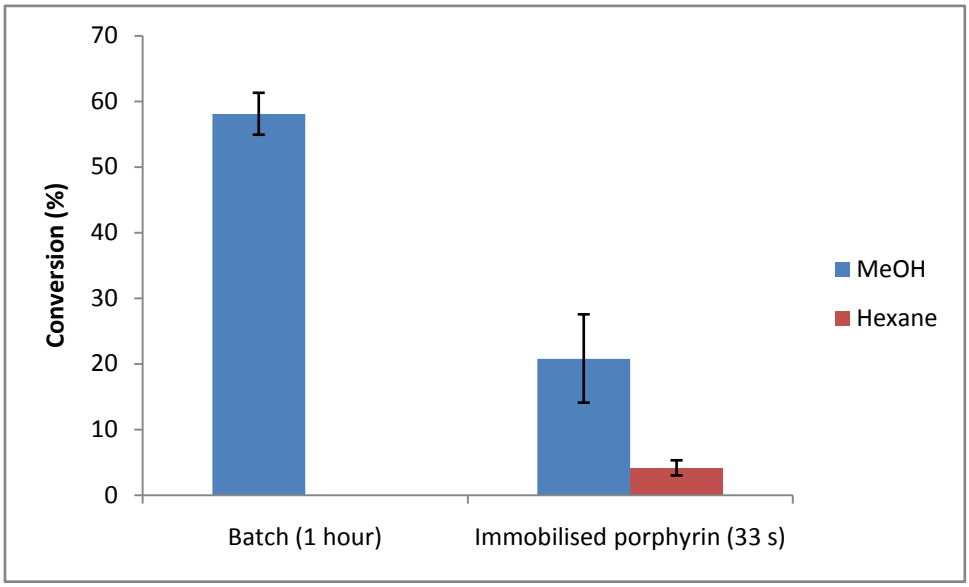

Figure 37: Graph showing the results from the oxidation of α-terpinene in batch and within the porphyrin-immobilised chip. Conversion is calculated by the ascaridole production as a % of starting α-terpinene concentration.

Over the one hour irradiation for the batch reaction, a high percentage was achieved on a consistent basis. However, this result included a large number of by-products which would need to be separated in order to obtain a pure product. The on-chip oxidation through the porphyrin-immobilised chip showed a good yield with fewer by-products, the batch reaction gave four unwanted products as opposed to the microfluidic reaction with no unwanted side products. However, overall the porphyrin-immobilised chip was not as high yielding as in batch which was expected from comparison with the cholesterol experiments. It also shows that an advantage with the on-chip reaction is the reduction in side reactions which could result in a much purer final compound with more optimisation. When the on-chip reaction was conducted in methanol the yield was much higher than in hexane. This was not the result that was expected; methanol has hydroxyl groups which are thought to quench the singlet

oxygen giving it a much shorter lifetime[214]. Therefore, in hexane the lifetime of the singlet oxygen should be longer and should produce a higher yield, as the singlet oxygen produced from the porphyrin immobilised on the surface should travel further into the solution. However, with the porphyrin being water soluble, and therefore having a greater solubility in methanol, it could be that the solvent was capable of carrying the α-terpinene closer to the porphyrin, and therefore to the singlet oxygen also. It is also likely that the hexane caused the porphyrin to be forced closer to the glass surface affecting the excited state of the porphyrin. In addition to this, the standard deviation from the results in methanol suggests that there were other factors that caused an increase in photo-oxidation. Further investigation may be required to determine reaction parameters that affect the photo-oxidation.

3.3.3. Photo-oxidation of citronellol using porphyrin-immobilised chip

The oxidation of citronellol (**16**) is another example of an ene-type oxidation using singlet oxygen. The reaction is very useful in the perfume industry as it enables the production of rose oxide[179] (Scheme 9, section 1.6.1). Therefore, an efficient method for achieving the oxidation of citronellol would be of value within an industrial setting. With the success of the cholesterol oxidation, it was presumed that this oxidation would occur in a similar manner. For routine analysis of this reaction RP-HPLC with UV detection of the components was used as described in section 6.7.4. However, this again proved difficult to analyse using LC-MS with ESI. Due to the low molecular weight it was considered possible that the ESI was destroying the molecules to the point at which none of the ions were detectable. Therefore, chemical ionisation (CI) was attempted as this was considered a less harsh method of giving the molecules charge. Unfortunately, this also proved ineffective. Therefore, a literature separation technique was found[259] and after the three batch experiments, the resulting mixtures were combined. The products were separated from remaining starting material and from the porphyrin used to sensitise this reaction by column chromatography. The fraction relating to the product was then analysed by NMR, and matched to the literature values, at which point it was again analysed on RP-HPLC/UV. The procedure is detailed in section 6.7.4. This enabled confirmation of the relevant peaks on the HPLC, in order to appropriately analyse the results.

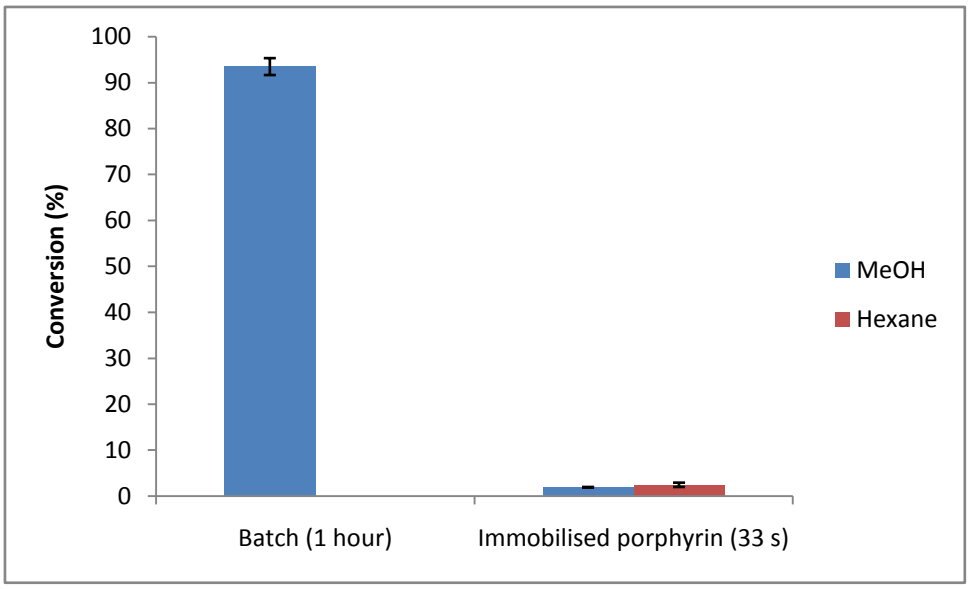

Figure 38: Graph showing the results from the oxidation of citronellol in batch and within the porphyrin-immobilised chip. Conversion calculated from oxidised citronellol products taken as a % of total citronellol species.

Figure 38 shows that the batch reaction of the oxidation of citronellol gave a much higher yield than that of cholesterol, and went almost to completion within 90 min irradiation, with few side reactions occurring. Comparing this with the on-chip reaction through the porphyrin-immobilised chip, there was a dramatic difference. The porphyrin-immobilised chip was only capable of producing a 2% conversion even with the use of different solvents, however, this was within 33 second residence time in comparison to the 1 hour reaction of the batch reaction. In comparison with the other ene reaction with cholesterol this is also very different. These results were unusual, and it may be due to a high concentration of citronellol used for this reaction. If the same number of moles of cholesterol and citronellol were being oxidised, the higher starting concentration would cause an apparently lower percentage yield. In order to ensure comparability it would be necessary to repeat the experiments with the same concentration of starting materials, or to compare the number of moles being oxidised. However, the same concentration of α-terpinene was used to that of citronellol and this still produced a higher yield through the microfluidic chip than that of

citronellol. The difference between the oxidation products when the reaction was conducted in MeOH and hexane is slightly different in this experiment, being higher in hexane. However, with such low percentage yields, neither is significantly better than the other.

3.3.4. Space-time yields

The results obtained for the oxidation of these products on-chip is clearly not as productive as the batch results. However, a benefit associated with the use microfluidic devices is their ability to deliver similar results to batch experiments in a much shorter time span, and in much smaller vessels. Another method for interpreting these results is by investigating the space-time yields. This takes into consideration the time that the reaction is taking place over, and the space confinements of the reaction. Shvydkiv *et al.* used the effective space time yields (STY) in their work, and it gave an indication of the efficiency within different reaction vessels[252]. STYs provide a more appropriate method for comparing the efficiency of reactions in batch and microfluidic devices:

$$STY = N_R/(V_R \times t)$$

Where N_R is the amount of reactant converted in mmol, V_R is the volume reactor vessel in L and t is the irradiation or residence time when relative to the microfluidic device in min.

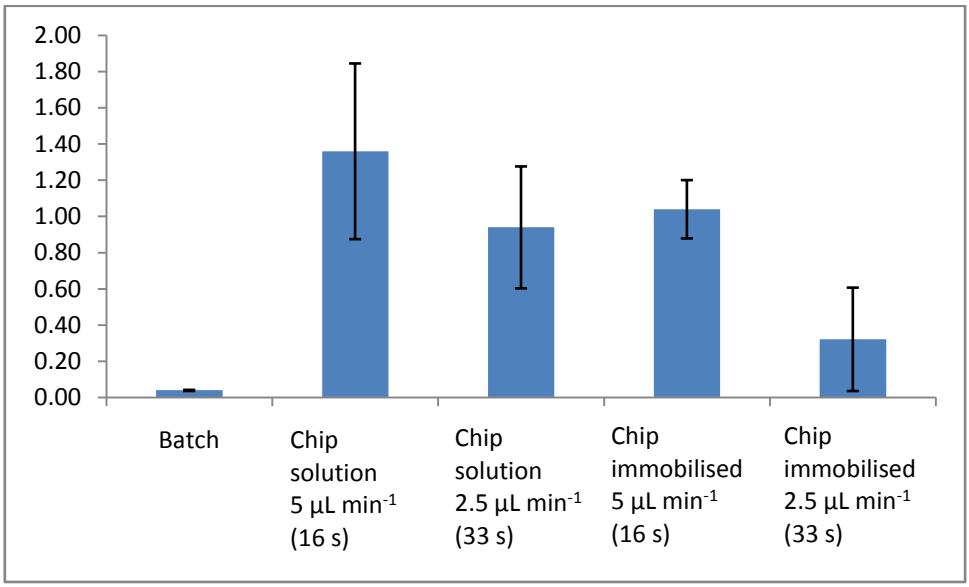

Figure 39: Graph showing the space time yield of the oxidation of cholesterol conducted in batch and in the microfluidic device.

Despite the large variability seen in Figure 39, which is associated with the on-chip reactions (determined through repeat experiments), it is clear that the STY for the oxidation of cholesterol is much higher than for the batch reaction. This suggests that the microfluidic method is more efficient than batch. By increasing residence time, it may be possible to produce yields equivalent to batch in a much shorter time. This could be done by slowing the flow rate, or by increasing the length of the microfluidic channels. These results indicate that it would be beneficial investigating these methods further in order to improve overall yield on-chip.

For the oxidation reaction of α-terpinene, and citronellol, the same calculations were performed (Figure 40).

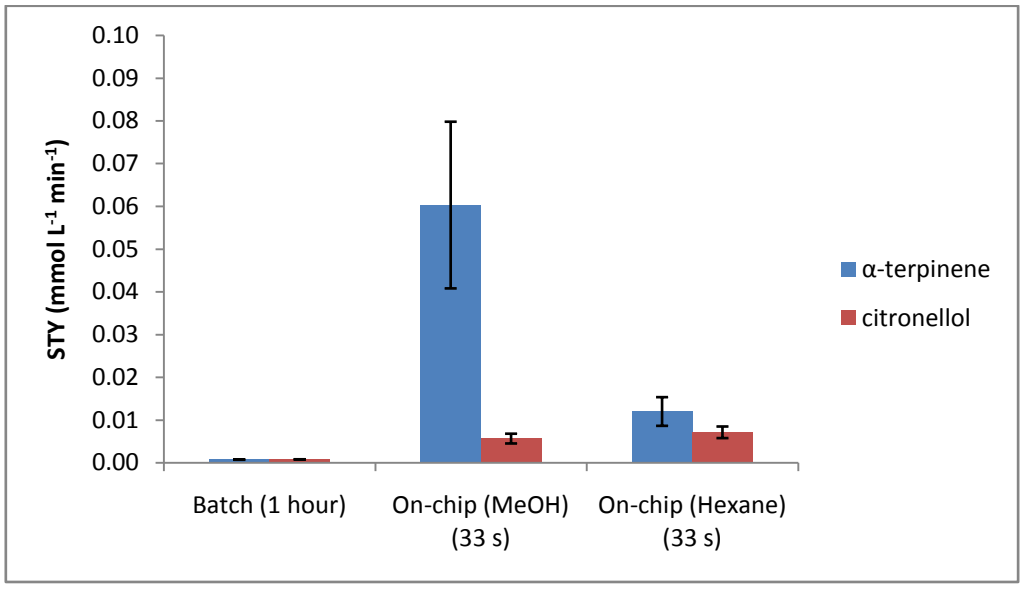

Figure 40: Graph showing the space-time yields for the oxidation of α-terpinene and citronellol in batch and on-chip.

The STYs from the oxidation of citronellol were shown to be better than those from the batch reaction. In comparison to those from the oxidation of α-terpinene, those in methanol are much lower; however, they were similar when conducted in hexane. The results from the α-terpinene reaction on-chip were much better than the batch reaction of the same. However, the errors, determined through repeated experiments, were very high, as was seen for the cholesterol oxidation. These results indicate that the α-terpinene reaction was occurring more efficiently, and would also improve with longer residence times. However, the citronellol reaction does not seem to follow the same trend, and it would be useful to investigate this reaction further to determine the reason for these results.

These space-time yields are a useful way of expressing the ability of the chip to efficiently conduct these singlet oxygen reactions. They show the potential of the application for chemical reactions, although it is also obvious that there is still much to do to optimise them.

3.4. Conclusion for chemical application of porphyrin-immobilised chip

The porphyrin-immobilised microfluidic device has been used to show its ability to produce ROS which can be used to conduct efficient oxidation reactions. In order to determine effective experimental parameters, the oxidation of cholesterol was used as a model reaction. This confirmed that a strong light source was required to effect the production of ROS from the immobilised porphyrin. It was also found advantageous to introduce oxygen to the system in order to optimise the oxidative potential of the porphyrin. Different flow rates were used, and little difference was found between 5 and 2.5 $\mu L\ min^{-1}$ with rose bengal as the photosensitiser. However, when porphyrin was used, it appeared that the slower flow rate was more productive. The photostability of the porphyrin was also investigated, and it was found to be relatively poor, and that after 40 min irradiation the singlet oxygen production was significantly decreased.

The porphyrin-immobilised chip was then used to explore the ability to initiate other oxidation reactions. Citronellol was used as an example of an industrially useful reaction of the same type (ene) as the cholesterol reactions and was shown to be less effective than the cholesterol oxidation on-chip. α-Terpinene was used as an example of another singlet oxygen reaction ([4+2]), and was shown to be more effective than the citronellol, and worthy of further investigation, especially with increased STYs.

Chapter 4.

Biological applications of porphyrin-immobilised chip

In this chapter the biological applications of the porphyrin-immobilised chip are discussed. Initially a method for pumping cultured cell lines through the microfluidic chip was established and determined not to affect cell survival. The effect on cell survival of other experimental parameters was then studied to ensure that any cell death observed was purely from the porphyrin-mediated oxidation. A more rigorous method of assaying the modes of cell death was established enabling on-chip results to be effectively measured against in-house cytotoxicity testing off-chip. The porphyrin-immobilised chips were then used to determine the effect on cell death, and when the cationic porphyrin appeared to cause dark toxicity, other porphyrin photosensitisers were investigated. Finally, the different modes of cell death and protein expression were investigated to determine the possibility of using this setup for providing cells that would initiate an immune response.

4.1. Aims for the biological application of porphyrin-immobilised chip

The aim was to use the porphyrin-immobilised chip to produce cytotoxic reactive oxygen species to kill cancer cells in a manner that would initiate immune responses. To achieve this, cultured cells were pumped through the porphyrin-immobilised chip and analysed to determine the effect on viability and the mode of cell death initiated. These were compared to the effect caused by the experimental parameters in the absence of porphyrin, and to immobilised porphyrin in the absence of light. It was the intention of these experiments to prove that immobilised porphyrin in the presence of light could cause apoptosis and necrosis in the cell population pumped through the chip. A number of cell surface markers have been implicated in the ability of PDT-treated cells to initiate an immune response to cancer cells (section 1.7.1).[295-303] Therefore, to determine the possibility of this system producing cells that would initiate an immune response an assay for one of these markers (HSP70) was performed.

4.2. The effect on cells of manipulation through the microfluidic device

Initially a method was needed to ensure that cells could be pumped through the microfluidic device efficiently. This would require enough cells to be collected from the chip to be counted and analysed. It was also necessary that the cells would not be unduly stressed by the process of being manipulated and pumped through the chip. Syringe pumping was chosen as the method for introducing cells onto chip as this required no further development of the basic microfluidic device. Electro-osmotic flow is often used for biological applications; however, this requires the addition of electrodes into the chip interface. Another option that was considered was the use of a pressure regulated pump; however, this would have required numerous measurements before being used to determine flow rate. The use of syringe pumping for working with cells does introduce complications that are not present with the chemical applications. Unlike homogeneous solutions of chemicals within a syringe, the cells are in a suspension, so that when oriented horizontally the cells will settle and possibly adhere to the lower surface of the syringe. Before any specific data on cells in chip was collected it was therefore necessary to determine a method of ensuring that the cells would travel from the syringe, through the interface to the chip and ultimately through the channels of the chip to be collected for analysis

Initial investigations were conducted with an adherent cell line, HT29 human colon adenocarcinoma cells which were used routinely in house for PDT cytotoxicity assays. However, with this cell line it was not possible to collect enough cells from the chip to analyse. At this point the cells were being counted using the haemocytometer, however, for an accurate count $15\text{-}50\times10^{4}$ cells mL^{-1} were required. With the syringe pump oriented horizontally, the cells were found to settle to the lower surface of the syringe. Regular

agitation of the syringe was conducted in an attempt to keep the cells in suspension. This was not successful as the cells would aggregate together causing a blockage in the capillaries or channels of the chip. Pulling the suspension of cells through the chip into the syringe was investigated next. This failed to solve the problem, as the cells would settle in the container rather than the syringe and not enough cells were collected from this method. Therefore a stand was constructed for the syringe pump which enabled it to be oriented almost vertically (Figure 41).

Figure 41: Syringe pump on wooden stand, constructed to ensure that the cells in the syringe did not settle to the sides of the syringe but were capable of being pumped through the chip.

Thus, any cells settling under gravity would be at the end of the syringe and be pumped through the chip. Although an improvement was seen in the total number of cells that could

be collected from the chip, it was found that the microfluidic device was still prone to blocking and the cells stuck to the channel surfaces. Therefore, a different cell line was selected that was non-adherent and would be less inclined to adhere to the syringe or microfluidic channels. The cell line chosen was human histocytic lymphoma (U937). With this cell line it was possible to get a profile of the number of cells exiting the chip. For the initial experiments both the parallel channel chip (design B) and the serpentine chip (design C) were used, so a comparison was conducted between the two designs (Figure 42)

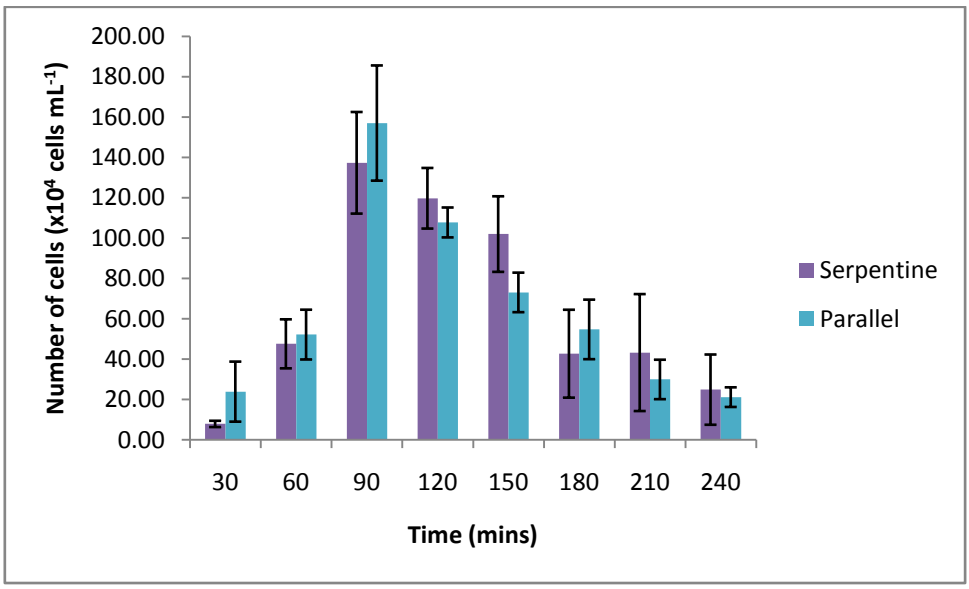

Figure 42: Concentration of cells retrieved from serpentine (design C) and parallel channel (design B) chip.

This experiment was conducted at a flow rate of 3 μL min^{-1} and each sample was collected over 30 min resulting in aliquots of ~100 μL. Figure 42 shows little difference between the results from the serpentine and parallel channel chips, suggesting that the longer, thinner channels in the serpentine device did not have detrimental effects on the ability of the cells to traverse the system. In the first three samples, up to 90 min, there were more cells from the parallel channel chip. This was to be expected as the serpentine channel had a longer

residence time, and it may have taken more time for the cells to reach the outlet and there was therfore an increased surface interaction.

With the chemical applications of the porphyrin-immobilised chip, a flow rate of 2.5 µL min^{-1} was optimum for oxidation reactions on-chip (section 3.3). A number of experiments were conducted to determine what effect a change in flow rate would have on the concentration and viability of cells on-chip (Figure 43). A flow rate of 5 µL min^{-1} and 2.5 µL min^{-1} was chosen, which relates to a speed of 0.76 mm s^{-1} and 0.38 mm s^{-1} and a residence time of 15.9 s and 31.8 s, respectively.

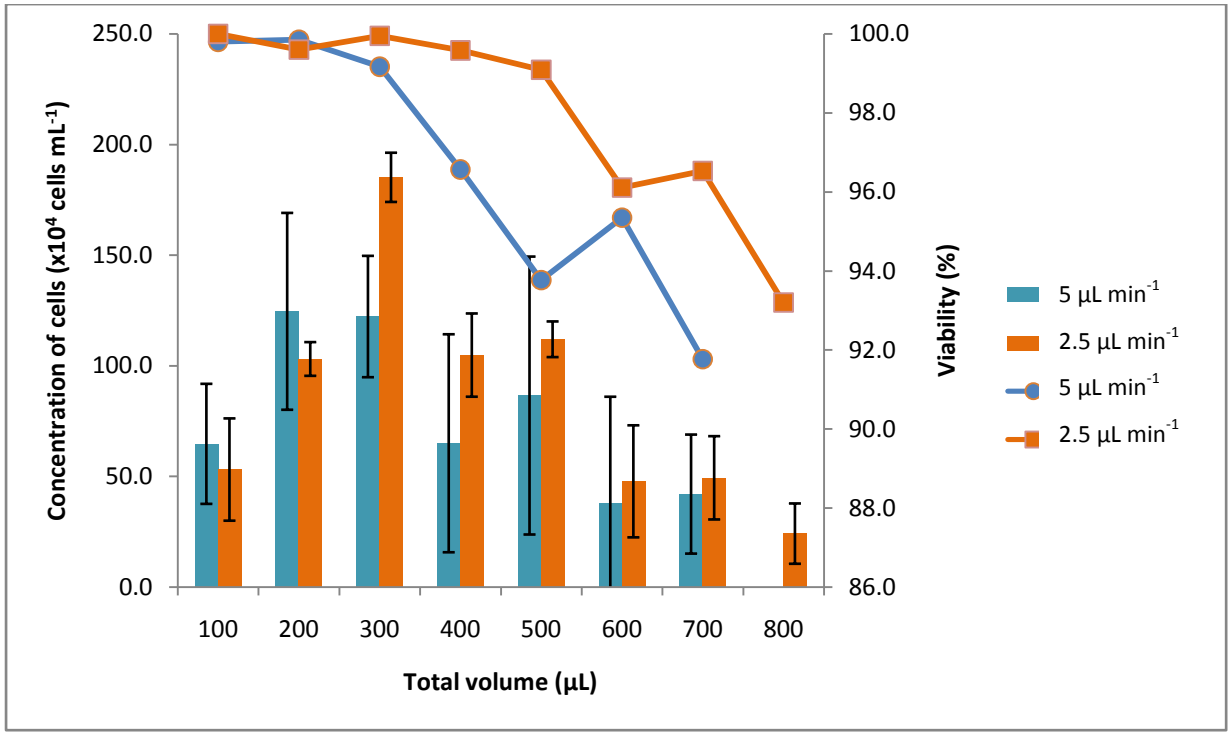

Figure 43: Graph showing the concentration of cells (as a % of starting concentration) (bars) and viability of cells (lines) pumped through the parallel channel chip at 5 µl min^{-1} and 2.5 µL min^{-1}

The scatter points on this graph represent the viability of the cells, whilst the bars represent the concentration of cells. The total volume collected was plotted against the time taken as 100 µL aliquots resulted in enough cells to analyse; therefore, for the flow rate of 5 µL min^{-1}

they were collected every 20 min and for the flow rate of 2.5 μL min^{-1} they were collected every 40 min. These results, as an accumulation of three experiments for each flow rate, show that the slower flow rate was more advantageous. In respect to cell numbers, the initial two aliquots resulted in a slightly greater concentration for the faster flow rate; however, for the following aliquots the slower flow rate was optimum. Equally for these first two aliquots the viability was comparable; however, as time passed the slower flow rate appeared to be advantageous in ensuring the cells survival. Although these results seemed encouraging with respect to cell survival, it was important to ensure that any cell death was insignificant with respect to control cells kept in the incubator. It was also interesting to note how the viability was affected specifically by pumping through the chip, as opposed to viability whilst outside the incubator over time (Figure 44).

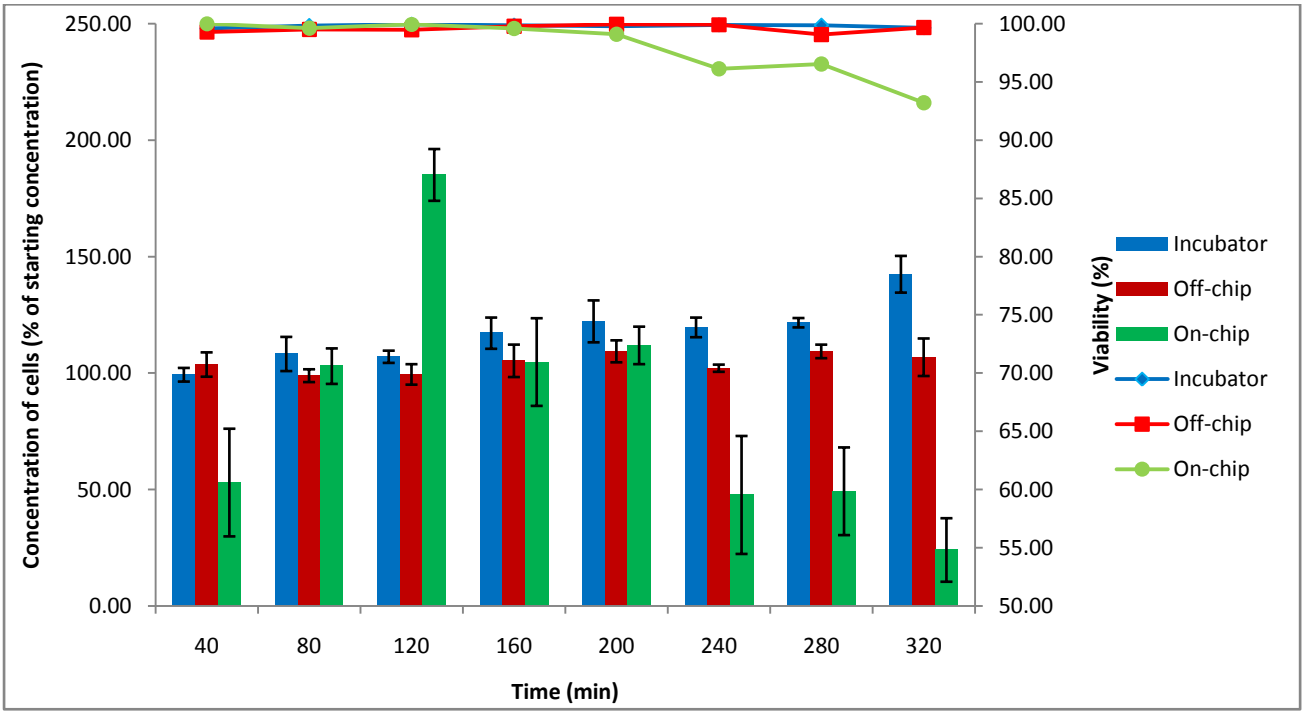

Figure 44: Graph showing the number of cells (bars) and viability (lines) of cells over time when left in the incubator, out of the incubator but off-chip and on-chip.

Again the viability was plotted as the line graph and the secondary y axis, whereas the concentration was plotted as bars with the primary y axis. This showed that within the first 2.5 h there was little difference in viability between the cells in all conditions. This is a good result as it indicates that the cells are not adversely affected by being on-chip and any cell death that occurs was not caused by this manipulation. After 3 h the cell viability did drop slightly compared to the control. However, this trend was also seen with the cells out of the incubator but off-chip. This suggested that the cells were dying whilst out of the incubator for long periods of time and coupled with the on-chip environment should not be used for more than 3 h at any one time.

These results enabled a basic setup to be established and a suitable cell line determined. The cells were travelling through the chip in sufficient numbers for further assays to be performed on them. In addition it was established that this setup was not overly detrimental to the viability of the cells. It was also necessary to determine whether other experimental parameters would cause cell death, to ensure that any cell death observed from the porphyrin-immobilised chip was a result of a photodynamic effect.

4.3. Establishing experimental parameters for biological applications

Other experimental parameters that could adversely affect the cells were light and oxygen. The cytotoxicity of the porphyrin itself, in the dark, was tested in tandem with the irradiated sample to ensure that the cells were treated in an equal manner and will be discussed in section 4.4. Cell cultivation is conducted in very strict conditions with specific media at 37 °C and with 5 % CO_2 in the atmosphere. These conditions most closely mimic conditions within the body and are optimum for cells to grow. Therefore the addition of other factors, such as excess heat or increased oxygen concentration could cause cell death. For use of cancer cells for vaccines, it has been shown that the manner of cell death is key to the immune response to the cells,[310] as explained in the introduction (section 1.7.1). To prove that cell death from the porphyrin-immobilised chip is from the reactive oxygen species implicated in PDT it is vital to show that these other parameters do not cause a significant amount of cell death.

During the chemical applications for the porphyrin-immobilised chip the introduction of oxygen was conducted via a number of capillaries from the oxygen cylinder as outlined in section 6.5.2. This enabled a low flow of oxygen through the chip and the production of uniform bubbles through the system. However, the chemical synthesis was conducted in organic solvents which have lower surface tensions than water and allowed the gas to dissipate at the outlet without causing foaming in the collected sample. On attempting the same technique with the aqueous solution of media that was used for these reactions, it was found that the bubbles remained in the solution received at the outlet causing foaming. This introduced problems with collecting and analysing samples from the chip. After several attempts to rectify the situation using different aqueous solutions that would be suitable for

cell suspensions (a media solution without FCS and PBS) it was decided that the time restraints were such that the remaining experiments were conducted without additional oxygen. It has been shown in section 3.2.3 that the addition of oxygen was advantageous to the oxidation of cholesterol; therefore, this would be worth investigating in the future. Options for rectifying this issue were discussed, such as oxygenating the cell suspension prior to taking up to the syringe or conducting the experiment using a pressure pump with oxygen, or air as the carrier gas. However, it was decided that it was more important to determine a proof of principle rather than optimising this step ahead of time.

Having shown that the Xe arc lamp was more capable of initiating the production of ROS than an LED during the chemical investigations, this was the lamp that was used here. However, this lamp produces a large quantity of heat in addition to the light that is produced. The effect that the heat has on the viability of the cells from the microfluidic device was investigated (Figure 45)

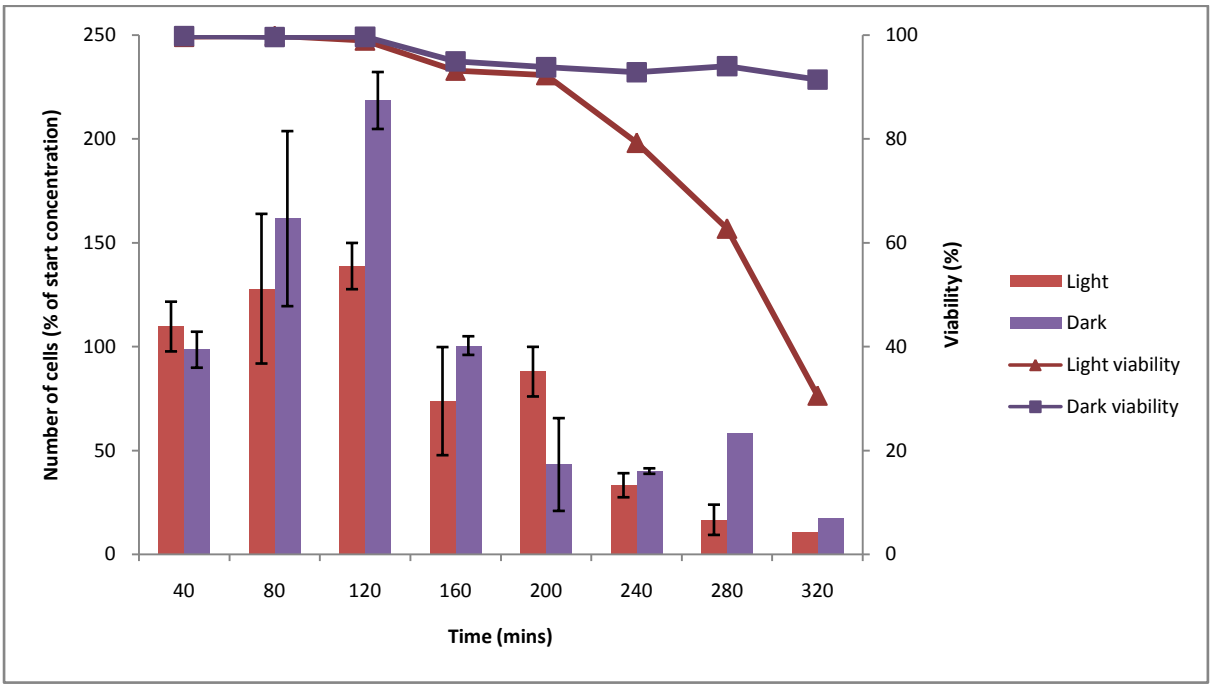

Figure 45: Graph showing the effect the Xe arc lamp light has on the cells from the microfludic device.

Here again, we see that up to 2 h through the microfluidic device, the light had a minimal affect on the cell viability. It does seem to have had a slightly detrimental effect on the number of cells through the chip. After 2 h the cells from both the light and dark experiments had a reduced viability, and after 4 h the light had a greater effect on the viability. This suggests that up to 2 h the light would not adversely affect the viability of the cells. This indicates that experiments should be limited to this time frame for meaningful results from the porphyrin-sensitised production of ROS.

Despite the seemingly positive results from the previous experiment, it cannot be forgotten, that for the cells to initiate an immune response certain DAMPs have been implicated in the process. One of these is HSP70 which is expressed on the cell surface after PDT and is thought to be integral in the immune response. If the temperature of the chip exceeds 37 °C it is likely to cause this protein to be expressed on the surface. It is unknown if heat-activated expression of HSP70 is as efficient at initiating this immune response as PDT-activated

expression. Thus, it is important that the damage to the cells is caused solely by the PDT action and not by other factors such as heat. Therefore, the chip temperature was measured throughout the experiment to determine the temperature reached during the experiment. In the basic setup that had been used up to this point the temperature was found to reach up to 70 °C over the course of an experiment (~4 h). This would certainly explain the increase in cell death observed in the previous experiment.

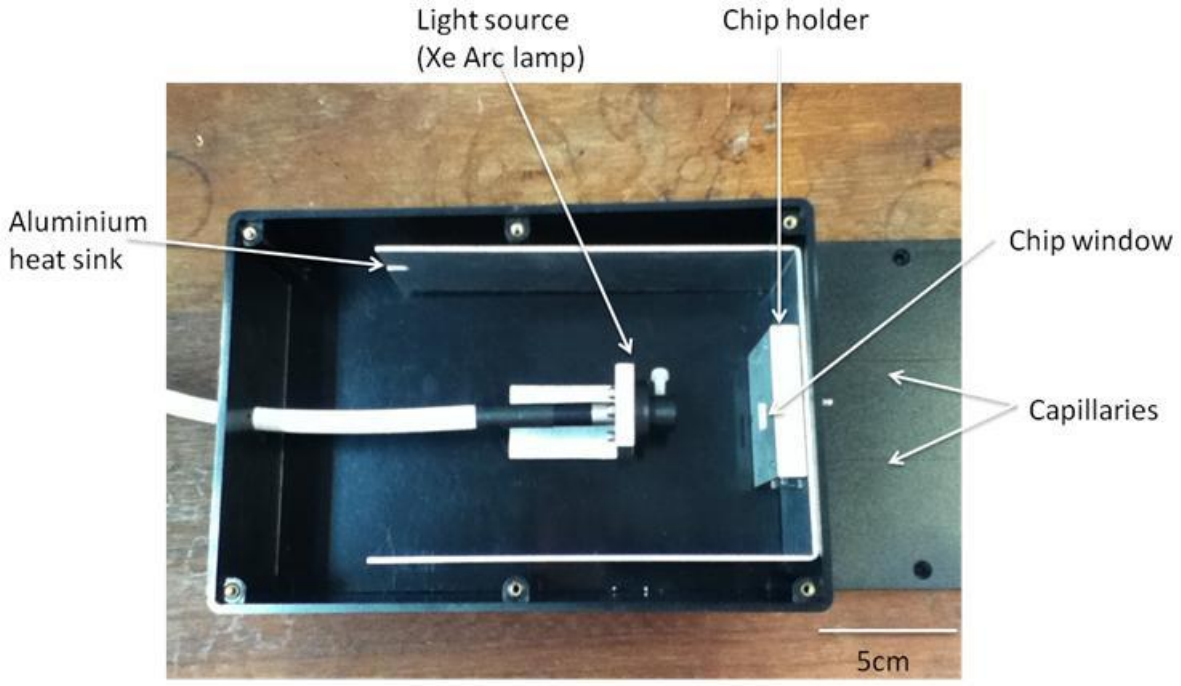

Figure 46: Black box set-up showing the aluminium heat sink around the box, the fibre optic for the Xe arc lamp, chip holder with window to the channels and capillaries for connecting to the syringe.

The chip holders were manufactured from aluminium which is known to transfer heat efficiently (thermal conductivity = 250 W m^{-1} K^{-1}). It was decided to add more aluminium to the set up which was hypothesised to aid in the removal of heat from the chip. In addition a heat transfer paste was used between the chip and the chip holder which would enable the heat to dissipate from the glass to the aluminium (Figure 46). A thermocouple was used to

measure the temperature at the chip surface to determine the effect that the extra aluminium had on the dispersion of heat (Figure 47).

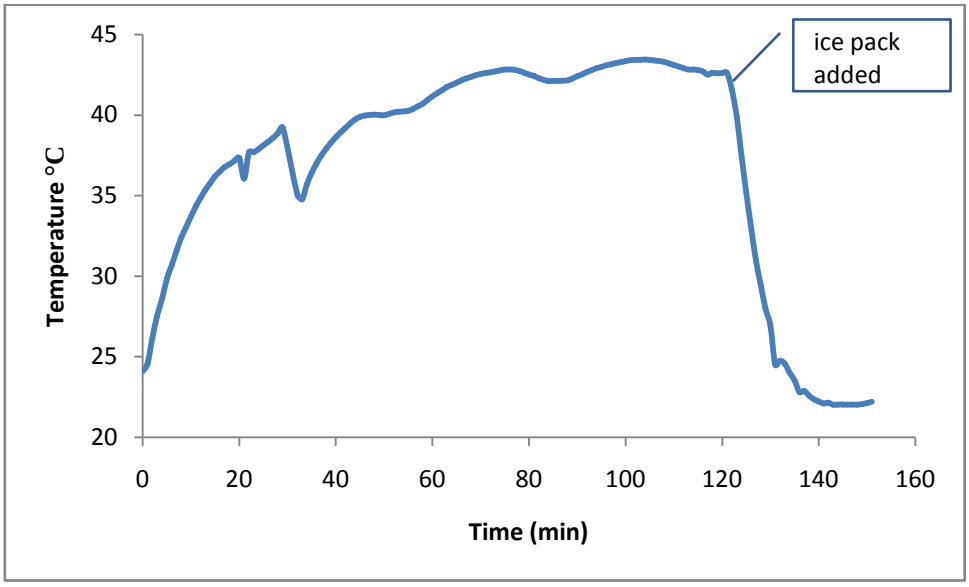

Figure 47: Temperature at chip surface over time with irradiation (ice pack placed next to aluminium after 2 h).

In this experiment the thermocouple was checked after 30 min which accounts for the dip in temperature at this time on the graph. Overall the temperature slowly rose throughout the experiment up to 43 °C after 2 h. This is too high for the cells, as even a slight temperature increase is enough to have a detrimental effect. To cool the chip down ice packs were used at the sides of the aluminium. This happened at 120 min and a dramatic effect can be noticed as the temperature drops to 22 °C within 20 min. Therefore a second experiment was conducted with ice packs in place from the start of the light experiment (Figure 48).

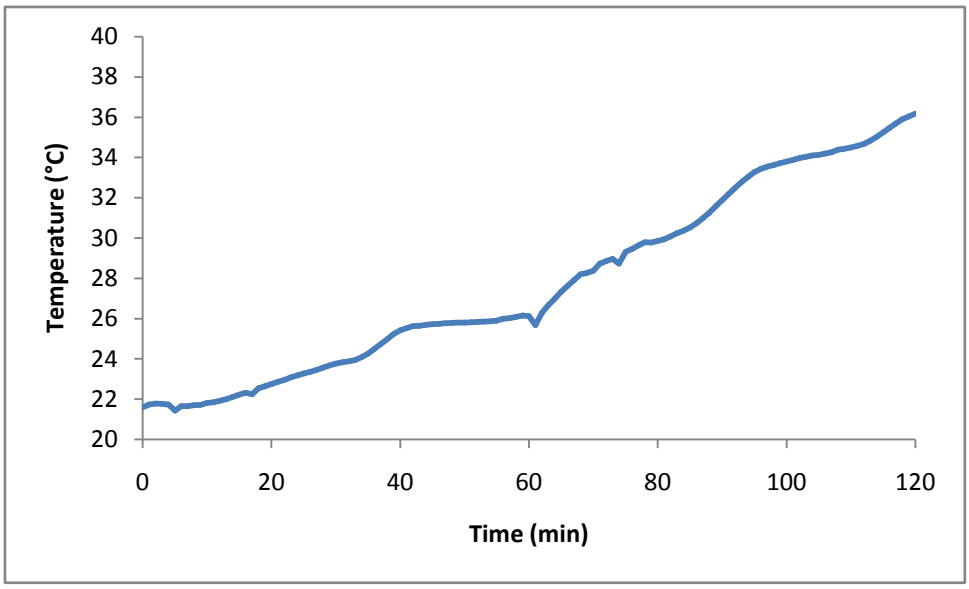

Figure 48: Graph showing the temperature change over time with light on the chip and ice packs cooling the aluminium frame.

This shows that, although the temperature was still rising over time the ice packs slowed this down, and over the 2 h time frame it remained below 37 °C. It was decided that to ensure the temperature did not rise over 37 °C the ice packs would be changed after 1 h for each experiment as this ensures a temperature below 30 °C.

This section has shown how the experimental parameters for the experiments were established to ensure that the cause of cell death could be confidently attributed to reactive oxygen species generated by the immobilised porphyrin. To continue with the experiments it was important to determine a suitable assay for determining the type of cell death.

4.4. Determination of an effective cell death assay

Up to this point the method for determining cell death was with a trypan blue test, as described in section 6.8. This stains the dead cells blue, whereas the live cells do not allow the dye to be taken up. However, this is a subjective method as it relies on human counting of the cells. Another method that was routinely used in house is the MTT assay which is a colourimetric method that measures lysed cells in the presence of the dye. The suspension is measured on a spectrometer and the details can be extrapolated from the known spectra of the compound (refer to section 6.8 for details). This is a time consuming assay, and requires a large volume and quantity of cells for an accurate measurement. The Annexin V-FITC/PI assay uses flow cytometry and staining the cells to determine those that are still viable and those that are apoptotic and necrotic. Although this assay still requires some work up, it gives more information about the cells. To ensure that it was comparable to the current in house method, the procedure used for testing cytotoxicity of products in solution was conducted in duplicate and the results from the MTT assay were compared with the results from the flow cytometry assay (Figure 49)

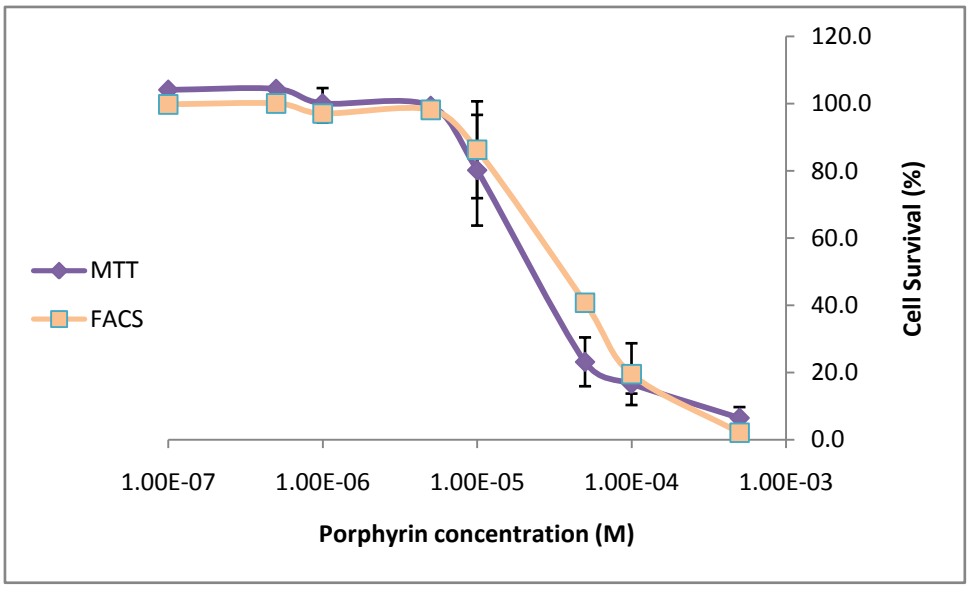

Figure 49: Graph showing the results from cytotoxicity experiments analysed through MTT assay and flow cytometry (FACS).

This showed that the two methods were comparable in respect to the results for cell survival. This suggests that the results achieved on-chip would be comparable to data for off-chip cytotoxicity testing, even though analysed using different methods. This also showed that the LD_{50} for U937 cells with cationic porphyrin off-chip was between 1×10^{-5} and 1×10^{-4} M.

4.5. Use of porphyrin-immobilised chip for initiating cell death

The first porphyrin that was immobilised on to the glass chip surface was 5-(4-isothiocyanatophenyl)-10,15,20-tetrakis-(4-*N*-methylpyridiniumyl) porphyrin triiodide (**35**). Several experiments were conducted in tandem with chips functionalised with the same porphyrin but kept dark (Figure 50).

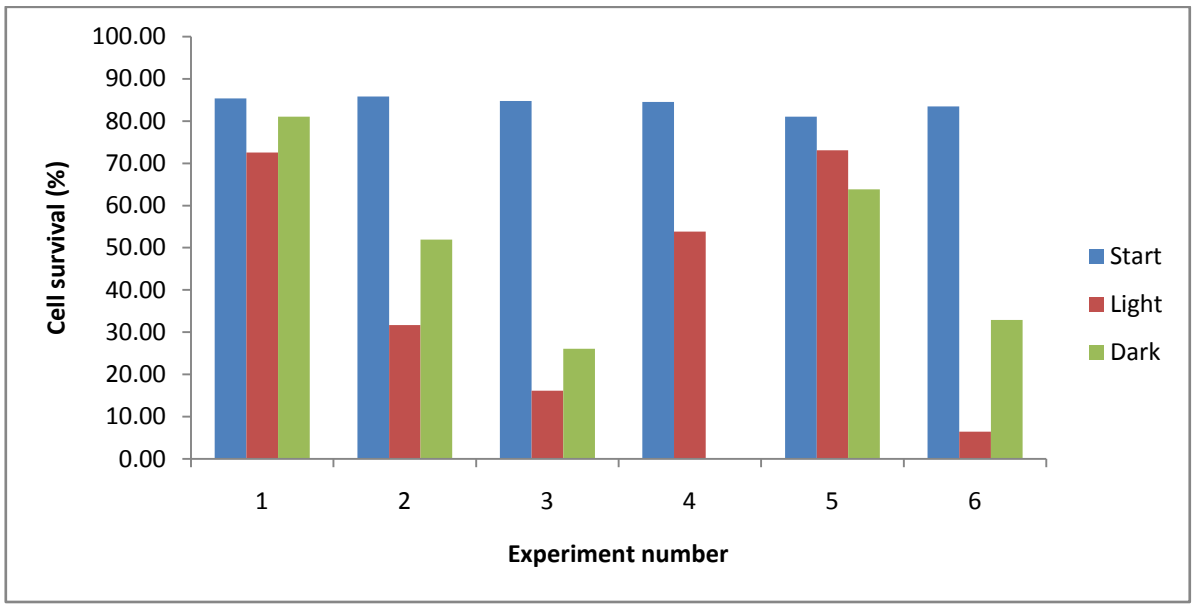

Figure 50: Experiments conducted with cationic porphyrin (iodide counter ions) showing the cell survival for cells from the start of the experiment (no manipulation) those on-chip with irradiation (light) and those on-chip without irradiation (dark).

These experiments showed that at times the light had a profound effect on the viability of the cells. However, there were some experiments for which the dark control produced as much if not more cell death. Taking all the paired values for light and dark results it was found that there is no significant difference ($P>0.05$) between the two results. This suggests that this cationic porphyrin was showing dark toxicity. It also would lead to the conclusion that the cell death in the light conditions could have been a result of the toxicity of the compound rather than from ROS.

To reduce the dark toxicity, it was hypothesised that using a cationic porphyrin with chloride counter ions may result in lower dark toxicity. If the counter ions were leaching into the aqueous media, they may have had a detrimental effect on the cells. Chloride ions are present *in vivo* and should have a reduced effect on the cells than iodide ions. Therefore the experiments were repeated with 5-(4-isothiocyanatophenyl)-10,15,20-tetrakis-(4-*N*-methylpyridiniumyl) porphyrin trichloride (**37**) immobilised to the glass channel surfaces (Figure 51).

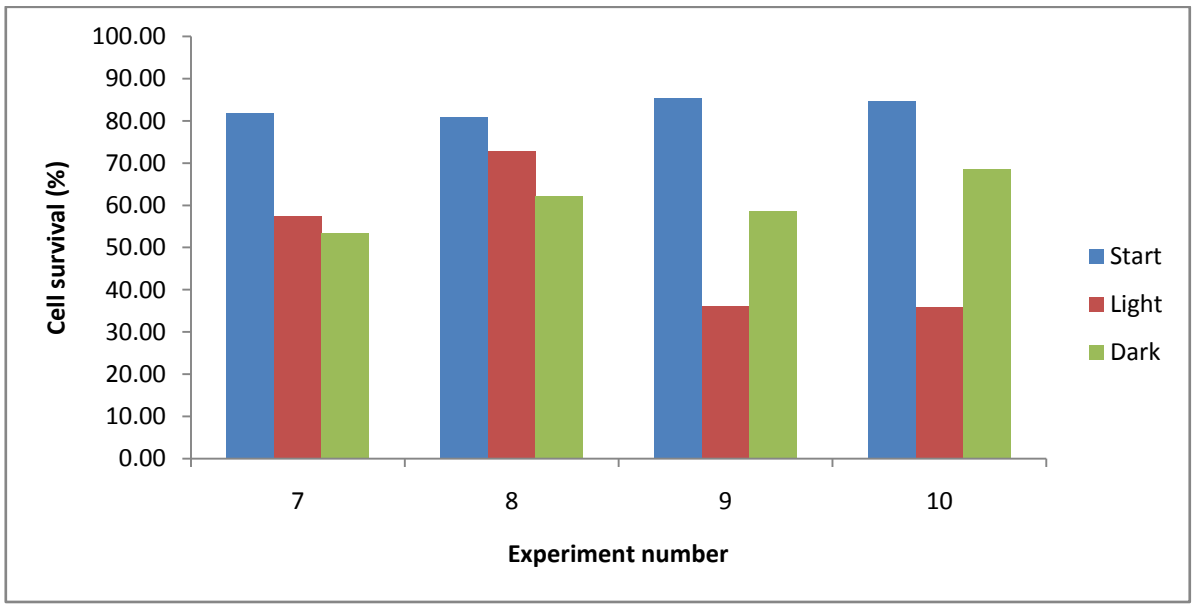

Figure 51: Graph showing cell survival from the start of the experiment and after irradiation on-chip (light) and on-chip with no irradiation (dark) with microfluidic device functionalised with cationic porphyrin with chloride counter ions.

Again this provided a variety of results; two of them showing that the light caused more cell death, and two in which the cell death was more similar with the dark conditions having higher cell death. By performing the paired t test on these results it was again found that the two experimental parameters were not statistically significant ($P>0.05$). This suggests that it is the cationic nature of the porphyrin that was having a detrimental effect on the cells. In comparison to off-chip results, this was unusual. With concentration lower than 2×10^{-5} M of

porphyrin in the media, dark toxicity has been found to be minimal. With the low concentration of porphyrin calculated for the glass chip surface, it would seem unlikely for this to have been a problem. However, considering the concentration at any one time on-chip, it is possible that this would be higher, and therefore, be causing the dark toxicity.

To determine whether this effect was limited to the cationic porphyrin or would be a problem with other porphyrins also, a neutral hydrophilic porphyrin (**41**) was immobilised to the glass surface and the experiments repeated (Figure 52).

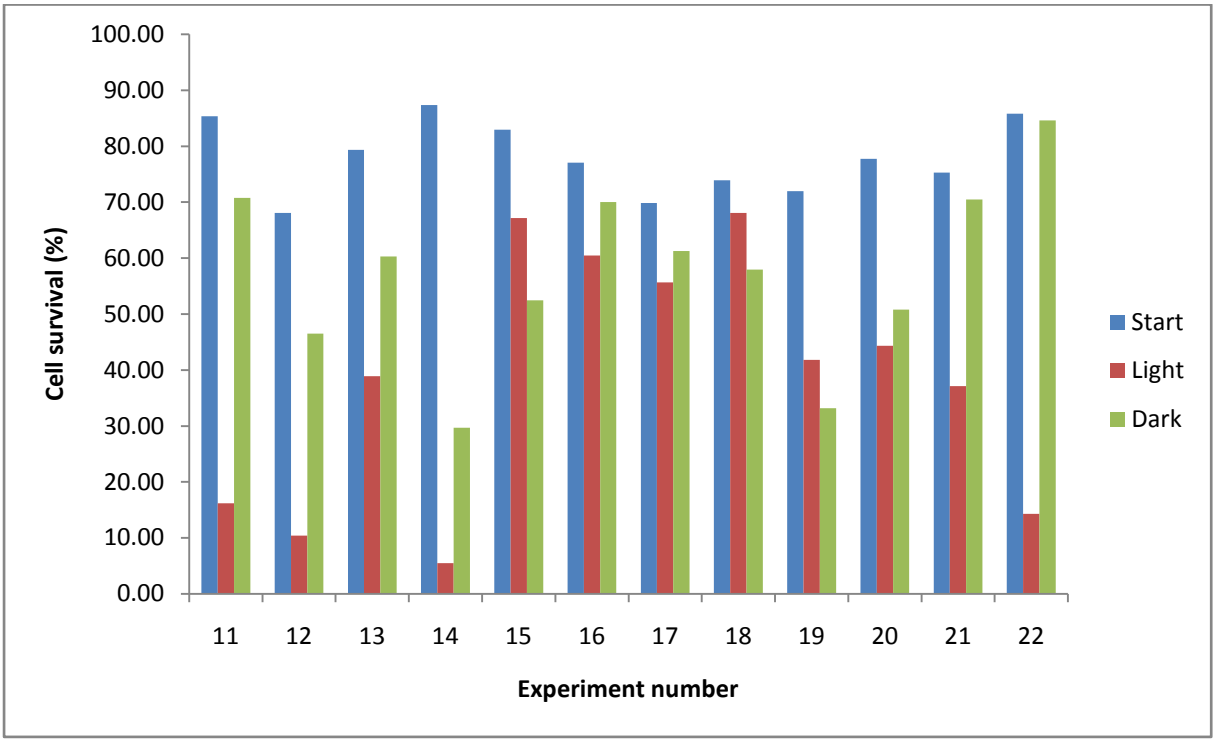

Figure 52: Graph showing cell survival 24 h after experiments conducted with the neutral porphyrin immobilised on glass microdevice channel surfaces.

These results showed that under conditions of irradiation cell death was more prominent than with those in the dark. There were still a small number of experiments in which there appeared to be dark toxicity; however, these were less significant over the scope of the experiments. This indicated that the neutral porphyrin displayed less dark toxicity and was

capable of causing cell death upon irradiation with light. Performing the paired t test on this data showed that the difference was statistically significance ($P<0.05$). These results were obtained on cells incubated for 24 h after the experiment was conducted to determine how the cells were affected over this time. However, to get a more rounded view of the cell death mechanism further experiments were conducted and the analyses conducted after just 1 h incubation of the cells (Figure 53).

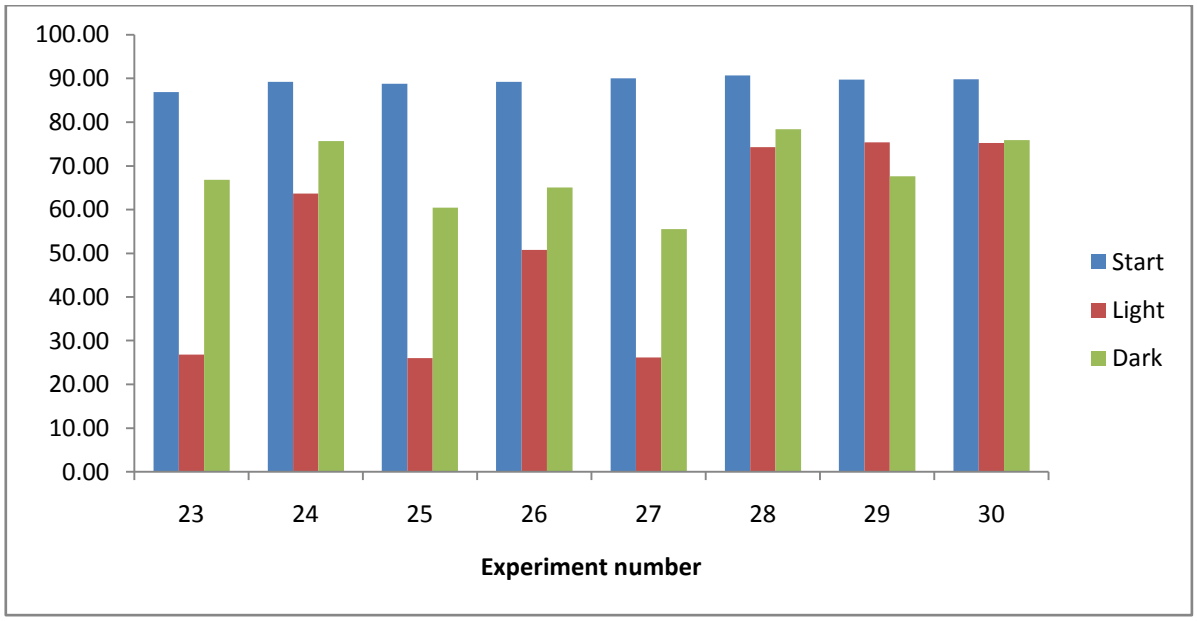

Figure 53: Graph showing the cell survival 1 h after the experiment was conducted on cells at the start and on-chip both irradiated (light) and non-irradiated (dark).

These results suggest that the cell survival rate after 1 h was similar to that after 24 h. It also confirms that the experiment conducted in the light conditions resulted in lower cell survival than those in the dark. The paired t test again showed that these results are statistically significant ($P<0.05$).

Although the results have been shown to be statistically significant the experiments still show that the cells from the experiment conducted in the dark were still not surviving as well as those that had not gone through the chip. This suggests that the porphyrin may still be having

some affect on the cells even when the channels are encased in the chip holder. The reason for this could be ambient light. The edges of the microfludic device were outside the chip holder; it could be possible that light within the room that the experiments were being conducted was affecting the porphryin immobilised on the channels. To show whether this is a significant affect it would be necessary to repeat these reactions with a chip holder that completely enclosed the microfluidic device or by covering the overlapping edges. This is something that should be done for any further work.

4.6. Modes of cell death from porphyrin-immobilised chip experiments

The previous results indicate the overall effect on cell survival from the experiments conducted on-chip functionalised with neutral porphyrin. The mode of cell death has been shown to be a factor affecting the immune response from PDT-generated vaccines.[310] Therefore, it is vital to be able to analyse the manner of cell death caused by these experiments. Initially this was analysed using the Annexin V-FITC/PI assay for the flow cytometer as outlined in section 5.8, and was achieved with the results for the cell survival, which also gave information on the number of cells that were apoptotic and those that were necrotic. Finally a number of experiments were pooled to allow an analysis of the expression of HSP70.

It has been suggested that a greater percentage of apoptotic cell death (40-50 %) over necrotic cell death (~10 %) is optimum for initiating an immune response against cancer.[310] The results showing the percentage of apoptosis and necrosis for the experiment after 24 h are shown in Figure 54. This indicates that there was a greater percentage of apoptotic cells for all experimental parameters. However, the percentage of apoptotic cells for the light experiment was significantly higher than for the dark experiment. It also falls within the 40-50 % range shown by Korbelik *et al.* to be useful in the initiation of anti-tumour immunity. This confirms the results from the cell survival parameters, and indicates that the cells are being killed via a PDT-mediated action.

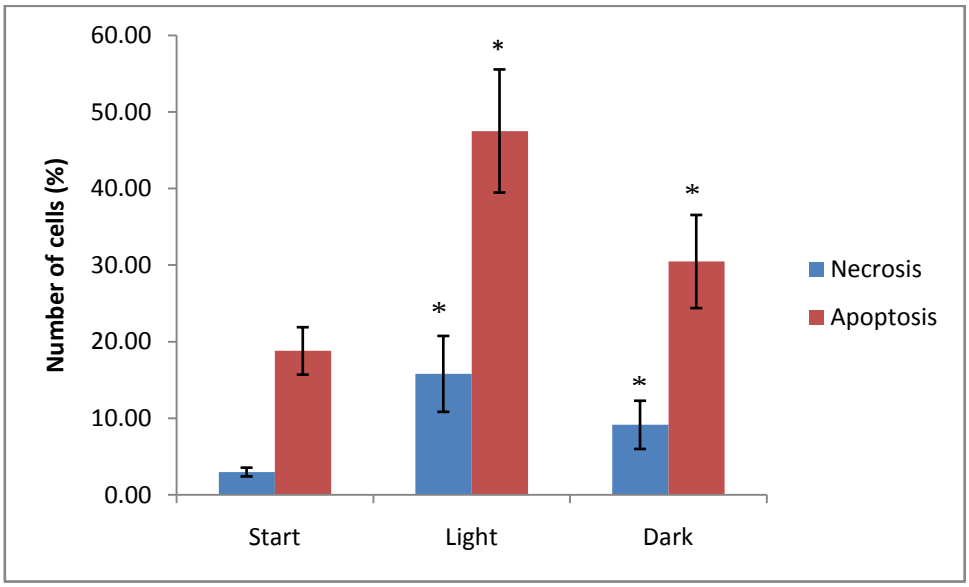

Figure 54: Graph showing the percentage of apoptosis and necrosis in the cell population from those analysed 24 h after experiment. Where * indicates statistical significance with a P<0.05

The percentage of apoptosis and necrosis after 1 h incubation were quite different (Figure 55). The percentage of necrotic cells in the light was much higher only 1 h after the experiment than 24 h after the experiment. Also the percentage of apoptotic cells in the light and in the dark was much more similar after 1 h and this was not statistically significant (P>0.05). By comparing the results after 1 h to those after 24 h, it was observed more cells became apoptotic over time both in the dark experiment and the light experiment. However, a greater percentage of the cells from the light experiment became apoptotic over time to make the difference statistically significant. This again seems to correlate with the data observed by Korbelik *et al.* that the cells require a post-treatment incubation time for apoptosis and related factors to mature.[310] Another interesting point to note is that the percentage of cell necrosis decreases in both the light and dark experiments. A possible explanation could be that necrotic cells, over 24 h, disintegrated to debris which was no longer analysed by the flow cytometer or was removed in the centrifugal supernatant.

Overall, it suggests that for a significant difference to be observed between apoptosis from the dark and light conditions the cells require time for apoptosis to become apparent.

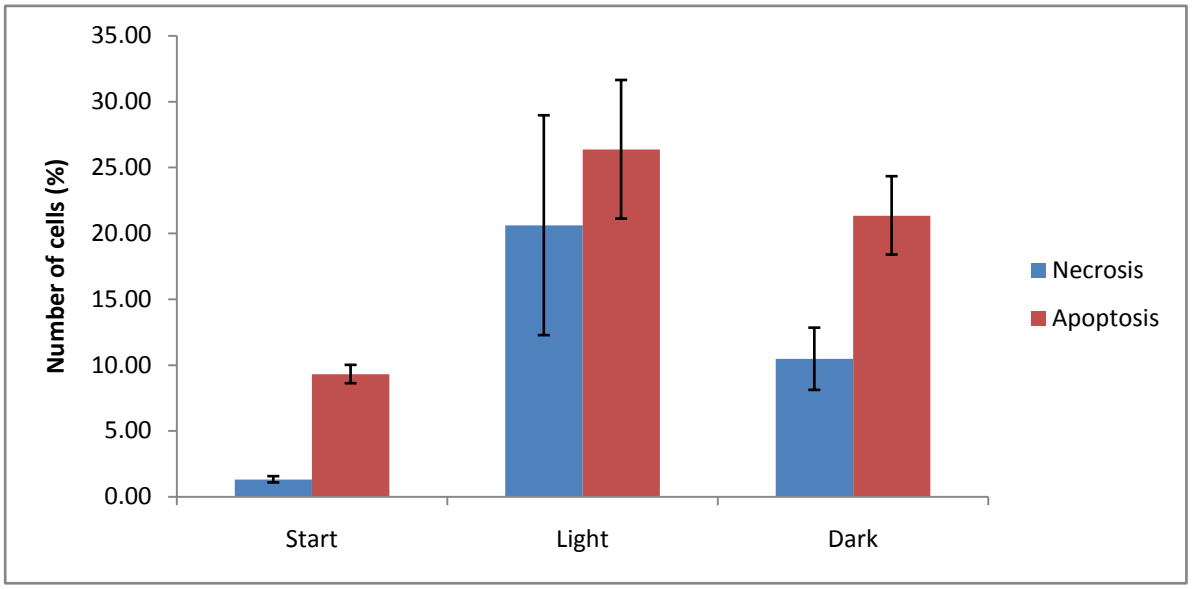

Figure 55: Graph showing the percentage of apoptotic and necrotic cells after 1 h incubation for cells at the start of the experiment and those irradiated on-chip (light) and non-irradiated on-chip (dark).

As with the results from the cell survival there is still a higher percentage of apoptosis and necrosis from the dark experiment than the cells from the start of the experiment. This again points to the possibility that some ambient light could have caused an affect on the cells classed as being from the "dark" experiment.

Other markers have been observed to be almost instantaneous after photosensitised treatment. HSP70 is one of these markers, it has been observed 1 h after treatment of cells.[298] As the name may imply, HSP70 is often expressed when the cells are exposed to temperatures above 37 °C. To determine the extent of HSP70 expression from excess temperatures the cells were incubated in a heat block for 1 h before analysing on the flow cytometer (Table 1) using the method in section 6.8.

Table 1: Expression of HSP70 on cells at 37 °C and those heated to 40 °C to determine normal expression over expression of stressed cells.

Temp (°C)	Positive	Negative	Ratio	Average
37	29.36	7.63	3.85	
37	26.16	6.48	4.04	3.94
40	37.00	6.94	5.33	
40	37.45	6.53	5.74	5.53

This suggested that there was not a large difference between normal and stressed expression of HSP70. To determine the effect that the porphyrin-immobilised chip would have on the cells it was necessary to collect more cells than a single experiment produced. Therefore, five separate experiments were conducted and 1 h after the experimental procedure the cells were frozen in liquid nitrogen. Once the final experiment was conducted they were thawed and pooled to analyse the expression of HSP70 (Table 2).

Table 2: Positive and Negative control results from a compilation of 5 experiments for cells at the start of the experiment and those irradiated (light) and non-irradiated (dark) on-chip

	Number of cells (x10^4 cell mL^{-1})	Positive	Negative	Ratio
Start	164	26.25	4.68	5.61
Light	42	29.04	9.27	3.13
Dark	21	28.68	9.72	2.95

Consideration of the ratio value suggests that there was a greater expression of HSP70 for the cells that had been unstressed due to processes on-chip. This value was closer to those seen for the stressed cells in the heat block. However, the negative values were unusual for the cells that had been on-chip. If these negative values were closer to that seen for the starting concentration of cells, then there would have been little difference between on-chip and off-chip cells. Finally the difference between irradiated cells and non-irradiated was negligible.

To determine significance more work would be required to determine a broader picture of the strange negative control results for cells on-chip and for the high result for the cells from the start of the reaction. Unfortunately for this project there was not time to determine all these factors. To gather this information some of the controls conducted for cell survival data would need to be conducted. It would also be useful to optimise the number of cells retrieved from the chip so that the HSP70 experiment could be conducted for each individual experiment allowing more data to be collected in a short space of time.

4.7. Conclusion for biological applications of porphyrin-immobilised chip

In this chapter the work conducted with biological applications for the porphyrin-immobilised chip was outlined. It was shown that the process of working with cells on-chip was not as straightforward as chemical solutions and required a setup more tailored to those needs. The syringe pump was required to be near vertical in orientation to ensure the cells did not settle to the bottom of the syringe, in addition to regular agitation of the suspension in the syringe. A system for cooling the chip was required to ensure that the temperature on-chip did not exceed 37 °C and adversely affect the cells. This was achieved through an aluminium chip holder and aluminium arms which could be cooled with ice-packs and through heat transfer cool the chip.

Once it was determined that the set up did not have an adverse affect on cell survival, experiments were conducted with the porphyrin-immobilised chip. It was found that cationic porphyrins on-chip had some dark toxicity and no statistical significance could be drawn between the cells irradiated and those in the dark. Therefore, a neutral porphyrin was immobilised, and it was found to have less dark toxicity, and enabled statistical significance of the results from irradiated samples and those in the dark. It was shown that the apoptosis of cells irradiated in the porphyrin-immobilised chip was higher after 24 h than after 1 h. However, the expression of HSP70, which is thought to be a fast reaction to stress, was not present 1 h after irradiation. The lack of HSP70 expression implies that the cells would not initiate an immune response, and therefore, would not be suitable for use as a PDT-generated vaccine.

Chapter 5. Overall Conclusion

The overall aim of this project was to produce a photosensitiser-immobilised microfluidic device as a simple and efficient method for generating a personalised cancer vaccine. There were three main areas of the project; the development of the photosensitiser-immobilised microfluidic device; proving the ability to produce singlet oxygen through chemical photo-oxidation reactions and; using the device for a PDT-generated cancer vaccine.

The development of the photosensitiser-immobilised device was achieved through the use of glass slide and glass beads to determine the effectiveness of the method. In addition rhodamine B isothiocyanate was used to gain a visual proof of the successful reaction both with the beads and within the microfluidic device. Finally a cationic porphyrin was immobilised to the glass beads and the glass channels of the chip.

The porphyrin-immobilised chip was used to achieve the photo-oxidation of cholesterol as a proof of having the porphyrin immobilised. This was compared with the same reaction using batch conditions and with the porphyrin in solution on-chip. It was found that the yield was much higher in the batch conditions, but that the immobilised porphyrin was more successful than the porphyrin in solution. To determine the scope of the porphyrin-immobilised porphyrin other photo-oxidation reactions were attempted; the [4+2] oxidation of α-terpinene and the ene oxidation of citronellol. The reaction of α-terpinene was found to be variable but good in methanol but poor in hexane. The reaction of citronellol was found to be poor in both methanol and hexane. However space-time yields showed that all the on-chip reactions were efficient in comparison with the relevant batch reactions.

The porphyrin-immobilised device was then used to determine how effective it was at producing a potential cancer vaccine. To do this the manner of cell death was analysed in

comparison to cell death in the absence of the photosensitiser and/or light. Initially it was found that the cationic porphyrins were causing dark toxicity on-chip which did not allow for statistically significant results for the irradiated samples. Therefore, a neutral hydrophilic porphyrin was used which provided a statistically significant difference and showed that the porphyrin-immobilised chip was causing both apoptosis and necrosis in the cells. An assay for the expression of heat shock protein-70, however was unsuccessful in showing the necessary difference between light and dark controls.

This has shown that the porphyrin-immobilised microfluidic device can be used for producing reactive oxygen species. However, there still requires a considerable amount of work to improve and perfect the device.

5.1. Further work

The preliminary nature of this thesis provides a large number of avenues for further investigation of the various aspects. Although the immobilisation procedure has been proven to work, it would be worth looking into this in more detail. With the details presented in the introduction (1.5.1) it would be advisable to look at the concentration of the silanising agent the reaction time and the curing procedure. In addition there are a number of other amino-functionalised silanising agents that may provide a greater degree of amino-reactivity for subsequent reactions. For the immobilisation technique, factors such as flow rate, reaction time and pH could be useful to investigate. To increase the concentration of photosensitiser on the surface, it could be beneficial to investigate the possibility of attaching multiple porphyrins to the available amines.

The use of the device for photo-oxidation reactions has been proven to be efficient; however, the low yields show that there is much room for improvement. Therefore, an investigation

into increasing the residence time, either by slowing the flow rate of increasing the channel length would be beneficial. However, as the device stands, there is still the possibility of using it for photo-oxidation reactions in which the reactant is scarce and such as natural product synthesis, it may be possible to repeat the reaction to improve the yields. In addition to this, it would be worth investigating modifications to the porphyrins, such as metal centres, which could improve the photostability.

For the use of the chip for the production of cancer vaccines much more work is necessary. The increase in effect for the chemical applications with the addition of oxygen shows that this would be a good place to start. It may be worthwhile to try oxygenating the suspension of cells before they are introduced on-chip. The use of a pressure driven pump may also be helpful as oxygen or air could be used directly. Finally, further work should be conducted into the expression of HSP70 of the cells to determine when it is expressed.

This project has proven the principle of creating singlet oxygen from immobilised porphyrin on the channel walls of a microfluidic device. Although much work needs to be done to optimise this system the results presented have been encouraging. The future for this work could lie in chemical or biological applications, and could have far-reaching benefits.

Chapter 6. Experimental

In this section the practical methods used in the project are detailed. The synthesis method for the porphyrins used is outlined, along with the characterisation that has been conducted. The silanisation methods and further functionalisation of the various glass surfaces are explained. Finally, various chemical and biological applications of the photosensitiser-immobilised glass channels of the chips are presented.

6.1. Materials and Chemicals

All chemicals were used as received unless otherwise stated. 4-Acetamidobenzaldehyde, 4-pyridinecarboxaldehyde, pyrrole, 1,1-thiocarbonyldi-2(*2H*)pyridine, iodomethane, (3-aminopropyl)triethoxysilane, rhodamine B isothiocyanate, 1,3-diphenylisobenzofuran, triethylamine, hydrogen peroxide and control pore glass and MTT (thiazolyl blue) were purchased from Sigma-Aldrich. Cholesterol was also purchased from Sigma-Aldrich and was purified by recrystalising in methanol before use. Sodium sulphate, potassium carbonate, dichloromethane, methanol, hydrochloric acid, hexane, diethyl ether, sulphuric acid, toluene and acetonitrile were purchased from Fisher Scientific. Propylamine, 4-acetamidobenzaldehyde, *N*,*N*-dimethylformamide, dimethylsulfoxide, α-terpinene and citronellol were purchased from Acros. (3-chloropropyl)trimethoxysilane, rose bengal, sodium borohydride, and propionic acid were purchased from Alfa Aesar. Deuterated solvents were purchased from Euriso-top. The glass slides were purchased from Thermo Scientific and were cut using a diamond glass cutter into smaller slides for use. Glass beads were purchased from Merck. Fused silica capillaries were from Polymicro Technologies LLC, Composite Metal Services Ltd. Tygon tubing was purchased from Cole-Parmer and poly(tetrafluoroethylene) (PTFE) tubing was from Supelco. Tefzel ferrules (1/16 inch), PEEK nuts (1/16 inch) and PEEK syringe adaptors (1/4-28 female to female luer adaptor)

were purchased from Anachem Ltd. Nanoport Ferrules (6-32 flat bottom-360/150 µm) and TinyTight PEEK nut (super flangeless fitting for 6-32 FB (flat bottom) ports) were purchased from Presearch Ltd. L-glutamine was purchased from Gibco, frozen in 4 mL batches, thawed before use. Fetal Calf Serum (FCS) was purchased from BioSera and frozen in 50 mL batches, thawed and filtered before use. The Annexin V:FITC assay kit for analysis on the flow cytometer was purchased from AbD Serotec as was the HSP-70 assay kit. The Annexin V:FITC assay kit contained propidium iodide and Annexin V:FITC dyes and the binding buffer, which was diluted 4x with distilled water before each experiment. The HSP-70 kit contained the positive and negative stains for HSP-70 expression in addition to fixation and permeation solutions.

6.2. Instrumentation

For detection of porphyrin on glass slides a Cary Win UV/Vis spectrometer was used (Varian Inc., 50 Bio). For the measurement of fluorescence of DPBF a Cary Eclipse fluorescence spectrometer was used (Varian Inc.). For illuminating samples a Paterson Lamp BL1000A PDT light was used (Phototherapeutics) fitted with a Xenon short arc lamp, used without a filter it produces light over the full visible spectrum and into ultraviolet (UV) and infrared (IR) (200-800 nm) with an intensity of 3.5 W. LED light were purchased from Farnell and set up in house, used as received producing light within the visible spectrum (400-750 nm) with an intensity of 0.27 W. The fluorescent imaging of glass substrates was conducted on an Eclipse TE2000-U (Nikon) microscope fitted with a CCD camera (Retiga-EXL, QImaging, Media Cybernetics UK). The cholesterol and citronellol samples were analysed using Shimadzu LC-6A HPLC pump connected to a 759A UV absorbance detector (Applied Biosystems). The confirmation of oxidised cholesterol peaks was conducted on a Varian 212 LC pump connected to a Varian 500-MS detector (Varian Inc.). The α-terpinene samples were analysed using GC-MS on an Agilent 6890 series GC connected to an Agilent 5973 Network MS detector. MTT assays were analysed on an ELX800 Universal Microplate Reader (Biotek) at 570 nm wavelength. The centrifuge used for cell work was a Biofuge Prima (Heraeus) and the incubator was a Hera Cell (Heraeus). Apoptosis and necrosis was conducted on Becton Dickinson FACSCalibur flow cytometer using the FL1: FL3 lasers to detect FITC and PI.

6.3. Chip Fabrication

Three microfluidic designs were utilised and are referred to as design A, B and C. (Figure 56)

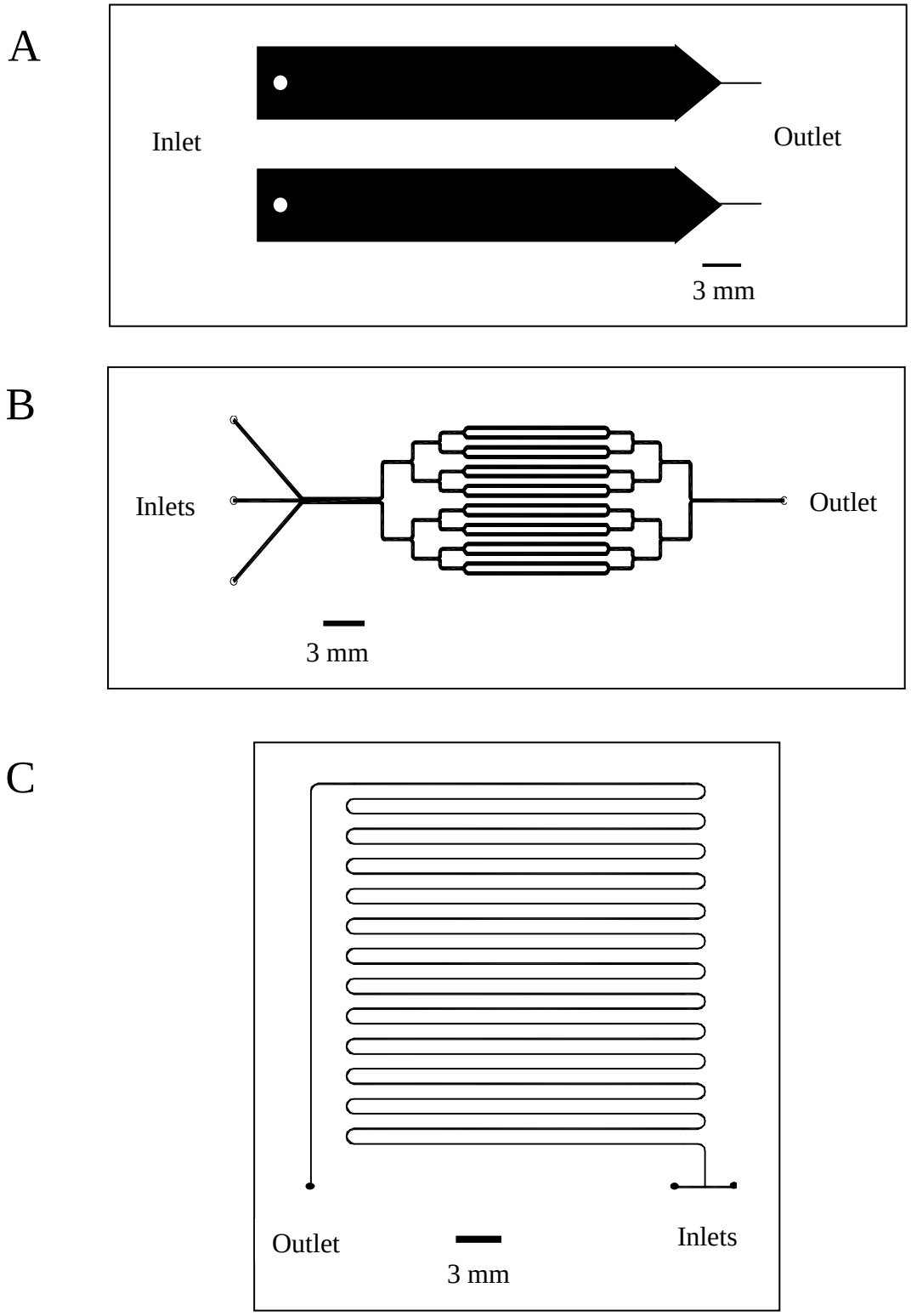

Figure 56: A) packed chip design, B) parallel channel chip design and C) serpentine chip design.

Design A featured a channel (duplicated on one chip) into which the control pore glass could be packed, with one inlet and one outlet for introduction and collection of reagents. The microchip had the following dimensions; top plate (main chamber) (B) 4.5 mm (w) x 30 μm (d) x 3.0 cm (l); bottom plate: small channel (outlet): 150 μm (w) x 50 μm (d), wider channel (main chamber + triangle to outlet) : 4.5 mm (w – at base) x 300 μm (w – at point) x 50 μm (d). The main chamber was deeper than the outlet section to provide a better volume for packing. Design B featured 16 parallel channels (200 μm (w) x 12 mm (l)) with 3 inlets allowing introduction of reagent solutions and oxygen gas, and one outlet for collecting the product (Figure 57).

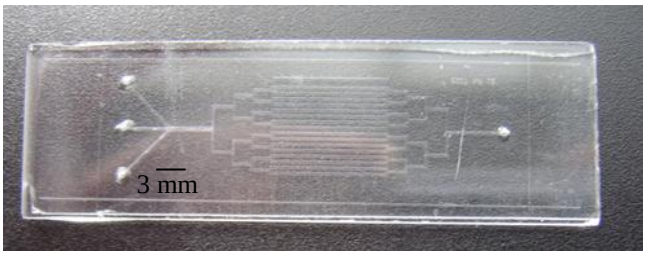

Figure 57: Chip design B before capillaries are glued or screwed in place.

Design C featured two inlets converging into a serpentine channel with 24 bends at 180° and the final bend to the outlet of 90° and a channel width of 75 μm (Figure 58).

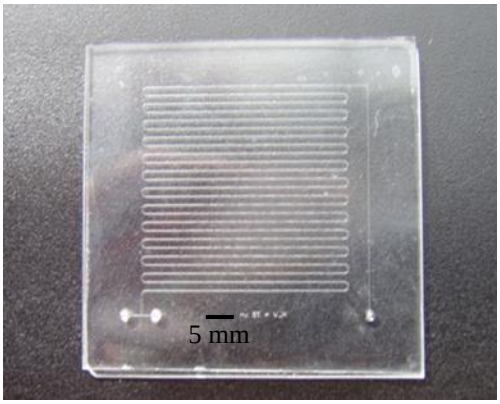

Figure 58: Chip design C before capillaries are glued in place.

They were all fabricated in borosilicate glass by the wet etching technique.[171] Briefly this involves a photolithographic glass plate with a chromium layer covered by a photoresist. The photoresist was removed in the area of the design by exposing these areas to UV light through a mask. To remove the UV-exposed photoresist layer the wafer was placed in a 1:1 solution of Microposit Developer Concentrate:purified water. This was followed by etching of the chromium layer using Microposit Chrom Etch 18 and then the glass in hydrofluoric acid. Access holes were drilled into the design, the photoresist and the chromium layer were removed and the resulting etched plate was bonded to a base plate in the furnace. For design A the top plate was etched for the main chamber, and the base plate was etched for this section and the remaining design, when bonded it gave a larger area for the chip to be packed. A 3D representation of this can be seen in Figure 59.

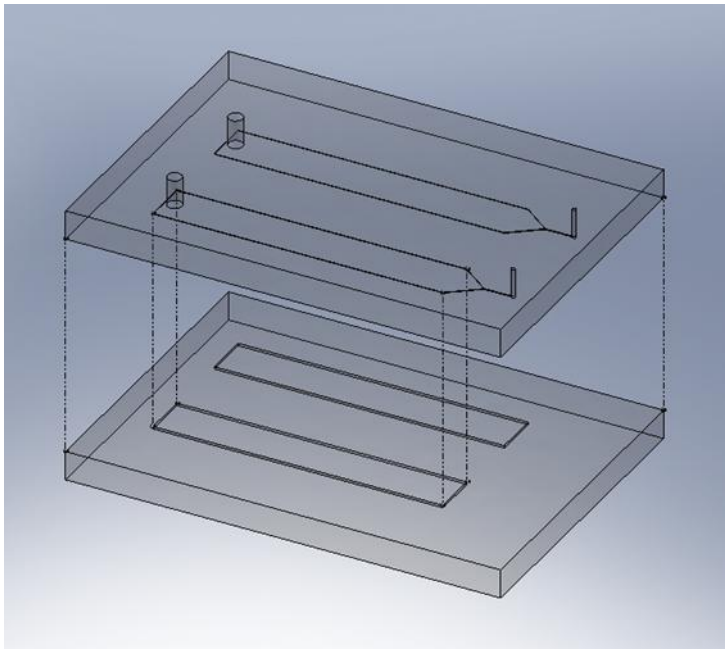

Figure 59: 3D schematic of chip design A showing the two plates etched for the chamber.

6.4. Porphyrin synthesis

The following porphyrin synthesis was adapted from the work of Sutton *et al.*[323]

Synthesis of 5-(4-acetamidophenyl)-10,15,20-tri-(4-pyridyl)porphyrin

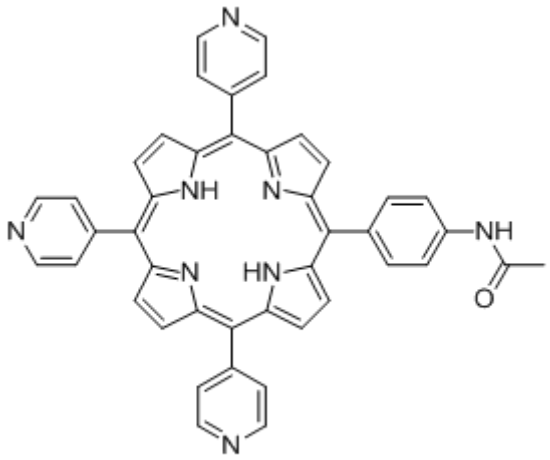

32

To a stirred solution of 4-acetamidobenzaldehyde (14.1 g, 86 mmol) in propionic acid (1 L) was added 4-pyridinecarboxaldehyde (19.5 mL, 207 mmol) and the solution was heated to reflux in a two necked flask equipped with a condenser. Pyrrole (20 mL, 288 mmol) was then added dropwise to the reaction mixture. Once the addition was complete the reaction mixture was held at reflux for 30 min and then cooled overnight. The solvent was then removed under reduced pressure and the residue purified by flash chromatography using dichloromethane:methanol (95:5) as eluent. The product was precipitated using methanol to yield **32** as a purple solid (1.082 g, 1.6 mmol, 2 %) ^{1}H-NMR ($CDCl_3$, 400 MHz) δ: -2.89 (s, 2H, N**H**); 2.39 (s, 3H, C**H**$_3$); 7.71 (s, 1H, N**H**COCH$_3$); 7.95 (d, 2H, J=8.4 Hz, 5-**Ph**-m); 8.10-8.29 (m, 8H, 6xH **Py**-o, 2xH **Ph**-o); 8.81 (d, 2H, J=4.9 Hz, **H**-β); 8.83-8.90 (m, 4H, **H**-β); 8.94 (d, 2H, J=4.9, **H**-β); 9.01-9.09 (m, 6H, H **Py**-m); R_f = 0.22 (DCM:MeOH, 19:1); UV/Vis (DCM) $\lambda_{max,}$ nm: 418, 514, 551, 589, 647; ESI-MS *m/z*: 675 (M + 1, 100%)

Synthesis of 5-(4-aminophenyl)-10,15,20-tri-(4-pyridyl)porphyrin

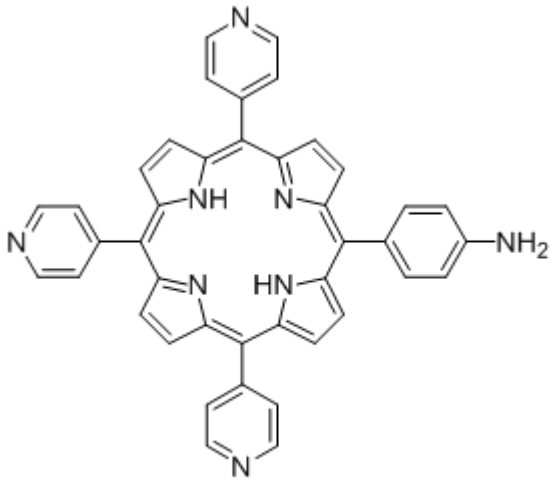

33

5-(4-Acetamidophenyl)-10,15,20-tri-(4-pyridyl)porphyrin (102.5 mg, 0.152 mmol) was dissolved in 5M HCl (aq) (100 mL) and the solution heated at reflux for 3 h with stirring. The hot reaction mixture was concentrated under reduced pressure to yield a green solid. This was then dissolved in a mixture of dichloromethane:triethylamine (9:1, 200 mL) and stirred for 10 min at room temperature. The solution was washed with water (4 x 200 mL), the organic layer was separated and dried over anhydrous sodium sulphate and concentrated under reduced pressure. The product was precipitated using methanol to yield **33** a purple solid (83.2 mg, 87 %). ^{1}H-NMR ($CDCl_3$, 400 MHz) δ: -2.83 (s, 2H, N**H**); 4.11 (s, 2H, N$\mathbf{H_2}$); 7.10 (d, 2H, J=8.44, 5-**Ph**-m); 7.99 (d, 2H, 8.44 Hz, 5-**Ph**-o); 8.17 (m, 6H, **Py**-o); 8.84 (m, 6H, **Py**-m); 9.02 (m, 8H, **H**-β); R_f = 0.31 (DCM/MeOH, 20:1); UV/Vis (DCM) λ_{max}, nm: 420, 516, 554, 591, 647; ESI-MS *m/z*: 633 (M + 1, 100%)

Synthesis of 5-(4-isothiocyanatophenyl)-10,15,20-tri-(4-pyridyl)porphyrin

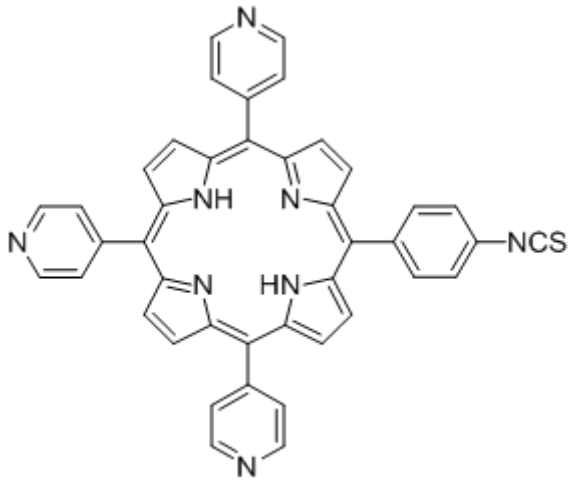

34

5-(4-Aminophenyl)-10,15,20-tri-(4-pyridyl)porphyrin (83.2 mg, 0.131 mmol) was dissolved in freshly distilled dichloromethane (20 mL) and 1,1-thiocarbonyldi-2(2*H*)-pyridone (65.2 mg, 0.281 mmol) was added. The reaction was allowed to stir at room temperature under nitrogen for 2 h and then concentrated under reduced pressure. The mixture was then separated using flash column chromatography with dichloromethane:methanol (96:4) and precipitated using hexane to yield **34** a purple solid (76.8 mg, 87 %). ^{1}H-NMR ($CDCl_3$, 400 MHz) δ: -2.91 (s, 2H, N**H**); 7.65 (d, 2H, J=7.84, 5-**Ph**-m); 8.14-8.23 (m, 8H, 6xH **Py**-o, 2xH 5-**Ph**-o); 8.86 (m, 8H, **H**-β); 9.06 (d, 6H, J=4.72, **Py**-m); R_f = 0.48 (DCM/MeOH, 96:4); UV/Vis (DCM:MeOH, 24:1) λ_{max} nm: 426, 513, 548, 588, 644; ESI-MS *m/z*: 674 (M^+)

Synthesis of 5-(4-isothiocyanatophenyl)-10,15,20-tris-(4-*N*-methylpyridiniumyl) porphyrin triiodide

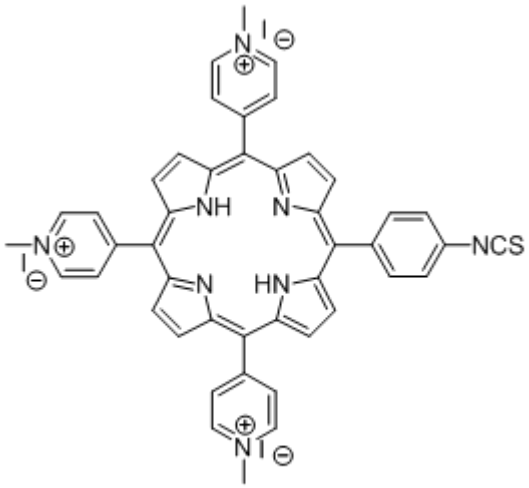

35

5-(4-Isothiocyanatophenyl)-10,15,20-tri-(4-pyridyl)porphyrin (76.8 mg, 0.114 mmol) was dissolved in 7.5 mL of dry DMF in a two necked flask equipped with a reflux condenser and a rubber septum. To the stirred solution a large excess of iodomethane (1.6 mL, 25.6 mmol) was added via syringe. The reaction mixture was stirred at 40 °C overnight and after cooling was precipitated with ice cold diethyl ether and washed thoroughly with the same solvent. The methylated porphyrin **35** was obtained as a purple/brown solid (121.6 mg, 97 %) ^{1}H-NMR (DMSO, 400MHz) δ: -3.13 (s, 2H, N**H**); 7.88 (d, 2H, J=8.30, 5-**Ph**-m); 8.24 (d, 2H, J=8.30, 5-**Ph**-o); 8.83-9.24 (m, 14H, 6xH **Py**-o, 8xH **H**-β); 9.42 (d, 6H, J=6.24, **Py**-m); UV/Vis (H_2O) λ_{max}, nm: 424, 520, 557, 585, 641;

Synthesis of 5-(4-isothiocyanatophenyl)-10,15,20-tris-(4-*N*-methylpyridiniumyl) porphyrin trichloride

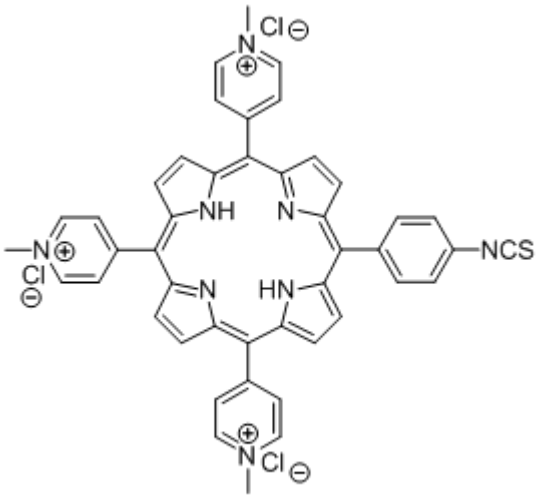

37

5-(4-Isothiocyanatophenyl)-10,15,20-tri-(4-pyridyl)porphyrin (70.9 mg, 0.105 mmol) was dissolved in 7 mL of dry DMF in a two necked flask equipped with a reflux condenser and a rubber septum. To the stirred solution a large excess of iodomethane (1.0 mL, 16 mmol) was added via syringe. The reaction mixture was stirred at 40 °C overnight and after cooling was precipitated with ice cold diethyl ether. It was redissolved in dimethylsulfoxide (DMSO) and precipitated by addition of ammonia hexafluorophosphate with water. After filtering the solid it was redissolved in acetone and precipitated by the addition of tetrabutylammonium chloride. The cationic porphyrin with the chloride counter ions, **37,** was obtained as a purple solid (94.2 mg, 86 % yield). ^{1}H-NMR (DMSO,400MHz) δ: -3.13 (s, 2H, N**H**); 4.71 (s, 9H, C**H**$_3$-pyr); 7.93 (d, 2H, J=8.16, 5-**Ph**-m); 8.28 (d, 2H, J=8.16, 5-**Ph**-o); 8.97-9.14 (m, 14H, 6xH **Py**-o, 8xH **H**-β); 9.49 (d, 6H, J=6.28, **Py**-m); UV/Vis (H_2O) λ_{max}, nm: 424, 520, 557, 584, 641

Synthesis of 5-(4-(*N*-propylthiocarbamido)-aminophenyl)-10,15,20-tris(4-*N*-methylpyridiniumyl) porphyrin triiodide

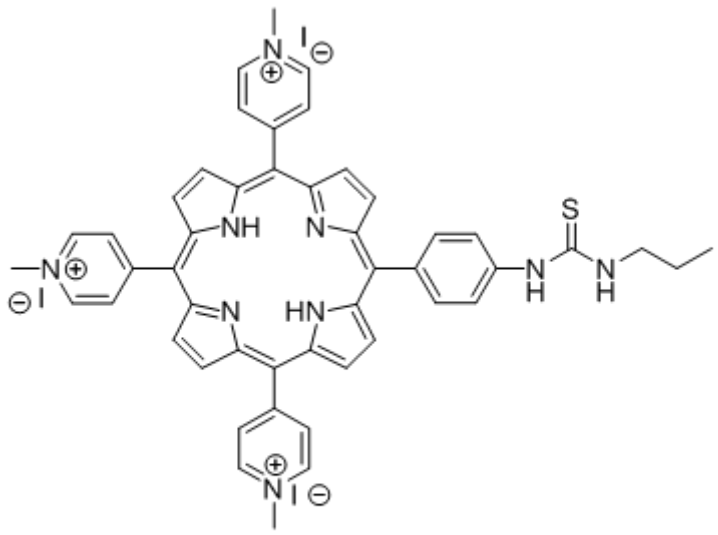

44

5-(4-Isothiocyanatophenyl)10,15,20-tris(4-*N*-methyldyridiniumyl)porphyrin triiodide (53.6 mg, 0.049 mmol) was dissolved in 5 mL dry DMF, to which propylamine (0.05 mL, 0.608 mmol) was added. The resulting mixture was stirred at room temperature for 1 h, after which the product was precipitated with ice cold diethyl ether to yield **44** as a purple/blue solid (43.4 mg, 77%). ^{1}H-NMR (DMSO, 400MHz) δ: -3.01 (s, 2H, N**H**); 0.99 (t, 3H, C**H**$_3$-CH$_2$-CH$_2$-NH-); 1.08 (t, 2H, CH$_3$-C**H**$_2$-CH$_2$-NH-); 1.65-68 (m, 2H, CH$_3$-CH$_2$-C**H**$_2$-NH-); 4.71 (s, 9H, C**H**$_3$-pyr); 8.03 (d, 2H, J=8.40, 5-**Ph**-m); 8.14 (d, 2H, J=8.4, 5-**Ph**-o); 8.95-9.15 (m, 14H, 6xH **Py**-o, 8xH **H**-β); 9.46 (d, 6H, J=6.8, **Py**-m); UV/Vis (H$_2$O) λ_{max} nm: 424, 520, 558, 583, 642

Synthesis of 5-(4-Acetamidophenyl)-10,15,20-tri-(3,5-dimethoxyphenyl) porphyrin

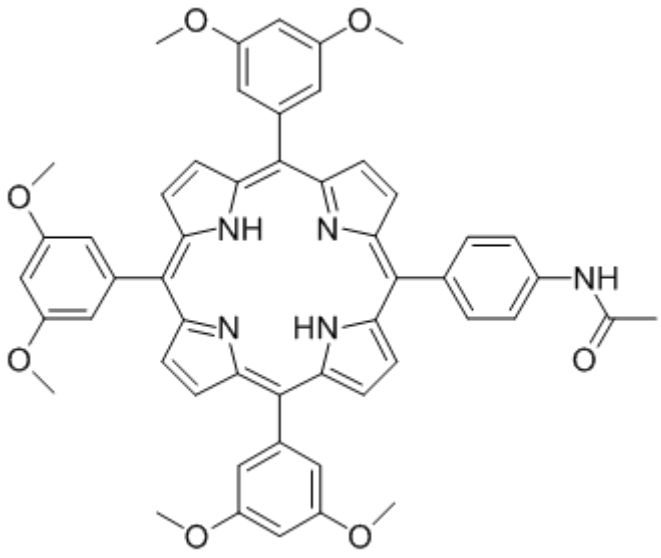

38

To a stirred solution of 4-acetamidobenzaldehyde (3.36 g, 20 mmol) in propionic acid (500 mL) was added 3,5-dimethoxybenzaldehyde (10.0 g, 60 mmol) and the solution was heated to reflux in a two necked flask equipped with a condenser. Pyrrole (5.5 mL, 80 mmol) was then added dropwise to the reaction mixture The crude reaction mixture was purified by chromatography, eluting with DCM/ethyl acetate (4:1) and yielded **38** as a purple crystalline solid (1.55 g, 9%); R_f = 0.50 (DCM/ethyl acetate, 4:1); UVvis (DCM) λ_{max}, nm: 421, 515, 551, 590, 650; ^{1}H-NMR (270 MHz, $CDCl_3$) δ: -2.96 (s, 2H, N**H**); 2.23 (s, 3H, C$\mathbf{H}_3$); 3.93 (s, 18H, 10+15+20-m-OC$\mathbf{H}_3$); 6.99 (s, 3H, 10+15+20-p-**Ar**); 7.07 (d, 2H, J=8, 5-m-**Ar**); 7.38 (s, 6H, 10+15+20-o-**Ar**); 7.44; ^{13}C-NMR (68 MHz, $CDCl_3$) δ: 20.4, 23.9, 103.9, 113.5, 117.3, 119, 119.4, 119.6, 120, 129, 131.1, 131.3, 131.4, 131.8, 134.5, 135.6, 139.3, 143.1, 158.6, 160.3, 167.9, 168.7; MALDIMS *m*/*z*: 852 (M^+, 100%)

Synthesis of 5-(4-Aminophenyl)-10,15,20-tri-(3,5-dimethoxyphenyl) porphyrin

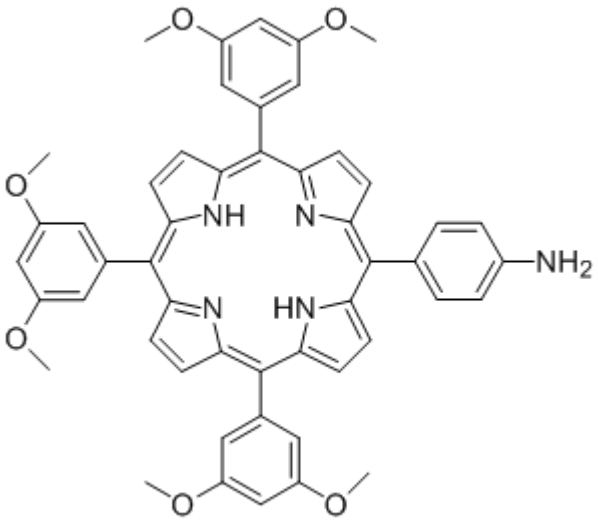

39

5-(4-Acetamidophenyl)-10,15,20-tri-(3,5-dimethoxyphenyl) porphyrin was dissolved in 5M HCl (aq) (100 mL) and the solution heated at reflux for 3 h with stirring. The hot reaction mixture was concentrated under reduced pressure to yield a green solid. This was then dissolved in a mixture of dichloromethane:triethylamine (9:1, 200 mL) and stirred for 10 min at room temperature. The solution was washed with water (4 x 200 mL), the organic layer was separated and dried over anhydrous sodium sulphate and concentrated under reduced pressure. The crude purple solid was purified by chromatography, eluting with DCM/ethyl acetate (4:1) and yielded the desired product (**39**) as a purple crystalline solid (426 mg, 89.7%); R_f = 0.89 (DCM/ethyl acetate, 4:1); UVvis (DCM) λ_{max}, nm: 422, 517, 553, 593, 651; ^{1}H-NMR (270 MHz, $CDCl_3$) δ: -2.80 (s, 2H, N**H**); 3.96 (s, 18H, 10+15+20-m-OC**H**$_3$); 6.90 (s, 3H, 10+15+20—p-**Ar**); 7.06 (d, 2H, j+8, 5-m-**Ar**); 7.40 (s, 6H, 10+15+20-o-**Ar**); 8.93 (m, 8H, **H**-β); ^{13}C-NMR (68 MHz, $CDCl_3$) δ; 20.13, 113.9, 114.3, 115.7, 119.8, 120.1, 121.4, 130.2, 131.4, 132.7, 136.1, 144.5, 144.6, 146.5, 159.3; MALDI-MS *m*/*z*: 809 (M^+, 100%)

Synthesis of 5-(4-Aminophenyl)-10,15,20-tri-(3,5-dihydroxyphenyl) porphyrin

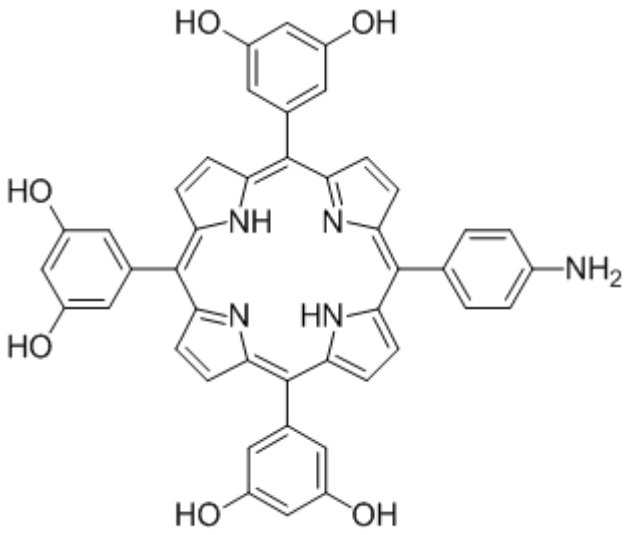

40

To a stirred solution of 5-(4-aminophenyl)-10,15,20-tri(3,5-dimethoxyphenyl) porphyrin (1 equiv) in freshly distilled DCM (50 mL) was added boron tribromide (15 equiv). The reaction was allowed to proceed under argon for 17 h at room temperature. The reaction mixture was cooled to 0 °C then treated with water and allowed to warm to room temperature for a further 1 h. The reaction was then concentrated in vacuo and redissolved in a (9:1) mixture of DCM/triethylamine (100 mL). The solution was washed with water (3 x 100 mL) and saturated brine (100 mL), the organic layer separated, dried (Na_2SO_4), and then concentrated in vacuo. The solid residue was chromatographed, eluting with $CHCl_3$/MeOH (9:1) to afford **40** as a purple crystalline solid; R_f = 0.19 ($CHCl_3$/MeOH, 9:1); UV-vis (DCM) λ_{max}, nm: 422, 517, 553, 592, 649; ^{1}H-NMR (270 MHz, DMSO) δ: -2.95 (s, 2H, N**H**); 5.56 (s, 2H, N**H**$_2$); 6.69 (s, 3H, 10+15+20-p-**Ar**); 7.02 (d, 2H, J=8, 5-m-**Ar**); 7.06 (s, 6H, 10+15+20-o-**Ar**); 7.87 (d, 2H, J=8, 5-o-**Ar**); 8.94 (s, 8H, **H**-β); 9.75 (s, 6H, 10+15+20-m-OH); ^{13}C-NMR 68 MHz, DMSO) δ: 102.3, 112.5, 113.9, 114.1, 119.2, 119.7, 121.5, 127.5, 128.3, 130.7-131.3, 135.5, 142.8, 142.9, 148.6, 156.4, 156.5; MALDI-MS *m*/*z*: 726 (M^+, 100%).

Synthesis of 5-(4-Isothiocyanatophenyl)-10,15,20-tri-(3,5-dihydroxyphenyl) porphyrin

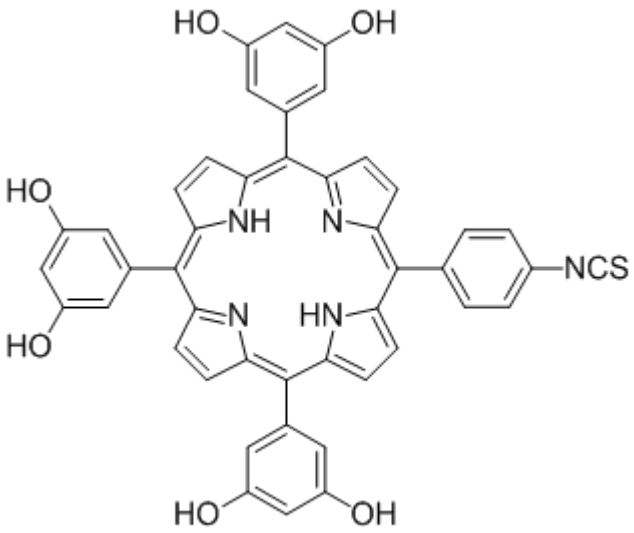

41

5-(4-Aminophenyl)-10,15,20-tri-(3,5-hydroxyphenyl)porphyrin (1 equiv) was dissolved in freshly distilled dichloromethane (20 mL) and 1,1-thiocarbonyldi-2(2*H*)-pyridone (1 equiv) was added. The reaction was allowed to stir at room temperature under nitrogen for 2 h and then concentrated under reduced pressure. The solid was purified by chromatography, eluting with $CHCl_3$/MeOH (9:1) which afforded the required product (**41**) as a purple crystalline solid; R_f = 0.29 ($CHCl_3$/MeOH, 9:1); UV-vis (MeOH) λ_{max}, nm: 422, 516, 552, 592, 648; ^{1}H-NMR (270 MHz, 25% CD_3OD in $CDCl_3$) δ: 6.77 (s, 3H, 10+15+20-p-**Ar**); 7.12 (s, 6H, 10+15+20-o-**Ar**); 7.64 (d, 2H, J=8, 5-m-**Ar**); 8.19 (d, 2H, J=8, 5-o-**Ar**); 8.76-9.0 (m, 8H, **H**-β); ^{13}C-NMR (68 MHz, 25% CD_3OD in $CDCl_3$) δ: 101, 107.1, 114.7, 117.6, 119.9, 120, 120.1, 123.9, 130.9, 134, 135.2, 136.1, 141.2, 142, 143.6, 155.8; ES-HRMS Anal. Calcd.for $C_{45}H_{29}N_5O_6S$ ($[M + H]^+$), 768.1914; found, 768.1908

6.5. Microfluidic chip setup and interface

6.5.1. Packed chip

The packed chip (design A) was fabricated in 3 mm thick B-270 glass. For the inlet 1/16 inch o.d. Teflon tubing with 395 µm o.d. was glued to the holes and interfaced to the syringe via a Tefzel ferrule a PEEK nut and PEEK syringe adaptor. For the outlet 360 µm o.d. Tub PEEK tubing was used with 150 µm i.d., glued to the outlet holes (Figure 60).

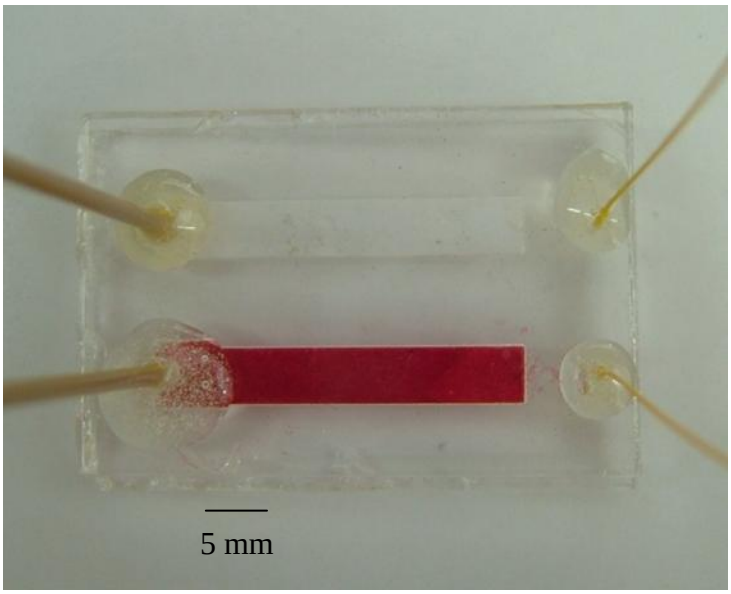

Figure 60: Packed chip with glued capillaries for introduction and collection of reagents.

6.5.2. Parallel channel chip

For the development of the functionalisation method, and for the first cholesterol experiments, fused glass capillaries of 365 µm o.d. and 150 µm i.d. were glued into the inlet and outlet holes using Araldite 2000 (Huntsman) glue. The system was interfaced to the syringe via PTFE tubing (0.3 mm i.d., 1.58 mm o.d.) attached to the end of the capillaries and inserted into the Tefzel ferrule. This was housed inside the PEEK nut and screwed into the PEEK syringe adaptor. For the outlet Tygon tubing was inserted onto the capillary.

In order to improve performance and avoid glue blocking capillaries, a chip holder was designed. This was fabricated in aluminium with holes matching those drilled into the chip. To interface this with the syringe the capillaries were inserted into NanoPort Ferrules which sat flush to the chip surface through the chip holder holes. This was then screwed securely in place with a TinyTight PEEK nut and sealed the capillary to the chip (Figure 61).

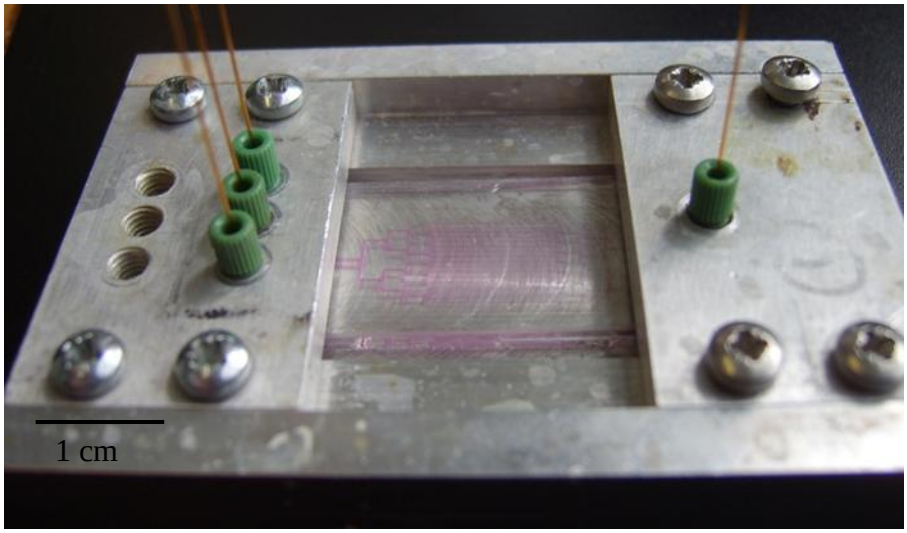

Figure 61: Parallel channel chip setup in the aluminium chip holder with capillaries screwed in place for interfacing to the syringe pump.

The oxygen was introduced on-chip (where used) through a series of fused silica capillaries with an internal diameter of 20 µm connected through PTFE tubing. The oxygen was taken straight from the cylinder through PTFE tubing (5 mm i.d.) fitted with a pipette tip with a capillary glued into the tip. This enabled fine control of the oxygen flow by increasing or decreasing the length of the capillary from the cylinder to the chip

6.5.3. Serpentine channel chip

The serpentine chip was set up in the same manner as the initial setup of the parallel channel chip with capillaries glued in place with Araldite glue. It was interfaced with the syringes via the PTFE tubing, ferrule and PEEK nut and syringe adaptor (Figure 62).

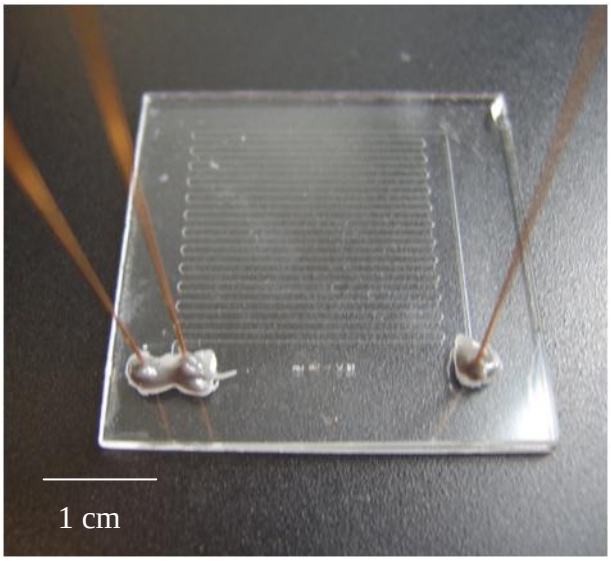

Figure 62: Serpentine chip design with capillaries glued in place for interfacing with the syringe pump.

6.6. Glass functionalisation

The method used for the silanisation and functionalisation were taken from a number of sources and altered to fit the purpose.[62-90] The justification for the procedures used is outlined in the introduction (section 1.5) and the final methods are outlined below.

6.6.1. Silanisation procedures

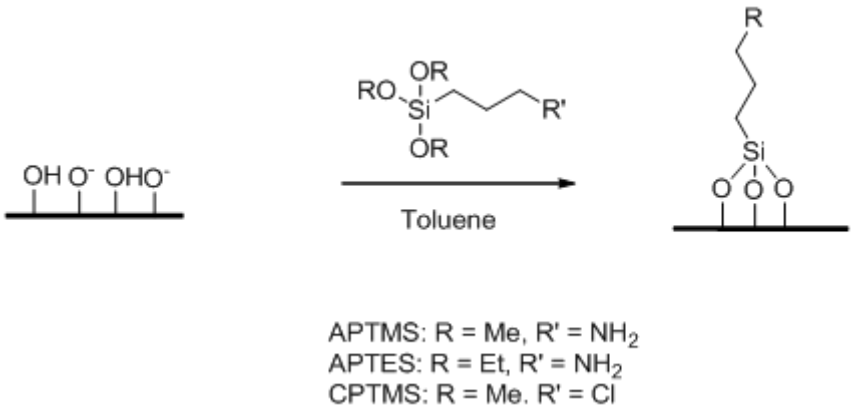

Scheme 16: Silanisation procedure from clean glass surfaces.

Glass slides

To ensure that the brorsilicate microscope glass slides are clean of any organic material they were cleaned in an acidic piranha solution. This method was adapted from a number of sources that used the same procedure.[55, 66, 69, 72, 74, 75, 87, 96, 100, 112, 117, 118, 129, 132, 134, 138, 161, 170, 270, 325, 328, 331] Glass slides were prepared by cleaning in freshly prepared piranha solution (H_2SO_4:35% H_2O_2 3:1 v/v) at 65 °C for 1 h and then washing thoroughly with deionised water and storing under deionised water until required.

To silanise the slides they were dried in the oven overnight (120 °C) then rinsed with methanol, methanol:toluene (1:1 v/v) and toluene, and dried in the oven (120 °C) for 10 min to ensure they were dry. When taken out of the oven the slides were cooled inside the round

bottomed flask under vacuum. Finally slides were immersed in a solution (concentrations change for each experiment) of silanising agent in dry toluene.

Silanisation was undertaken at both room temperature and at reflux under a nitrogen atmosphere. After the appropriate time (times vary according to experiment) the glass slides were rinsed with toluene, sonicated under toluene for 10 min, and then rinsed with methanol:toluene (1:1 v/v). Slides were then dried and stored under nitrogen until required.

Glass beads

Glass beads were prepared by cleaning with piranha solution (as with glass slides), they were then washed with deionised water, and allowed to dry in the oven (120 °C) overnight.

To silanise, the beads were removed from the oven and allowed to cool, then rinsed with methanol, methanol:toluene (1:1 v/v) and toluene. Beads were dried again in the oven (120 °C) for a further 30 min, and then placed into a flask with the silanising agent in dry toluene. The reaction proceeded at reflux with different concentrations and times for each experiment. On completion they were rinsed with toluene, sonicated in toluene for 5 min and washed again with toluene. Finally the silanised beads were dried and stored under nitrogen.

Glass microdevice

Chips (design B or design C) cleaned in the furnace were washed with deionised water and the channels filled with water before treatment with piranha solution. After piranha cleaning (as with glass slides) they were sonicated in water, and cleaned with more water before the fused glass capillaries were glued in place, or screwed in place using a chip holder as detailed in section 6.5.

To silanise with APTES, methanol was pumped through the chip, followed by filling the channels with an aqueous sodium hydroxide (1 mM) solution for 1 h. The sodium hydroxide solution was rinsed out with methanol, followed by rinsing with toluene. The channels were filled with a 5 % (v/v) APTES solution in dry toluene for 1 h. The APTES solution rinsed out with toluene, sonicated in toluene and rinsed again with toluene. They were dried with nitrogen and placed in the oven at 120 °C for 1 h in order to cure them. If not used immediately they were sealed to the air until needed.

To silanise with CPTMS, 1 mL was pumped through the chip with no dilution at 10 μL min^{-1} and then rinsed with toluene and sonicated in toluene.

6.6.2. Functionalisation procedures

Immobilisation with a thiourea bond

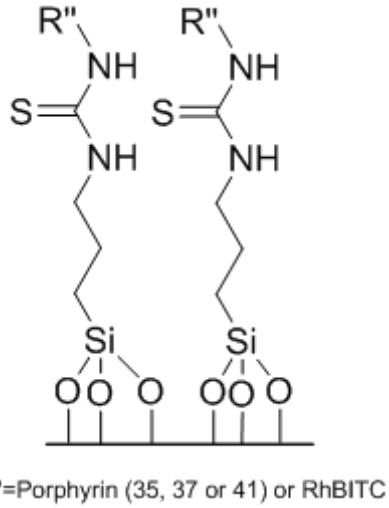

Figure 63: Thiourea bond between porphyrin or rhodamine B on glass surface.

Porphyrin and glass slides

An excess of potassium carbonate (~10 mg, 7μM) was added to a clean dry flask. To this 9.9 mL of dimethylsulfoxide (DMSO) was added followed by 0.1 mL of a 10 mM stock solution

of porphyrin in DMSO with stirring. This was modified from a reaction for coupling with antibodies.[323] The reaction vessel was kept under nitrogen, and the glass slides were added. The concentration of the solution and of the porphyrin on glass slides was measured by UV/Vis spectrometry before glass slides were added and after 1 h and 24 h of reaction.

Rhodamine B and glass beads

The glass beads were transferred to a solution of RhBITC (7.5 mg) in 10 mL methanol with 0.05 mL of triethylamine. The reaction was stirred under nitrogen at room temperature for 24 h. The beads were then washed with methanol, sonicated in methanol and washed again in methanol. Finally the beads were dried using a stream of nitrogen.

Porphyrin and glass beads

A 10 mM stock solution of 5-(4-isothiocyanatophenyl)-10,15,20-tris-(4-*N*-methyl pyridiniumyl) porphyrin triiodide in DMSO was prepared. 0.1 mL of this was added to 9.9 mL DMSO with K_2CO_3 (~10 mg), and the glass beads were transferred into the vessel. The beads were stirred under a nitrogen atmosphere for 5 hrs, after which the beads were washed with water, sonicated for 5 min in DMSO/water, washed again with water and then rinsed with methanol.

Rhodamine B and glass microdevice

Methanol was used to fill the chip (design B) before the solution of RBITC (~0.7 mg) in methanol (1 mL) and triethylamine (~50 μL) was pumped through the chip at 5 μL min^{-1}. This method was modified from a reaction conducted in our group. The channels were then rinsed with methanol, sonicated in methanol for 5 min, and then rinsed again with methanol,

before drying with a flow of nitrogen. Successful immobilisation was observed by a pink colour to the channels and a fluorescent image under a fluorescent microscope.

Porphyrin and glass microdevice

Methanol was used to fill the chip (design B) before the solution of 5-(4-isothiocyanatophenyl)-10,15,20-tris-(4-*N*-methylpyridyniumyl) porphyrin triiodide (1.0 mg) in methanol (1 mL) and triethylamine (~50 μL) was pumped through the chip at 5 μL min^{-1}. The channels were then rinsed with methanol, sonicated in methanol for 5 min, and rinsed again with methanol, before drying with a flow of nitrogen. Successful immobilisation could be visually verified by a faint yellow colour to the channels.

Immobilising with a carboxylate ester bond

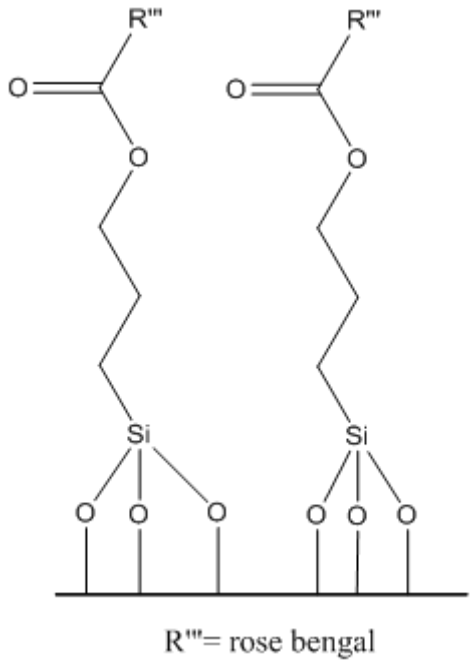

Figure 64: Immobilisation of rose bengal to glass surface with an ester bond.

Rose bengal and control pore glass

Controlled pore glass (0.75 g) was added to a stirred solution of (3-chloropropyl)-trimethoxysilane (2.22 mL, 12.00 mmol) in anhydrous toluene (10 mL) and heated to reflux, under N_2, for 8 hr. The resulting reaction mixture was filtered under suction and washed with toluene (10 mL) then DCM (20 mL), prior to oven drying at 60°C to afford (3-chloropropyl)-functionalised controlled pore glass (CPG-Cl) (16.0 mmol g^{-1}).

Based on a protocol reported by Blossey *et* al.[200] (3-chloropropyl)-functionalised controlled pore glass (0.20 g, assumed 3.2 mmol) was added to a stirred solution of Rose Bengal (4.07 g, 4.00 mmol, 1.25 eq.) in anhydrous DMF (50 mL) prior to heating the reaction mixture to 80°C for 24 hr. The resulting reaction mixture was filtered under suction and washed with DI

water (1500 mL), followed by MeOH (200 mL), ethyl acetate (200 mL) and DCM (200 mL) to afford the immobilised Rose Bengal as a free flowing red solid.

Rose bengal and microfluidic device

RB (4.7 mM) in DMF was pumped through the silanised chip at 5 μL min^{-1} at room temperature or heated to 40 °C. The chip was rinsed with water and methanol and sonicated in methanol.

6.7. Singlet oxygen generation

6.7.1. Diphenylisobenzofuran

Batch

A 10mM stock solution of DPBF in acetonitrile was freshly prepared for each experiment. A 10 mM stock solution of rose bengal in acetonitrile was prepared separately. For the experiments the rose bengal stock solution was diluted to 0.1 mM. The following amount of DPBF and RB were made up to 4 mL for the experiments

Table 3: Concentrations used for experiments with DPBF and RB.

DPBF	RB	RB concentration
30 μL	40 μL	1 μM
30 μL	80 μL	2 μM
30 μL	120 μL	3 μM

Light from a Xe source was shone on the solution from underneath the sample through a bandpass filter (320 – 680 nm) for 1 min intervals with stirring (giving a fluence rate of 39.6 J cm^{-2}), and samples of the solution were analysed using the fluorescence spectrophotometer.

Packed chip

The chip (design A) was packed with control pore glass, one channel had blank glass, with no immobilised photosensitiser, the other channel had control pore glass immobilised with rose bengal. A fresh 300 μM solution of DPBF was pumped through the microchip at a flow rate of 1 μL min^{-1} and collected for 5 min at a time. Light was used to irradiate the chip for the 5 min collections time (fluence rate = 437 J cm^{-2}). Samples were then diluted and analysed by

fluorescence spectrophotometry. When no further change in the fluorescence intensity was observed between samples the light was switched off and the solution monitored until fluorescence intensity was recovered.

6.7.2. Cholesterol

Batch

5 mL of the photosensitiser solution (20 μM) was mixed with 5 mL of cholesterol solution (10 mM) in 10% methanol in dichloromethane. Parallel experiments were performed with and without bubbling of oxygen through the sample. The solutions were then irradiated with the Xe light source for 1 h (fluence rate = 2376 J/cm^2) while surrounded with aluminium foil to maximise the light dose.

Packed Chip

A 5 mM solution of cholesterol in 10% methanol in dichloromethane was pumped through the chip (design A) at different flow rates. Untreated porous glass beads were used as a blank, while the rose bengal immobilised beads were used for the experiment. The chip was then illuminated with the Xe light source while the solution was pumped through. The flow rates used, time allowed to collect the sample and fluence rates for both light sources are displayed below:

Table 4: Table showing flow rates and fluence rates for the oxidation of cholesterol through the CPG-RB packed chip experiments.

Flow rate (μL min^{-1})	Time collected (min)	Fluence rate for Xe arc lamp (J cm^{-2})	Fluence rate for LED (J cm^{-2})
10	20	43.7	7.28
5	40	87.5	14.6

Two samples were collected with the light off (before and after irradiation) and one with the light on (irradiated)

Microchannel chip (solution)

A mixture of a solution of photosensitiser (20 μM) and a solution of cholesterol (10 mM) in 10% methanol in dichloromethane in a 1:1 ratio was pumped through the chip (design B) at various flow rates, as follows (with the relevant fluence rates):

Table 5: Table showing flow rates and fluence rates for the oxidation of cholesterol in solution with porphyrin through the parallel channel chip.

Flow rate (μL min^{-1})	Time collected (min)	Fluence rate for Xe arc lamp (J cm^{-2})
5	20	10.5
2.5	40	21.0

The light source used was the Xe lamp and was conducted with and without the addition of oxygen as outlined in section 6.5.2. When oxygen was used it was introduced directly onto the chip, so the solution and gas were mixed as they entered the chip.

Microchannel chip (immobilised photosensitiser)

The chip (design B) with the photosensitiser immobilised to the glass surface was used for this experiment. A 5 mM solution of cholesterol in 10% methanol in dichloromethane was pumped through the chip at various flow rates as follows:

Table 6: Table showing flow rates and fluence rates for the oxidation of cholesterol through the porphyrin-immobilised parallel channel chip.

Flow rate ($\mu L\ min^{-1}$)	Time collected (min)	Fluence rate ($J\ cm^{-2}$)
5	20	10.5
2.5	40	21.0

The light source used was the unfiltered Xe lamp and was conducted with oxygen introduced directly onto the chip as detailed in section 6.5.2

RP-HPLC analysis

Samples collected from the cholesterol experiments were all tested using RP-HPLC. The mobile phase was 60:40 (v/v) methanol:acetonitrile at 1 mL min^{-1} using a 250 x 46 mm C18 phenomenex HPLC column. Eluting material was monitored using a UV detector set at 205 nm. The oxidised cholesterol products eluted between 6-9 min, while cholesterol eluted at 13 min.

6.7.3. α-Terpinene

Batch

5 mL of the photosensitiser solution (20 μM) was mixed with 5 mL of α-terpinene solution (0.15 mM) in methanol. The sample was bubbled with oxygen and the solutions were then irradiated with the unfiltered Xe light source over 2 h (fluence rate = 4752 J cm^{-2}). Samples were taken at the start, and then after 1 and 60 min for analysis on GC-MS

Microchannel chip (immobilised photosensitiser)

The chip (design B) with the photosensitiser immobilised to the glass surface was used for this experiment. A 0.15 mM solution of α-terpinene in methanol was pumped through the chip at 2.5 μL min^{-1}. The unfiltered Xe arc lamp was used to irradiate it with oxygen introduced directly onto the chip (fluence rate = 21.0 J cm^{-2})

GC-MS

Samples collected from the α-terpinene experiments were analysed using GC-MS. The column used was a HP-1 column (0.2 mm x 12 m x 0.33 μm) using He carrier gas at 1 ml min^{-1}. The injector temperature and detector temperature was 250 °C and 280 °C respectively and the sample size was 1 μL with a split ration of 52:1:1. The initial oven temperature was 40°C held for 2 min and then ramped at 20 °C up to 280 °C and then held for 1 min. α-Terpinene eluted at 3.9 min, ascaridole eluted at 5.5 min. Other products included eucalyptol at 3.8 min and other oxidation products around 5 min.

6.7.4. Citronellol

Batch

5 mL of the photosensitiser solution (20 μM) was mixed with 5 mL of citronellol solution (0.15 mM) in methanol. The sample was bubbled with oxygen and the solutions were then irradiated with the Xe light source over 2 h giving a fluence of 0.66 W/cm^2. Samples were taken at the start, and then after 1, 30, 60, 90 and 120 min for analysis on RP-HPLC. (E)-7-hydroperoxy-3-7-dimethyloct-7-en-1-ol: ^{1}H-NMR ($CDCl_3$, 400 MHz) δ: 1.28 (s.6H, 2 x 7**Me**), 5.49-5.62 (m, 2H, C**H**=C**H**) and 6-hydroperoxy-3,7-dimethyloct-7-en-1-ol: ^{1}H-NMR ($CDCl_3$, 400 MHz) δ = 1.65 (s,3H, 7**Me**), 4.17-4.21 (m, 1H, C**H**-OOH), 4.90 (s, 2H, C=C**H$_2$**)

Microchannel chip (immobilised photosensitiser)

The chip (design B) with the photosensitiser immobilised to the glass surface was used for this experiment. A 0.15 mM solution of citronellol in methanol was pumped through the chip at 2.5 μL min^{-1}. The Xe arc lamp was used to irradiate it with oxygen introduced directly onto the chip (fluence rate = 21.0 J cm^{-2})

RP-HPLC

Samples collected from the citronellol experiments were routinely tested using RP-HPLC and analysed with NMR to identify peaks. The mobile phase was 70:30 (v/v) acetonitrile:0.1 M formic acid at 1 mL min^{-1} using a 250 x 46 mm C18 phenomenex HPLC column. Eluting material was monitored using a UV detector set at 215 nm. The oxidised citronellol products eluted 3.2 min, while citronellol eluted at 5.5 and 6.5 min.

6.8. Singlet oxygen generation (biological applications)

Cell culture

U937, histiocytic lymphoma cells were cultured at 37 °C in 5% CO_2 in RPMI 1640 with 10% fetal calf serum (FCS) and 1% L-glutanine. They were used at a density of $1x10^6$ cell mL^{-1} for the on-chip experiments in phosphate buffered solution (PBS).

Batch

Cells were suspended in media without FCS to a concentration of $1x10^6$ cells mL^{-1} and mixed with a solution of capped porphyrin (**44**) to a range of concentrations as specified in section 4.4. The mixture was incubated for 1 h at 37 °C and 5% CO_2 for 1 h before washing with a 3x excess of media to eliminate any unbound porphyrin. The pellets of cells were then resuspended in media and 4x 100 μL of each concentration was plated into two 96 well plates. One plate was irradiated with white light at a fluence rate of 18 J/cm^2 (two plates if one was for flow cytometry analysis), while the other served as a dark control. After the experiment 5 μL of FCS was added to each well and they were returned to the incubator overnight before analysis. Analysis was initinally carried out using a Trypan blue stain. It was then carried out using an MTT assay or with Annexin V-FITC/PI flow cytometry as the research progressed.

Trypan blue assay

10 μL of the cell suspension was mixed with 10 μL of Trypan blue and the cells counted on an haemocytometer to determine those that allowed the dye to stain them (non viable) and those that did not (viable).

MTT Assay

The cell viability was determined using MTT (3-[4,5-dimethylthiazol-2-yl]-2,5 diphenyltetrazolium bromide) colorimetric assay.[213] 10 µL of 12 mM MTT solution was added to each well and incubated between 1 and 4 h at 37 °C to allow MTT metabolisation. The crystals formed were dissolved by adding 150 µL of acid-alcohol mixture (0.04 M HCL in absolute 2-propanol). The absorbance at 570 nm was measured and the results were expressed with respect to control values.

Microchannel chip

Cells were suspended in PBS to a concentration of $1x10^6$ cells mL^{-1}. The chip was cleaned with ethanol and then backfilled with PBS. The cell suspension was pumped through the porphyrin-immobilised chip at a flow rate of 2.5 µL min^{-1} over 2 h at a fluence rate of 21.0 J cm^{-2}. The cells were resuspended in complete media, left in the incubator until analysed.

Flow cytometry

Apoptosis and necrosis were detected using an Annexin V-FITC/PI detection kit as per manufacturer's instruction (AbD Serotec). 10,000 events were collected for each sample and analysed using quadrant stats on the software.

HSP 70 expression was detected using a fix and perm method followed by positive and negative determination for the expression of HSP70. 10,000 events were collected for each sample and analysed by taking the ratio of the positive and negative means from the flow cytometer software.[337]

Statistics

To analyse the biological data a paired t test was performed on the mean values. A null hypothesis was proposed that the mean difference between the two sets of data (results from the experiment in the light and the dark) was zero. To show that the two sets of data are statistically significant it was therefore necessary to disprove this null hypothesis. For each experiment, the difference between the two values was calculated. The mean of these values was then divided by the standard deviation to yield the t test value. This value was compared to the t test table with the degrees of freedom being equal to one less than the number of pairs. If the test value was greater than or equal to the value in the table then the difference between the two experiments could be classed as being statistically significant to the probability stated in the table.

References

1. J. Gabriel, ed., *The biology of cancer*, John Wiley & Sons Ltd, Chichester, 2007.
2. D. Hanahan and R. A. Weinberg, *Cell*, 2000, **100**, 57-70.
3. V. A. McCormack and P. Boffetta, *Ann. Oncol.*, 2011, **22**, 2349-2357.
4. A. C. De Freitas, A. P. A. D. Gurgel, B. S. Chagas, E. C. Coimbra and C. M. M. Do Amaral, *Gynecol Oncol*, 2012, **126**, 304-311.
5. F. L. Meyskens Jr, *Oncology (Williston Park, N.Y.)*, 1992, **6**, 15-24.
6. L. A. Hindorff, E. M. Gillanders and T. A. Manolio, *Carcinogenesis*, 2011, **32**, 945-954.
7. H. A. A. Aly, *J Immunol Methods*, 2012, **382**, 1-23.
8. M. Korbelik and J. Sun, *Cancer Immunol. Immunother.*, 2006, **55**, 900-909.
9. S. O. Gollnick, L. Vaughan and B. W. Henderson, *Cancer Res.*, 2002, **62**, 1604-1608.
10. L. B. Josefsen and R. W. Boyle, *Met-Based Drugs*, 2008, **2008**.
11. A. E. O'Connor, W. M. Gallagher and A. T. Byrne, *Photochem. Photobiol.*, 2009, **85**, 1053-1074.
12. E. S. Nyman and P. H. Hynninen, *J. Photochem. Photobiol. B*, 2004, **73**, 1-28.
13. K. Smith, N. Malatesti, N. Cauchon, D. Hunting, R. Lecomte, J. E. Van Lier, J. Greenman and R. W. Boyle, *Immunology*, 2011, **132**, 256-265.
14. W. Tang, H. Xu, R. Kopelman and M. A. Philbert, *Photochem. Photobiol.*, 2005, **81**, 242-249.
15. J. P. Tardivo, A. Del Giglio, C. S. De Oliveira, D. S. Gabrielli, H. C. Junqueira, D. B. Tada, D. Severino, R. De Fátima Turchiello and M. S. Baptista, *Photodiagn. Photodyn. Ther.*, 2005, **2**, 175-191.

16. D. B. Tada, L. L. R. Vono, E. L. Duarte, R. Itri, P. K. Kiyohara, M. S. Baptista and L. M. Rossi, *Langmuir*, 2007, **23**, 8194-8199.

17. Y. Chen, W. Zheng, Y. Li, J. Zhong, J. Ji and P. Shen, *Cancer Sci.*, 2008, **99**, 2019-2027.

18. A. Riva, F. Trifiró and F. Santarelli, *J. Mol. Catal.*, 1981, **11**, 283-291.

19. D. Gryglik, J. S. Miller and S. Ledakowicz, *Solar Energy*, 2004, **77**, 615-623.

20. A. P. Schaap, A. L. Thayer, E. C. Blossey and D. C. Neckers, *J. Am. Chem. Soc.*, 1975, **97**, 3741-3745.

21. A. P. Schaap, A. L. Thayer, K. A. Zaklika and P. C. Valenti, *J. Am. Chem. Soc.*, 1979, **101**, 4016-4017.

22. S. Tamagaki, C. E. Liesner and D. C. Neckers, *J. Org. Chem.*, 1980, **45**, 1573-1576.

23. J. Paczkowski and D. C. Neckers, *Macromolecules*, 1985, **18**, 1245-1253.

24. B. Paczkowska, J. Paczkowski and D. C. Neckers, *Macromolecules*, 1986, **19**, 863-870.

25. R. Alcántara, L. Canoira, P. G. Joao, J. G. Rodriguez and I. Vázquez, *J. Photochem. Photobiol. A., Chem.*, 2000, **133**, 27-32.

26. R. C. R. Wootton, R. Fortt and A. J. De Mello, *Org. Process Res. Dev.*, 2002, **6**, 187-189.

27. M. Oelgemöller, C. Jung, J. Ortner, J. Mattay and E. Zimmermann, *Green Chem.*, 2005, **7**, 35-38.

28. O. Leal, D. L. Anderson, R. G. Bowman, F. Basolo and R. L. Burwell, *J. Am. Chem. Soc.*, 1975, **97**, 5125-5129.

29. X. Qian, Z. Tai, X. Sun, S. Xiao, H. Wu, Z. Lu and Y. Wei, *Thin Solid Films*, 1996, **284-285**, 432-435.

30. A. G. Griesbeck and T. T. El-Idreesy, *Photochem. Photobiol. Sci*, 2005, **4**, 205-209.

31. I. J. MacDonald and T. J. Dougherty, *J. Porphyrins Phthalocyanines*, 2001, **5**, 105-129.

32. R. Bonnett, *Chem. Soc. Rev.*, 1995, **24**, 19-33.

33. R. W. Redmond and J. N. Gamlin, *Photochem. Photobiol.*, 1999, **70**, 391-475.

34. M. C. DeRosa and R. J. Crutchley, *Coordin. Chem. Rev.*, 2002, **233**, 351-371.

35. J. E. Van-Lier, *Photobiological Techniques*, Plenum Press, New York, 1991.

36. A. A. Gorman and M. A. J. Rodgers, *Chem. Soc. Rev.*, 1981, **10**, 205-231.

37. C. Schweitzer and R. Schmidt, *Chem. Rev.*, 2003, **103**, 1685-1757.

38. R. K. Pandey and G. Zheng, 6, Academic Press, 2000.

39. J. J. Schuitmaker, P. Baas, H. L. L. M. Van Leengoed, F. W. Van Der Meulen, W. M. Star and N. Van Zandwijk, *J. Photochem. Photobiol. B*, 1996, **34**, 3-12.

40. B. W. Henderson, T. M. Busch and J. W. Snyder, *Laser Surg. Med.*, 2006, **38**, 489-493.

41. E. L. Clennan, *Tetrahedron*, 2000, **56**, 9151-9179.

42. E. L. Clennan and A. Pace, *Tetrahedron*, 2005, **61**, 6665-6691.

43. Y. Tang, Y. Dong and J. L. Vennerstrom, *Med. Res. Rev.*, 2004, **24**, 425-448.

44. A. Siwicka, Z. Molęda, K. Wojtasiewicz, A. Zawadzka, J. K. Maurin, M. Panasiewicz, T. Pacuszka and Z. Czarnocki, *J. Pineal Res.*, 2008, **45**, 40-49.

45. D. I. Pattison, A. S. Rahmanto and M. J. Davies, *Photochem. Photobiol. Sci*, 2012, **11**, 38-53.

46. M. J. Davies, *Biochem. Biophys. Res. Commun.*, 2003, **305**, 761-770.

47. G. M. Whitesides, *Nature*, 2006, **442**, 368-373.

48. K. Huikko, R. Kostiainen and T. Kotiaho, *Eur. J. Pharm. Sci.*, 2003, **20**, 149-171.

49. J. El-Ali, P. K. Sorger and K. F. Jensen, *Nature*, 2006, **442**, 403-411.

50. M. A. Shoffner, J. Cheng, G. E. Hvichia, L. J. Kricka and P. Wilding, *Nucleic Acids Res.*, 1996, **24**, 375-379.

51. P. Watts and C. Wiles, *Chem. Commun.*, 2007, 443-467.

52. A. J. DeMello, *Nature*, 2006, **442**, 394-402.

53. E. E. Coyle and M. Oelgemoller, *Photochem. Photobiol. Sci*, 2008, **7**, 1313-1322.

54. A. A. Lapkin, V. M. Boddu, G. N. Aliev, B. Goller, S. Polisski and D. Kovalev, *Chem. Eng. J.*, 2008, **136**, 331-336.

55. H. Lu, M. A. Schmidt and K. F. Jensen, *Lab Chip*, 2001, **1**, 22-28.

56. A. Ulman, *Chem. Rev.*, 1996, **96**, 1533-1554.

57. W. C. Bigelow, D. L. Pickett and W. A. Zisman, *J. Colloid Sci.*, 1946, **1**, 513-538.

58. H. Ishida and J. L. Koenig, *Polym. Eng. Sci.*, 1978, **18**, 128-145.

59. H. Ishida, *Polym. Compos.*, 1984, **5**, 101-123.

60. C. H. Chiang, H. Ishida and J. L. Koenig, *J. Colloid Interf. Sci.*, 1980, **74**, 396-404.

61. C. H. Chiang, N. I. Liu and J. L. Koenig, *J. Colloid Interf. Sci.*, 1982, **86**, 26-34.

62. G. S. Caravajal, D. E. Leyden, G. R. Quinting and G. E. Maciel, *Anal. Chem.*, 1988, **60**, 1776-1786.

63. B. Arkles, *Chemtech*, 1977, **7**, 766-778.

64. E. T. Vandenberg, L. Bertilsson, B. Liedberg, K. Uvdal, R. Erlandsson, H. Elwing and I. Lundstrom, *J. Colloid Interf. Sci.*, 1991, **147**, 103-118.

65. C. W. Chu, D. P. Kirby and P. D. Murphy, *J. Adhes. Sci. Technol.*, 1993, **7**, 417-433.

66. J. Kim, P. Seidler, L. S. Wan and C. Fill, *J. Colloid Interf. Sci.*, 2009, **329**, 114-119.

67. A. Simon, T. Cohen-Bouhacina, M. C. Porte, J. P. Aime and C. Baquey, *J. Colloid Interf. Sci.*, 2002, **251**, 278-283.

68. I. Haller, *J. Am. Chem. Soc.*, 1978, **100**, 8050-8055.

69. R. Wilson and D. J. Schiffrin, *Analyst*, 1995, **120**, 175-178.

70. W. Wang and M. W. Vaughn, *Scanning*, 2008, **30**, 65-77.

71. G. Arslan, M. Ozmen, B. Gunduz, X. Zhang and M. Ersoz, *Turk. J. Chem.*, 2006, **30**, 203-210.

72. J. A. Howarter and J. P. Youngblood, *Langmuir*, 2006, **22**, 11142-11147.

73. K. M. R. Kallury, P. M. Macdonald and M. Thompson, *Langmuir*, 1994, **10**, 492-499.

74. N. K. Kamisetty, S. P. Pack, M. Nonogawa, K. C. Devarayapalli, T. Kodaki and K. Makino, *Anal. Bioanal. Chem.*, 2006, **386**, 1649-1655.

75. M. H. Lee, D. A. Brass, R. Morris, R. J. Composto and P. Ducheyne, *Biomaterials*, 2005, **26**, 1721-1730.

76. T. Nakagawa, T. Tanaka, D. Niwa, T. Osaka, H. Takeyama and T. Matsunaga, *J Biotechnol*, 2005, **116**, 105-111.

77. G. K. Toworfe, R. J. Composto, I. M. Shapiro and P. Ducheyne, *Biomaterials*, 2006, **27**, 631-642.

78. F. Zhang and M. P. Srinivasan, *Langmuir*, 2004, **20**, 2309-2314.

79. J. Zhao, Y. Li, H. Guo and L. Gao, *Chinese J. Anal. Chem.*, 2006, **34**, 1235-1238.

80. H. Okabayashi, I. Shimizu, E. Nishio and C. J. O'Connor, *Colloid Polym. Sci.*, 1997, **275**, 744-753.

81. J. K. Kim, D. S. Shin, W. J. Chung, K. H. Jang, K. N. Lee, Y. K. Kim and Y. S. Lee, *Colloids Surf., B*, 2004, **33**, 67-75.

82. W. D. Bascom, *Macromolecules*, 1972, **5**, 792-798.

83. S. Naviroj, S. R. Culler, J. L. Koenig and H. Ishida, *J. Colloid Interf. Sci.*, 1984, **97**, 308-317.

84. K. M. R. Kallury, U. J. Krull and M. Thompson, *Anal. Chem.*, 1988, **60**, 169-172.

85. T. G. Waddell, D. E. Leyden and M. T. DeBello, *J. Am. Chem. Soc.*, 1981, **103**, 5303-5307.

86. D. F. S. Petri, G. Wenz, P. Schunk and T. Schimmel, *Langmuir*, 1999, **15**, 4520-4523.

87. J. Kim, P. Seidler, C. Fill and L. S. Wan, *Surf. Sci.*, 2008, **602**, 3323-3330.

88. J. H. Moon, J. W. Shin, S. Y. Kim and J. W. Park, *Langmuir*, 1996, **12**, 4621-4624.

89. K. Bierbaum, M. Kinzler, C. Wöll, M. Grunze, G. Hähner, S. Heid and F. Effenberger, *Langmuir*, 1995, **11**, 512-518.

90. E. Metwalli, D. Haines, O. Becker, S. Conzone and C. G. Pantano, *J. Colloid Interf. Sci.*, 2006, **298**, 825-831.

91. R. C. R. Wootton and A. J. DeMello, *Lab Chip*, 2006, **6**, 471-473.

92. J. A. Fracassi Da Silva, C. L. Do Lago and R. Furlan, *J. Braz. Chem. Soc.*, 2007, **18**, 1531-1536.

93. B. Wang, Z. Abdulali-Kanji, E. Dodwell, J. H. Horton and R. D. Oleschuk, *Electrophoresis*, 2003, **24**, 1442-1450.

94. G. Sui, J. Wang, C. C. Lee, W. Lu, S. P. Lee, J. V. Leyton, A. M. Wu and H. R. Tseng, *Anal. Chem.*, 2006, **78**, 5543-5551.

95. W. Cai, J. Jing, B. Irvin, L. Ohler, E. Rose, H. Shizuya, U. J. Kim, M. Simon, T. Anantharaman, B. Mishra and D. C. Schwartz, *Proc Natl Acad Sci U S A*, 1998, **95**, 3390-3395.

96. V. Chan, D. J. Graves, P. Fortina and S. E. McKenzie, *Langmuir*, 1997, **13**, 320-329.

97. J. Jing, J. Reed, J. Huang, X. Hu, V. Clarke, J. Edington, D. Housman, T. S. Anantharaman, E. J. Huff, B. Mishra, B. Porter, A. Shenker, E. Wolfson, C. Hiort, R.

Kantor, C. Aston and D. C. Schwartz, *Proc Natl Acad Sci U S A*, 1998, **95**, 8046-8051.

98. B. Joos, H. Kuster and R. Cone, *Anal Biochem*, 1997, **247**, 96-101.

99. L. Li, H. Hu and R. G. Larson, *Rheologica Acta*, 2004, **44**, 38-46.

100. S. J. Oh, S. J. Cho, C. O. Kim and J. W. Park, *Langmuir*, 2002, **18**, 1764-1769.

101. N. Zammatteo, L. Jeanmart, S. Hamels, S. Courtois, P. Louette, L. Hevesi and J. Remacle, *Anal Biochem*, 2000, **280**, 143-150.

102. W. Cai, H. Aburatani, V. P. Stanton Jr, D. E. Housman, Y. K. Wang and D. C. Schwartz, *Proc Natl Acad Sci U S A*, 1995, **92**, 5164-5168.

103. Z. Guo, R. A. Guilfoyle, A. J. Thiel, R. Wang and L. M. Smith, *Nucleic Acids Res.*, 1994, **22**, 5456-5465.

104. A. A. Vaidya and M. L. Norton, *Langmuir*, 2004, **20**, 11100-11107.

105. T. H. Nguyen, S. S. Choi, D. W. Kim and Y. U. Kim, *J. Korean Phys. Soc.*, 2007, **50**, 1942-1946.

106. T. H. Nguyen, V. C. Bui, Y. U. Kim and S. S. Choi, *J. Bionanosci.*, 2009, **3**, 1-6.

107. R. L. DeRosa, J. A. Cardinale and A. Cooper, *Thin Solid Films*, 2007, **515**, 4024-4031.

108. J. R. Falsey, M. Renil, S. Park, S. Li and K. S. Lam, *Bioconjugate Chem.*, 2001, **12**, 346-353.

109. H. G. Hong, M. Jiang, S. G. Sligar and P. W. Bohn, *Langmuir*, 1994, **10**, 153-158.

110. U. Jönsson, M. Malmqvist, G. Olofsson, I. Rönnberg and M. Klaus, in *Methods Enzymol*, Academic Press, 1988, vol. Volume 137, pp. 381-388.

111. A. Antoniou, G. Herlem, C. André, Y. Guillaume and T. Gharbi, *Talanta*, 2011, **84**, 632-637.

112. Y. Lee, S. Park, J. Park and W. G. Koh, *Biomed. Microdevices*, 2010, **12**, 457-464.

113. M. Qin, S. Hou, L. Wang, X. Feng, R. Wang, Y. Yang, C. Wang, L. Yu, B. Shao and M. Qiao, *Colloids Surf., B*, 2007, **60**, 243-249.

114. C. Ryu, C. Kim, H. Chae and J. D. Nam, *J. Korean Phys. Soc.*, 2007, **51**, 1160-1165.

115. H. Y. Shim, S. H. Lee, D. J. Ahn, K. D. Ahn and J. M. Kim, *Mater. Sci. Eng. C*, 2004, **24**, 157-161.

116. M. Yamaguchi, O. Nishimura, S. H. Lim, K. Shimokawa, T. Tamura and M. Suzuki, *Colloids Surf., A*, 2006, **284-285**, 532-534.

117. S. R. Kim and N. L. Abbott, *Langmuir*, 2002, **18**, 5269-5276.

118. A. Heise, H. Menzel, H. Yim, M. D. Foster, R. H. Wieringa, A. J. Schouten, V. Erb and M. Stamm, *Langmuir*, 1997, **13**, 723-728.

119. S. L. Zhu, J. B. Zhang, L. Y. L. Yue, D. Hartono and A. Q. Liu, *Adv. Mater. Res.*, 2009, **74**, 95-98.

120. S. K. Arya, A. K. Prusty, S. P. Singh, P. R. Solanki, M. K. Pandey, M. Datta and B. D. Malhotra, *Anal Biochem*, 2007, **363**, 210-218.

121. H. Tang, W. Zhang, P. Geng, Q. J. Wang, L. T. Jin, Z. R. Wu and M. Lou, *Anal. Chim. Acta*, 2006, **562**, 190-196.

122. K. Webb, V. Hlady and P. A. Tresco, *J Biomed Mater Res*, 1998, **41**, 422-430.

123. K. Webb, V. Hlady and P. A. Tresco, *J Biomed Mater Res*, 2000, **49**, 362-368.

124. Y. X. Liu, X. J. Wang, J. Lu and C. B. Ching, *J. Phys. Chem. B*, 2007, **111**, 13971-13978.

125. N. Balachander and C. N. Sukenik, *Langmuir*, 1990, **6**, 1621-1627.

126. S. Prakash, T. M. Long, J. C. Selby, J. S. Moore and M. A. Shannon, *Anal. Chem.*, 2007, **79**, 1661-1667.

127. M. Sharma, A. Dube and J. R. Engstrom, *J. Am. Chem. Soc.*, 2007, **129**, 15022-15033.

128. L. Netzer and J. Sagiv, *J. Am. Chem. Soc.*, 1983, **105**, 674-676.

129. Y. P. Wang, K. Yuan, Q. L. Li, L. P. Wang, S. J. Gu and X. W. Pei, *Mater. Lett.*, 2005, **59**, 1736-1740.

130. Y. Liu, V. N. Khabashesku and N. J. Halas, *J. Am. Chem. Soc.*, 2005, **127**, 3712-3713.

131. M. Chen, W. Brett Caldwell and C. A. Mirkin, *J. Am. Chem. Soc.*, 1993, **115**, 1193-1194.

132. L. Basabe-Desmonts, F. D. Van Baan, R. S. Zimmerman, D. N. Reinhoudt and M. Crego-Calama, *Sensors*, 2007, **7**, 1731-1746.

133. Q. Gu and X. Cheng, *Appl. Surf. Sci.*, 2007, **253**, 6800-6806.

134. H. S. Ki, J. H. Yeum, S. Choe, J. H. Kim and I. W. Cheong, *Compos. Sci. Technol.*, 2009, **69**, 645-650.

135. Y. J. Na, S. J. Park, S. W. Lee and J. S. Kim, *Ultramicroscopy*, 2008, **108**, 1297-1301.

136. A. Sridharan, J. Muthuswamy, J. T. LaBelle and V. B. Pizziconi, *Langmuir*, 2008, **24**, 8078-8089.

137. F. Da Cruz, K. Driaf, C. Berthier, J. M. Lameille and F. Armand, *Thin Solid Films*, 1999, **349**, 155-161.

138. Z. Zhang, R. Hu and Z. Liu, *Langmuir*, 2000, **16**, 1158-1162.

139. T. J. Savenije, C. H. M. Marée, F. H. P. M. Habraken, R. B. M. Koehorst and T. J. Schaafsma, *Thin Solid Films*, 1995, **265**, 84-88.

140. J. Wienke, F. J. Kleima, R. B. M. Koehorst and T. J. Schaafsma, *Thin Solid Films*, 1996, **279**, 87-92.

141. X. Zhang, M. Gao, X. Kong, Y. Sun and J. Shen, *J. Chem. Soc., Chem. Commun.*, 1994, 1055-1056.

142. A. G. Schick and Z. Sun, *Thin Solid Films*, 1994, **248**, 86-91.

143. D. W. J. McCallien, P. L. Burn and H. L. Anderson, *J. Chem. Soc., Perkin Trans 1*, 1997, 2581-2586.

144. P. A. Heiney, K. Grüneberg, J. Fang, C. Dulcey and R. Shashidhar, *Langmuir*, 2000, **16**, 2651-2657.

145. J. Fang, M. S. Chen and R. Shashidhar, *Langmuir*, 2001, **17**, 1549-1551.

146. S. C. Jain, V. K. Tanwar, V. Dixit, S. P. Verma and S. B. Samanta, *Appl. Surf. Sci.*, 2001, **182**, 350-356.

147. R. Rosario, D. Gust, M. Hayes, F. Jahnke, J. Springer and A. A. Garcia, *Langmuir*, 2002, **18**, 8062-8069.

148. B. C. Bunker, B. I. Kim, J. E. Houston, R. Rosario, A. A. Garcia, M. Hayes, D. Gust and S. T. Picraux, *Nano Lett.*, 2003, **3**, 1723-1727.

149. R. Bonnett, S. Ioannou, A. G. James, C. W. Pitt and M. M. Z. Soe, *J. Mater. Chem.*, 1993, **3**, 793-799.

150. D. L. Pilloud, C. C. Moser, K. S. Reddy and P. L. Dutton, *Langmuir*, 1998, **14**, 4809-4818.

151. S. M. Borisov, P. Lehner and I. Klimant, *Anal. Chim. Acta*, 2011, **690**, 108-115.

152. T. L. Blair, J. R. Allen, S. Daunert and L. G. Bachas, *Anal. Chem.*, 1993, **65**, 2155-2158.

153. S. T. Yang and L. G. Bachas, *Talanta*, 1994, **41**, 963-968.

154. C. Y. Liu, T. Hasty and A. J. Bard, *J. Electrochem. Soc.*, 1996, **143**, 1914-1918.

155. J. Xiao and M. E. Meyerhoff, *Anal. Chem.*, 1996, **68**, 2818-2825.

156. H. Dong, C. M. Li, Q. Zhou, J. B. Sun and J. M. Miao, *Biosens. Bioelectron.*, 2006, **22**, 621-626.

157. J. C. Ehrhart, B. Bennetau, L. Renaud, J. P. Madrange, L. Thomas, J. Morisot, A. Brosseau, S. Allano, P. Tauc and P. L. Tran, *Biosens. Bioelectron.*, 2008, **24**, 467-474.

158. T. G. Henares, F. Mizutani, R. Sekizawa and H. Hisamoto, *Sensors and Materials*, 2007, **19**, 249-259.

159. L. S. Jang and H. J. Liu, *Biomed. Microdevices*, 2009, **11**, 331-338.

160. C. Jönsson, M. Aronsson, G. Rundström, C. Pettersson, I. Mendel-Hartvig, J. Bakker, E. Martinsson, B. Liedberg, B. MacCraith, O. Öhman and J. Melin, *Lab Chip*, 2008, **8**, 1191-1197.

161. D. N. Kim, Y. Lee and W. G. Koh, *Sensor. Actuat. B-Chem.*, 2009, **137**, 305-312.

162. O. Alptekin, S. S. Tükel, D. Yildirim and D. Alagöz, *Journal of Molecular Catalysis B: Enzymatic*, 2009, **58**, 124-131.

163. T. Liu, S. Wang and G. Chen, *Talanta*, 2009, **77**, 1767-1773.

164. G. Stojkovič and P. Žnidaršič-Plazl, *Acta Chim. Solv.*, 2010, **57**, 144-149.

165. Y. J. Chuang, J. W. Huang, H. Makamba, M. L. Tsai, C. W. Li and S. H. Chen, *Electrophoresis*, 2006, **27**, 4158-4165.

166. D. G. Pijanowska and W. Torbicz, *ITBM-RBM*, 2008.

167. X. Zhang, P. Jones and S. J. Haswell, *Chem. Eng. J.*, 2007, **135**.

168. W. Tan and T. A. Desai, *JALA - Journal of the Association for Laboratory Automation*, 2003, **8**, 40-43.

169. K. Aran, L. A. Sasso, N. Kamdar and J. D. Zahn, *Lab Chip*, 2010, **10**, 548-552.

170. H. Nakamura, X. Li, H. Wang, M. Uehara, M. Miyazaki, H. Shimizu and H. Maeda, *Chem. Eng. J.*, 2004, **101**, 261-268.

171. N. G. Wilson and T. McCreedy, *Chem. Commun.*, 2000, 733-734.

172. N. Hoffmann, *Chem. Rev.*, 2008, **108**, 1052-1103.

173. A. Albini and M. Fagnoni, *Green Chem.*, 2004, **6**, 1-6.

174. M. Prein and W. Adam, *Angewandte Chemie-International Edition in English*, 1996, **35**, 477-494.

175. M. Stratakis and M. Orfanopoulos, *Tetrahedron*, 2000, **56**, 1595-1615.

176. G. Ohloff, *Pure Appl. Chem.*, 1975, **43**, 481-502.

177. P. Kluson, M. Drobek, T. Strasak and A. Kalaji, *React. Kinet. Catal. Lett.*, 2008, **95**, 231-238.

178. F. Lévesque and P. H. Seeberger, *Org. Lett.*, 2011, **13**, 5008-5011.

179. N. Monnerie and J. Ortner, *J. Sol. Energ.-T. Asme*, 2001, **123**, 171-174.

180. O. Suchard, R. Kane, B. J. Roe, E. Zimmerman, C. Jung, P. A. Waske, J. Mattay and M. Oelgemoller, *Tetrahedron*, 2006, **62**, 1467-1473.

181. C. S. Foote, S. Wexler, W. Ando and R. Higgins, *J. Am. Chem. Soc.*, 1968, **90**, 975-981.

182. R. A. Bourne, X. Han, M. Poliakoff and M. W. George, *Angew. Chem. Int. Edit.*, 2009, **48**, 5322-5325.

183. W. C. Eisenberg, A. Snelson, J. Veltman and R. W. Murray, *Tetrahedron Lett.*, 1981, **22**, 1949-1952.

184. W. Spiller, H. Kliesch, D. Wöhrle, S. Hackbarth, B. Röder and G. Schnurpfeil, *J. Porphyrins Phthalocyanines*, 1998, **2**, 145-158.

185. L. Roitman, B. Ehrenberg and N. Kobayashi, *J. Photochem. Photobiol. A*, 1994, **77**, 23-28.

186. K. D. Belfield, M. V. Bondar and O. V. Przhonska, *J. Fluoresc.*, 2006, **16**, 111-117.

187. J. R. Kanofsky, P. D. Sima and C. Richter, *Photochem. Photobiol.*, 2003, **77**, 235-242.

188. M. Uemi, G. E. Ronsein, S. Miyamoto, M. H. G. Medeiros and P. Di Mascio, *Chem. Res. Toxicol.*, 2009, **22**, 875-884.

189. M. Kulig and L. L. Smith, *J. Org. Chem.*, 1973, **38**, 3639-3642.

190. L. S. Tsai and C. A. Hudson, *J. Am. Oil Chem. Soc.*, 1981, **58**, 931-934.

191. G. Maerker, E. H. Nungesser and I. M. Zulak, *J Agric Food Chem*, 1988, **36**, 61-63.

192. C. S. J. Shen and A. J. Sheppard, *Chromatographia*, 1983, **17**, 469-471.

193. A. S. Csallany, S. E. Kindom, P. B. Addis and J. H. Lee, *Lipids*, 1989, **24**, 645-651.

194. M. F. Caboni, A. Costa, M. T. Rodriguez-Estrada and G. Lercker, *Chromatographia*, 1997, **46**, 151-155.

195. L. Lakritz and K. C. Jones, *J. Am. Oil Chem. Soc.*, 1997, **74**, 943-946.

196. P. Manini, R. Andreoli, M. Careri, L. Elviri and M. Musci, *Rapid Commun Mass Spectrom*, 1998, **12**, 883-889.

197. W. Korytowski and A. W. Girotti, *Photochem. Photobiol.*, 1999, **70**, 484-489.

198. K. Osada, A. Ravandi and A. Kuksis, *J. Am. Oil Chem. Soc.*, 1999, **76**, 863-871.

199. A. Grandgirard, L. Martine, C. Joffre, P. Juaneda and O. Berdeaux, *J. Chromatogr. A*, 2004, **1040**, 239-250.

200. E. C. Blossey, D. C. Neckers, A. L. Thayer and A. P. Schaap, *J. Am. Chem. Soc.*, 1973, **95**, 5820-5823.

201. M. Nowakowska, M. Kępczyński and K. Szczubiałka, *Pure Appl. Chem.*, 2001, **73**, 491-495.

202. X. Han, R. A. Bourne, M. Poliakoff and M. W. George, *Chem. Sci.*, 2011, **2**, 1059-1067.

203. W. R. Midden and S. Y. Wang, *J. Am. Chem. Soc.*, 1983, **105**, 4129-4135.

204. C. M. Krishna, Y. Lion and P. Riesz, *Photochem. Photobiol.*, 1987, **45**, 1-6.

205. M. I. Burguete, F. Galindo, R. Gavara, S. V. Luis, M. Moreno, P. Thomas and D. A. Russell, *Photochem. Photobiol. Sci*, 2009, **8**, 37-44.

206. T. Hino, T. Anzai and N. Kuramoto, *Tetrahedron Lett.*, 2006, **47**, 1429-1432.

207. G. D. Panagiotou, M. D. Tzirakis, J. Vakros, L. Loukatzikou, M. Orfanopoulos, C. Kordulis and A. Lycourghiotis, *Appl. Catal.*, 2009, **372**, 16-25.

208. J. Vakros, G. Panagiotou, C. Kordulis, A. Lycourghiotis, G. C. Vougioukalakis, Y. Angelis and M. Orfanopoulos, *Catal. Lett.*, 2003, **89**, 269-273.

209. D. Latassa, O. Enger, C. Thilgen, T. Habicher, H. Offermanns and F. Diederich, *J. Mater. Chem.*, 2002, **12**, 1993-1995.

210. S. Lacombe, J. P. Soumillion, A. El Kadib, T. Pigot, S. Blanc, R. Brown, E. Oliveros, C. Cantau and P. Saint-Cricq, *Langmuir*, 2009, **25**, 11168-11179.

211. V. Latour, T. Pigot, P. Mocho, S. Blanc and S. Lacombe, *Catal. Today*, 2005, **101**, 359-367.

212. N. Soggiu, H. Cardy, J. L. Habib Jiwan, I. Leray, J. P. Soumillion and S. Lacombe, *J. Photochem. Photobiol. A., Chem.*, 1999, **124**, 1-8.

213. J. L. Bourdelande, J. Font, G. Marquès and M. Valiente, *J. Photochem. Photobiol. A., Chem.*, 1996, **95**, 235-238.

214. J. L. Bourdelande, J. Font, G. Marques, A. A. Abdel-Shafi, F. Wilkinson and D. R. Worrall, *J. Photochem. Photobiol. A., Chem.*, 2001, **138**, 65-68.

215. M. J. Moreno, E. Monson, R. G. Reddy, A. Rehemtulla, B. D. Ross, M. Philbert, R. J. Schneider and R. Kopelman, *Sensor. Actuat. B-Chem.*, 2003, **90**, 82-89.

216. R. Gerdes, O. Bartels, G. Schneider, D. Wohrle and G. Schulz-Ekloff, *Polym. Advan. Technol.*, 2001, **12**, 152-160.

217. V. Iliev, A. Ileva and L. Bilyarska, *J. Mol. Catal. A: Chem.*, 1997, **126**, 99-108.

218. E. L. Clennan and M. F. Chen, *J. Org. Chem.*, 1995, **60**, 6004-6005.

219. K. Feng, M. L. Peng, D. H. Wang, L. P. Zhang, C. H. Tung and L. Z. Wu, *Dalton Trans.*, 2009, 9794-9799.

220. M. Benaglia, A. Puglisi and F. Cozzi, *Chem. Rev.*, 2003, **103**, 3401-3429.

221. A. Maldotti, A. Molinari and R. Amadelli, *Chem. Rev.*, 2002, **102**, 3811-3836.

222. J. Wahlen, D. E. De Vos, P. A. Jacobs and P. L. Alsters, *Adv. Synth. Catal.*, 2004, **346**, 152-164.

223. S. Lacombe and T. Pigot, in *Photochemistry*, 2011, vol. 38, pp. 307-329.

224. D. Faust, K. H. Funken, G. Horneck, B. Milow, J. Ortner, M. Sattlegger, M. Schafer and C. Schmitz, *Solar Energy*, 1999, **65**, 71-74.

225. F. M. P. R. Van Laar, F. Holsteyns, I. F. J. Vankelecom, S. Smeets, W. Dehaen and P. A. Jacobs, *J. Photochem. Photobiol. A., Chem.*, 2001, **144**, 141-151.

226. M. Benaglia, T. Danelli, F. Fabris, D. Sperandio and G. Pozzi, *Org. Lett.*, 2002, **4**, 4229-4232.

227. C. J. Rogers, T. J. Dickerson, P. Wentworth Jr and K. D. Janda, *Tetrahedron*, 2005, **61**, 12140-12144.

228. M. J. Fuchter, B. M. Hoffman and A. G. M. Barrett, *J. Org. Chem.*, 2006, **71**, 724-729.

229. J. Mosinger, O. Jirsak, P. Kubat, K. Lang and B. Mosinger, *J. Mater. Chem.*, 2007, **17**, 164-166.

230. V. Titov, E. Krivykh, T. Ageeva, T. Shikova, A. Solov'eva, V. Timofeeva, I. Vershinina, V. Rybkin and H. Choi, *Polym. Sci., Ser. A*, 2008, **50**, 841-847.

231. M. Pineiro, S. M. Ribeiro and A. C. Serra, *Arkivoc*, 2010, **2010**, 51-63.

232. S. M. Ribeiro, A. C. Serra and A. M. d. A. Rocha Gonsalves, *J. Catal.*, 2008, **256**, 331-337.

233. S. M. Ribeiro, A. C. Serra and A. M. d. A. Rocha Gonsalves, *Tetrahedron*, 2007, **63**, 7885-7891.

234. A. G. Griesbeck and A. Bartoschek, *Chem. Commun.*, 2002, 1594-1595.

235. A. G. Griesbeck, T. T. El-Idreesy and A. Bartoschek, *Adv. Synth. Catal.*, 2004, **346**, 245-251.

236. A. G. Griesbeck, T. T. El-Idreesy and J. Lex, *Tetrahedron*, 2006, **62**, 10615-10622.

237. J. Inbaraj, M. V. Vinodu, R. Gandhidasan, R. Murugesan and M. Padmanabhan, *J. Appl. Polym. Sci.*, 2003, **89**, 3925-3930.

238. V. Chirvony, V. Bolotin, E. Matveeva and V. Parkhutik, *J. Photochem. Photobiol. A., Chem.*, 2006, **181**, 106-113.

239. S. M. Ribeiro, A. C. Serra and A. M. d. Rocha Gonsalves, *J. Mol. Catal. A: Chem.*, 2010.

240. H. Shimakoshi, T. Baba, Y. Iseki, A. Endo, C. Adachi, M. Watanabe and Y. Hisaeda, *Tetrahedron Lett.*, 2008, **49**, 6198-6201.

241. D. Aebisher, N. S. Azar, M. Zamadar, N. Gandra, H. D. Gafney, R. Gao and A. Greer, *J. Phys. Chem. B*, 2008, **112**, 1913-1917.

242. L. M. Rossi, P. R. Silva, L. L. R. Vono, A. U. Fernandes, D. B. Tada and M. S. Baptista, *Langmuir*, 2008, **24**, 12534-12538.

243. M. Trytek, J. Fiedurek, A. Lipke and S. Radzki, *J. Sol-Gel Sci. Technol.*, 2009, **51**, 272-286.

244. S. A. Chavan, W. Maes, L. E. M. Gevers, J. Wahlen, I. F. J. Vankelecom, P. A. Jacobs, W. Dehaen and D. E. De Vos, *Chem. -Eur. J.*, 2005, **11**, 6754-6762.

245. D. Wöhrle, A. K. Sobbi, O. Franke and G. Schulz-Ekloff, *Zeolites*, 1995, **15**, 540-550.

246. C. J. Liu, W. Y. Yu, S. G. Li and C. M. Che, *J. Org. Chem.*, 1998, **63**, 7364-7369.

247. L. Shi, B. Hernandez and M. Selke, *J. Am. Chem. Soc.*, 2006, **128**, 6278-6279.

248. K. Lang, P. Bezdička, J. L. Bourdelande, J. Hernando, I. Jirka, E. Káfuňková, F. Kovanda, P. Kubát, J. Mosinger and D. M. Wagnerová, *Chem. Mater.*, 2007, **19**, 3822-3829.

249. T. Fukuyama, Y. Hino, N. Kamata and I. Ryu, *Chem. Lett.*, 2004, **33**, 1430-1431.

250. B. D. A. Hook, W. Dohle, P. R. Hirst, M. Pickworth, M. B. Berry and K. I. Booker-Milburn, *J. Org. Chem.*, 2005, **70**, 7558-7564.

251. H. Maeda, H. Mukae and K. Mizuno, *Chem. Lett.*, 2005, **34**, 66-67.

252. O. Shvydkiv, A. Yavorskyy, S. B. Tan, K. Nolan, N. Hoffmann, A. Youssef and M. Oelgemoller, *Photochem. Photobiol. Sci*, 2011.

253. K. Tsutsumi, K. Terao, H. Yamaguchi, S. Yoshimura, T. Morimoto, K. Kakiuchip, T. Fukuyama and I. Ryu, *Chem. Lett.*, 2010, **39**, 828-829.

254. B. Dunk and R. Jachuck, *Green Chem.*, 2000, **2**.

255. S. Fuse, N. Tanabe, M. Yoshida, H. Yoshida, T. Doi and T. Takahashi, *Chem. Commun.*, 2010, **46**, 8722-8724.

256. A. Sugimoto, Y. Sumino, M. Takagi, T. Fukuyama and I. Ryu, *Tetrahedron Lett.*, 2006, **47**, 6197-6200.

257. O. Shvydkiv, S. Gallagher, K. Nolan and M. Oelgemoller, *Org. Lett.*, 2010, **12**, 5170-5173.

258. K. Ueno, F. Kitagawa and N. Kitamura, *Lab Chip*, 2002, **2**, 231-234.

259. S. Meyer, D. Tietze, S. Rau, B. Schafer and G. Kreisel, *J. Photochem. Photobiol. A., Chem.*, 2007, **186**, 248-253.

260. C. P. Park, R. A. Maurya, J. H. Lee and D. P. Kim, *Lab Chip*, 2011, **11**, 1941-1945.

261. K. Jahnisch and U. Dingerdissen, *Chem. Eng. Technol.*, 2005, **28**, 426-427.

262. E. L. Clennan, W. Zhou and J. Chan, *J. Org. Chem.*, 2002, **67**, 9368-9378.

263. X. G. Fu, L. P. Zhang, L. Z. Wu and C. H. Tung, *J. Photosci.*, 2003, **10**, 175-180.

264. X. Y. Li and V. Ramamurthy, *J. Am. Chem. Soc.*, 1996, **118**, 10666-10667.

265. R. J. Robbins and V. Ramamurthy, *Chem. Commun.*, 1997, 1071-1072.

266. P. C. Lee and M. A. J. Rodgers, *J. Phys. Chem.*, 1984, **88**, 4385-4389.

267. M. Krieg, *J. Biochem. Biophys. Methods*, 1993, **27**, 143-149.

268. C. H. Tung, L. Z. Wu, L. P. Zhang and B. Chen, *Accounts Chem. Res.*, 2003, **36**, 39-47.

269. C. H. Tung, L. Z. Wu, L. P. Zhang, H. R. Li, X. Y. Yi, K. Song, M. Xu, Z. Y. Yuan, J. Q. Guan, H. W. Wang, Y. M. Ying and X. H. Xu, *Pure Appl. Chem.*, 2000, **72**, 2289-2298.

270. M. Miyazaki, J. Kaneno, M. Uehara, M. Fujii, H. Shimizu and H. Maeda, *Chem. Commun. (Cambridge, U.K.)*, 2003, 648-649.

271. A. Kussrow, E. Kaltgrad, M. L. Wolfenden, M. J. Cloninger, M. G. Finn and D. J. Bornhop, *Anal. Chem.*, 2009, **81**, 4889-4897.

272. A. E. Niotis, C. Mastichiadis, P. S. Petrou, I. Christofidis, A. Siafaka-Kapadai, K. Misiakos and S. E. Kakabakos, *Anal. Bioanal. Chem.*, 2009, **393**, 1081-1086.

273. J. Kobayashi, Y. Mori, K. Okamoto, R. Akiyama, M. Ueno, T. Kitamori and S. Kobayashi, *Science*, 2004, **304**, 1305-1308.

274. G. Stojkovič, I. Plazl and P. Žnidaršič-Plazl, *Microfluid. Nanofluid.*, 2011, **10**, 627-635.

275. R. Gorges, S. Meyer and G. Kreisel, *J. Photochem. Photobiol. A., Chem.*, 2004, **167**, 95-99.

276. Y. Matsushita, S. Kumada, K. Wakabayashi, K. Sakeda and T. Ichimura, *Chem. Lett.*, 2006, **35**, 410-411.

277. Y. Matsushita, N. Ohba, S. Kumada, K. Sakeda, T. Suzuki and T. Ichimura, *Chem. Eng. J.*, 2007, **135**, S303-S308.

278. Y. Matsushita, N. Ohba, S. Kumada, T. Suzuki and T. Ichimura, *Catal. Commun.*, 2007, **8**, 2194-2197.

279. G. Takei, T. Kitamori and H. B. Kim, *Catal. Commun.*, 2005, **6**, 357-360.

280. S. Teekateerawej, J. Nishino and Y. Nosaka, *J. Appl. Electrochem.*, 2005, **35**, 693-697.

281. S. Teekateerawej, J. Nishino and Y. Nosaka, *J. Photochem. Photobiol. A., Chem.*, 2006, **179**, 263-268.

282. N. Kitamura, K. Yamada, K. Ueno and S. Iwata, *J. Photochem. Photobiol. A., Chem.*, 2006, **184**, 170-176.

283. T. Carofiglio, P. Donnola, M. Maggini, M. Rossetto and E. Rossi, *Adv. Synth. Catal.*, 2008, **350**, 2815-2822.

284. K. Oda, S. I. Ogura and I. Okura, *J. Photochem. Photobiol. B*, 2000, **59**, 20-25.

285. S. K. Pushpan, S. Venkatraman, V. G. Anand, J. Sankar, D. Parmeswaran, S. Ganesan and T. K. Chandrashekar, *Curr. Med. Chem.: Anti-Cancer Agents*, 2002, **2**, 187-207.

286. M. Wainwright, *Chem. Soc. Rev.*, 1996, **25**, 351-359.

287. J. Banchereau and R. M. Steinman, *Nature*, 1998, **392**, 245-252.

288. E. Buytaert, M. Dewaele and P. Agostinis, *Biochim. Biophys. Acta - Rev. Cancer*, 2007, **1776**, 86-107.

289. I. Cecic, B. Stott and M. Korbelik, *Int. Immunopharmacol.*, 2006, **6**, 1259-1266.

290. S. O. Gollnick, X. Liu, B. Owczarczak, D. A. Musser and B. W. Henderson, *Cancer Res.*, 1997, **57**, 3904-3909.

291. S. O. Gollnick, B. Owczarczak and P. Maier, *Laser Surg. Med.*, 2006, **38**, 509-515.

292. M. Korbelik, *Laser Surg. Med.*, 2006, **38**, 500-508.

293. M. Korbelik, I. Cecic, S. Merchant and J. Sun, *Int J Cancer*, 2008, **122**, 1411-1417.

294. T. Kushibiki, T. Tajiri, Y. Tomioka and K. Awazu, *Int. J. Clin. Exp. Med.*, 2010, **3**, 110-114.

295. S. O. Gollnick, E. Kabingu, P. C. Kousis and B. W. Henderson, Stimulation of the host immune response by photodynamic therapy (PDT), 2004.

296. A. D. Garg, D. Nowis, J. Golab, P. Vandenabeele, D. V. Krysko and P. Agostinis, *Biochim. Biophys. Acta - Rev. Cancer*, 2010, **1805**, 53-71.

297. C. J. Gomer, S. W. Ryter, A. Ferrario, N. Rucker, S. Wong and A. M. R. Fisher, *Cancer Res.*, 1996, **56**, 2355-2360.

298. M. Korbelik, J. Sun and I. Cecic, *Cancer Res.*, 2005, **65**, 1018-1026.

299. F. Zhou, D. Xing and W. R. Chen, *Cancer Lett*, 2008, **264**, 135-144.

300. F. Zhou, D. Xing and W. R. Chen, *Int J Cancer*, 2009, **125**, 1380-1389.

301. N. Etminan, C. Peters, D. Lakbir, E. Bünemann, V. Börger, M. C. Sabel, D. Hänggi, H. J. Steiger, W. Stummer and R. V. Sorg, *Br. J. Cancer*, 2011, **105**, 961-969.

302. M. Korbelik, W. Zhang and S. Merchant, *Cancer Immunol. Immunother.*, 2011, **60**, 1431-1437.

303. A. D. Garg, D. V. Krysko, P. Vandenabeele and P. Agostinis, *Cancer Immunol. Immunother.*, 2012, **61**, 215-221.

304. G. Cantl, D. Lattuada, A. Nicolin, P. Taroni, G. Valentinl and R. Cubeddu, *Anti-Cancer Drugs*, 1994, **5**, 443-447.

305. M. Korbelik and I. Cecic, *Cancer Lett*, 1999, **137**, 91-98.

306. M. Korbelik and G. J. Dougherty, *Cancer Res.*, 1999, **59**, 1941-1946.

307. M. Korbelik, G. Krosl, J. Krosl and G. J. Dougherty, *Cancer Res.*, 1996, **56**, 5647-5652.

308. J. A. Hendrzak-Henlon, T. L. Knisely, L. Cincotta, E. Cincotta and A. H. Cincotta, *Photochem. Photobiol.*, 1999, **69**, 575-581.

309. E. Gilboa, *J. Clin. Invest.*, 2007, **117**, 1195-1203.

310. M. Korbelik, B. Stott and J. Sun, *Br. J. Cancer*, 2007, **97**, 1381-1387.

311. A. Jalili, M. Makowski, T. Świtaj, D. Nowis, G. M. Wilczyński, E. Wilczek, M. Chorązy-Massalska, A. Radzikowska, W. Maśliński, Ł. Białły, J. Sieńko, A. Sieroń, M. Adamek, G. Basak, P. Mróz, I. W. Krasnodębski, M. Jakóbisiak and J . Gołąb, *Clin. Cancer Res.*, 2004, **10**, 4498-4508.

312. S. M. Bae, Y. W. Kim, S. Y. Kwak, D. Y. Ro, J. C. Shin, C. H. Park, S. J. Han, C. H. Oh, C. K. Kim and W. S. Ahn, *Cancer Sci.*, 2007, **98**, 747-752.

313. J. S. Friedberg, A. Rao, T. Laksman, J. Collins, J. Cantor and M. Shive, *Lung Cancer*, 2006, **54**, 58.

314. H. Zhang, W. Ma and Y. Li, *Lasers Med Sci*, 2009, **24**, 549-552.

315. V. Cuchelkar, P. Kopečková and J. Kopeček, *Macromol. Biosci.*, 2008, **8**, 375-383.

316. S. Kim, T. Y. Ohulchanskyy, H. E. Pudavar, R. K. Pandey and P. N. Prasad, *J. Am. Chem. Soc.*, 2007, **129**, 2669-2675.

317. T. Y. Ohulchanskyy, I. Roy, L. N. Goswami, Y. Chen, E. J. Bergey, R. K. Pandey, A. R. Oseroff and P. N. Prasad, *Nano Lett.*, 2007, **7**, 2835-2842.

318. F. Yan and R. Kopelman, *Photochem. Photobiol.*, 2003, **78**, 587-591.

319. D. C. Hone, P. I. Walker, R. Evans-Gowing, S. FitzGerald, A. Beeby, I. Chambrier, M. J. Cook and D. A. Russell, *Langmuir*, 2002, **18**, 2985-2987.

320. M. E. Wieder, D. C. Hone, M. J. Cook, M. M. Handsley, J. Gavrilovic and D. A. Russell, *Photochem. Photobiol. Sci*, 2006, **5**, 727-734.

321. A. C. S. Samia, X. Chen and C. Burda, *J. Am. Chem. Soc.*, 2003, **125**, 15736-15737.

322. A. J. Bullous, C. M. A. Alonso and R. W. Boyle, *Photochem. Photobiol. Sci*, 2011, **10**, 721-750.

323. J. M. Sutton, O. J. Clarke, N. Fernandez and R. W. Boyle, *Bioconjugate Chem.*, 2002, **13**, 249-263.

324. S. Flink, F. C. J. M. van Veggel and D. N. Reinhoudt, *J. Phys. Org. Chem.*, 2001, **14**, 407-415.

325. H. Li, J. Zhang, X. Zhou, G. Lu, Z. Yin, G. Li, T. Wu, F. Boey, S. S. Venkatraman and H. Zhang, *Langmuir*, 2010, **26**, 5603-5609.

326. M. Ozmen, K. Can, I. Akin, G. Arslan, A. Tor, Y. Cengeloglu and M. Ersoz, *J. Hazard. Mater.*, 2009, **171**, 594-600.

327. Y. Wang, W. Qian, Y. Tan and S. Ding, *Biosens. Bioelectron.*, 2008, **23**, 1166-1170.

328. Y. Lv, H. Liu, Z. Wang, L. Hao, J. Liu, Y. Wang, G. Du, D. Liu, J. Zhan and J. Wang, *Polym. Advan. Technol.*, 2008, **19**, 1455-1460.

329. Y. C. Lin, B. Y. Yu, W. C. Lin, Y. Y. Chen and J. J. Shyue, *Chem. Mater.*, 2008, **20**, 6606-6610.

330. J. U. Choi, C. B. Lim, J. H. Kim, T. Y. Chung, J. H. Moon, J. H. Hahn, S. B. Kim and J. W. Park, *Synthetic Met.*, 1995, **71**, 1729-1730.

331. G. Arslan, M. Özmen, I. Hatay, I. H. Gübbük and M. Ersöz, *Turk. J. Chem.*, 2008, **32**, 313-321.

332. K. Jahnisch, V. Hessel, H. Lowe and M. Baerns, *Angew. Chem. Int. Edit.*, 2004, **43**, 406-446.

333. N. Tagmatarchis and H. Shinohara, *Org. Lett.*, 2000, **2**, 3551-3554.

334. A. De Mello and R. Wootton, *Lab Chip*, 2002, **2**, 7N-13N.

335. Y. Matsushita, T. Ichimura, N. Ohba, S. Kumada, K. Sakeda, T. Suzuki, H. Tanibata and T. Murata, *Pure Appl. Chem.*, 2007, **79**, 1959-1968.

336. S. Wolf, C. S. Foote and J. Rebek, *J. Am. Chem. Soc.*, 1978, **100**, 7770-7771.

337. R. V. Vince, A. W. Midgley, G. Laden and L. A. Madden, *Cell Stress Chaperones*, 2011, **16**, 339-343.